NASA Contractor Report 177589

The Development of Laser Speckle Velocimetry for the Study of Vortical Flows

A. Krothapalli

CONTRACT NAG2-314
July 1991

National Aeronautics and
Space Administration

NASA Contractor Report 177589

The Development of Laser Speckle Velocimetry for the Study of Vortical Flows

A. Krothapalli

Fluid Mechanics Research Laboratory
Department of Mechanical Engineering
FAMU / FSU College of Engineering
The Florida State University
Tallahassee, Florida 32306

Prepared for
Ames Research Center
CONTRACT NAG2-314
July 1991

National Aeronautics and
Space Administration

Ames Research Center
Moffett Field, California 94035-1000

Introduction

A research program was undertaken to develop a new experimental technique commonly known as "particle image displacement velocimetry" to measure a instantaneous two dimensional velocity field in a selected plane of the flow field. Such a technique was successfully developed and applied to the study of several aerodynamic problems. The detailed description of the technique is given in Appendix I, which is a broad review of all the research activity carried out under this grant.

The application of PIDV to unsteady flows with large scale vortical structures is demonstrated in Appendix II, which describes the temporal evolution of the flow past an impulsively started circular cylinder.

The instantaneous two dimensional flow in the transition region of a rectangular air jet was measured using PIDV and the details are given in Appendix III and IV. This experiment clearly demonstrates PIDV's capability in the measurement of turbulent flows.

Preliminary experiments were also conducted to measure the instantaneous flow over a circular bump in a transonic flow. Several other experiments are now routinely using PIDV as a non-intrusive measurement technique to obtain instantaneous two dimensional velocity fields.

A list of Technical publications is given in the next section.

Technical Publications:

Lourenco, L., Krothapalli, A., and Smith, C. A., "Particle Image Velocimetry", *Advances in Fluid Mechanics Measurements*, Editor: M. Gad-el-Hak, Springer-Verlag, 1989, pp128-199.

Lourenco, L., and Krothapalli, A., "Particle Image Displacement Velocimetry Measurements of a Three Dimensional Jet", *The Physics of Fluids*, 31, No. 7, 1988, pp 1835-1837.

Lourenco, L., and Krothapalli, A., "The Role of Photographic Parameters in Laser Speckle or Particle Image Displacement Velocimetry", *Experiments in Fluids*, 5, No. 1, 1987, pp 29-32.

Lourenco, L., and Krothapalli, A., "Application of PIDV to the Study of the Temporal Evolution of the Flow Past a Circular Cylinder", *Laser Anemometry in Fluid Mechanics - III*, Editors: R. J. Adrian et. al, Ladon-Instituto Superior Tecnico, Lisbon, Portugal, 1987, 161-177.

Lourenco, L., Krothapalli, A., Buchlin, J. M., and Riethmuller, M. C., "An Non-Invasive Technique for the Measurement of Unsteady Velocity Fields", *AIAA Journal*, 24, No. 10, 1986, pp 1715-1717.

Krothapalli, A., Lourenco, L., and Shih, C., "Vortex Interactions in the Transition Region of a Rectangular Jet", *IUTAM Symposium on Separated Flows and Jets*, Novosibirsk, USSR, July 1990.

Lourenco, L., and Krothapalli, A., and Smith, C. A., "On the Instability of a Rectangular Jet", *Proceedings of Fourth International Symposium on Applications of Laser Anemometry to Fluid Mechanics*, Lisbon, Portugal, July 1988.

Lourenco, L., and Krothapalli, A., "Instantaneous Velocity Field Measurements of a Turbulent Rectangular Jet Using PIDV", AIAA Paper 88-0498, *26th Aerospace Sciences Meeting*, Reno, January 1988.

Krothapalli, A., and Lourenco, L., "Unsteady Separated Flows: A Novel Experimental Approach", AIAA Paper 87-0459, *25th Aerospace Sciences Meeting*, Reno, Nevada, January 1987.

Lourenco, L., and Krothapalli, A., Buchlin, J. M., and Riethmuller, M. L., "Application of PIDV to the Study of Unsteady Fluid Flows", *AGARD Symposium on Aerodynamic and Related Hydrodynamic Studies Using Water Facilities*, Montery, October 1986, AGARD CP-413, 23.1-23.9.

Smith, C. A., Lourenco, L., and Krothapalli, A., "The Development of Laser Speckle Velocimetry for the Measurement of Vorticle Flow Fields", AIAA Paper 86-0768-CP, *14th Aerodynamic Testing Conference*, March 1986.

Buzyna, G., Lourenco, L., and Krothapalli, A., "PIDV Measurements in a Transonic Flow", *42nd Annual Meeting of Fluid Dynamics, Bulletin of American Physical Society*, **34**, No. 10, November 1989.

Lourenco, L., and Krothapalli, A., "The Development of Laser Speckle or Particle Image Displacement Velocimetry Part I: The Role of Photographic Parameters", Fluid Mechanics Research Laboratory TR-1, The Florida State University, May 1986. Also appeared in NASA CP-2477, 1987.

Professional Personnel

Graduate Students

Mr. Ramesh Arjunji	M. S. (12/88)
Mr. David Wishart	M. S. (5/91) **
Miss. Melissa Styer	M. S. (8/91) *

* Expected
** Currently a Ph.D. student in our department.

Professors Krothapalli, Lourenco, Van Dommelen, and Shih have participated in the program.

APPENDIX I

PARTICLE IMAGE VELOCIMETRY

L. M. Lourenco, and A. Krothapalli
Department of Mechanical Engineering
FAMU/FSU College of Engineering
P.O Box 2175, Tallahassee, FL 32316
and
C. A. Smith
NASA Ames Research Center
Moffett Field, CA 94035

Reprinted from

Lecture Notes In Engineering 45
Advances in Fluid Mechanics Measurements
Edited by M. Gad-el-Hak
Springer-Verlog, 1989

Particle Image Velocimetry

Outline

1. Introduction

One of the most challenging and time-consuming problems in experimental fluid mechanics is the measurement of the overall flow field properties, such as the velocity, vorticity, and pressure fields. Local measurements of the velocity field (i.e., at individual points) are now done routinely in many experiments using hot-wire (HW) or laser velocimetry (LV). However, many of the flow fields of current interest, such as coherent structures in shear flows or wake flows, are highly unsteady. HW or LV data of such flows are difficult to interpret, as both spatial and temporal information of the entire flow field are required and these methods are commonly limited to simultaneous measurements at only a few spatial locations.

Interpretation of these flow fields would be easier if a quantitative flow visualization technique was used in conjunction with the flow field measurements. Such a technique would provide both spatial and temporal information. One such method is termed particle tracing (Gharib, Dyne, Thomas, and Yap, 1987) and consists of measuring the streak lengths and orientation generated by injected particles. However, this method only provides partial results, because of its limitations in accuracy and spatial resolution (Lourenco, 1986).

Although the vorticity field is an essential property of most flows of current interest, measurements of this quantity have exceeded experimental capability. This difficulty arises from the fact that vorticity is a quantity defined in terms of local velocity gradients. In contrast, the currently available flow measurement techniques, such as hot-wire anemometry or laser velocimetry, are sensitive only to the local velocity. Hence, measurements must be made over several points and the resulting velocity components are then analyzed by finite difference schemes. However, the errors produced by the necessary differentiations limit the accuracy and spectral range. In addition, the spatial resolution of this method is often not sufficient to measure small-scale fluid motions of rapidly changing velocity gradients. As a consequence, the measured vorticity field is a type of spatially averaged estimate of the actual vorticity field. Finally, this method provides information at only a single point. If information on the entire flow field is required, measurements must be carried out sequentially one point at a time. This sequential method, although laborious, is straightforward in applications involving steady flows. However, the method becomes very difficult, if not impossible, when studying unsteady flows. Direct measurement of vorticity has

been tried, for instance by the injection of spherical particles which rotate in the flow with an angular velocity proportional to the local vorticity (Frish and Webb, 1981). Such methods suffer the same drawback of insufficient spatial resolution just mentioned and also can be quite complex.

Recently, a novel velocity measurement technique, commonly known as Laser Speckle Velocimetry (LSV) or Particle Image Velocimetry (PIV), has become available. This technique provides the simultaneous visualization of the two-dimensional streamline pattern in unsteady flows as well as the quantification of the velocity field over an entire plane. The advantage of this technique is that the velocity field can be measured over an entire plane of the flow field simultaneously, with both accuracy and spatial resolution. From this the instantaneous vorticity field can be easily obtained. This constitutes a great asset for the study of a variety of flows that evolve stochastically in both space and time, such as unsteady flow separation or vortex-surface interaction. This article describes the principle of this technique, various methods of data acquisition and reduction, some parameters that affect its utilization, and some examples of its use.

2. Principle of The Technique

The application of PIV to the measurement of the velocity in a fluid involves two steps. First it is necessary to "create" a selected plane or surface within the flow field. The orientation of this plane should be such that it contains the dominant flow direction, if one exists. For instance, if the technique is used to measure the velocity field over a model in a wind tunnel, the plane will be parallel to the wind tunnel flow axis. The plane itself is created by seeding the flow with small tracer particles, such as those used in LV applications, and illuminating them with a thin sheet of coherent light, as depicted in Figure 1. A pulsed laser, such as a Ruby or a Nd-Yag laser, or a CW laser with a shutter, is normally used as the light source. The laser sheet itself is formed, for example, by focusing the laser beam first with a long focal length spherical lens (to obtain minimum thickness), and then diverging the beam in one dimension with a cylindrical lens. The light scattered by the tracer particles in the illuminated plane provides a moving pattern. When the seeding concentration is low, the instantaneous pattern consists of resolved, diffraction-limited images of the particles. When the concentration increases, the images overlap and interfere to produce a random speckle pattern. A multiple-exposure photograph, of two or more of the instantaneous patterns and taken in quick succession, is used to record the data. When the time interval between exposures is appropriately chosen, the tracer particles will have moved only a few diameters, far enough to resolve their motion but less than the smallest length scale of the flow. Thus, information on the local fluid velocity is stored on the photographic image and can be retrieved by subsequent analysis.

In a second step the local fluid velocity is derived from the ratio of the measured spacing between the images of the same particle, or speckle grain, and the time between exposures. The recorded image, whether formed by isolated disks, in the case of low particle concentration, or speckle grains for high particle concentration, is a complicated random pattern. Several methods exist to convert the information contained in the multiple-exposed photograph, or specklegram, to flow field data such as velocity, streamlines, or vorticity. These methods can be grouped into two broad categories. In the first category the distance between particle pairs is evaluated directly. That is, the absolute locations of the particles' corresponding images in the photograph are measured, for instance using a digitized version of the photograph, and the velocity is determined by computing the relative position of the corresponding images. The second category covers those techniques that evaluate the particles' image spacings indirectly. They exploit the property that all particles in a small region (small relative to the length

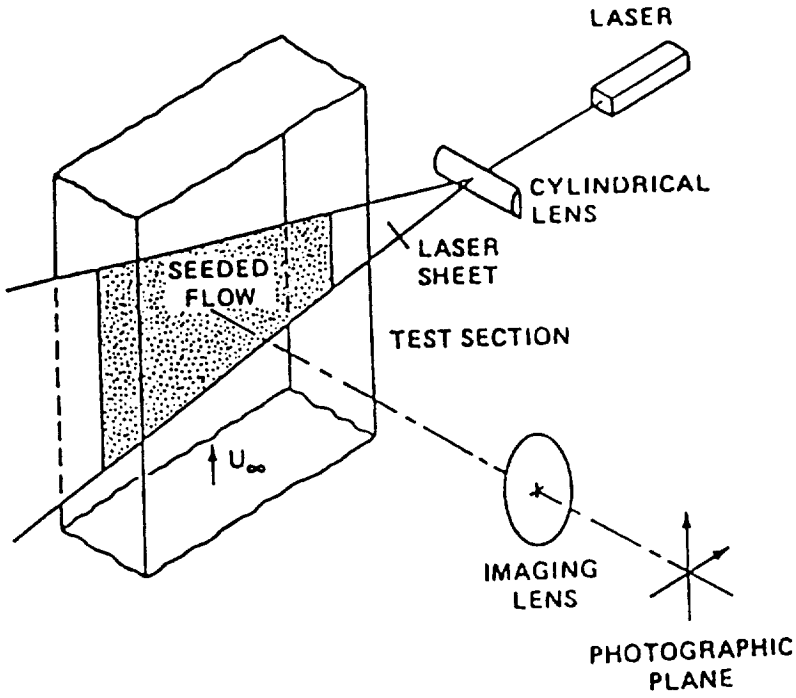

Figure 1. Schematic of Experimental Setup for Particle Image Velocimetry

scales of the fluid under study) are displaced roughly the same amount between exposures. This property is exploited in several ways in both hardware and software recently developed in digital image processing to determine the velocity. One specific method in this second category, evaluation by Young's fringes, is described in detail in Section 4.2, following a brief overview of other techniques in Section 4.1. However, a brief background of how this analysis technique first originated is described first.

For instance, it is conceivable to measure the local displacements by visual or computer-aided inspection. The data reduction systems that have been proposed are based on the digitization of the entire photograph into a very large number of pixels and the development of algorithms to permit computer identification of individual streaks or pairs of particles. Methods for this direct analysis of these images have been developed, but with limited success. Gharib et al, (1987), Elkins et al (1977), and Dimotakis et al (1981) are recent studies where this technique has been used. Photographs based on these techniques are difficult to interpret when the mean distance between two independent particles is the same order of magnitude as the particle displacement. This difficulty is usually circumvented by using low particle concentrations. However, flow field information is then restricted to those isolated locations where particles are present. This results in velocity measurements with low spatial density. Spatial derivatives of the velocity (e.g., vorticity) are then difficult to estimate and must be inferred by indirect arguments, such as described by Dimotakis, et al, (1981).

It is important to realize that the multiple-exposure photograph produces a locally periodic random image. This periodicity is proportional to the local velocity and can be determined using Fourier or autocorrelation techniques. To obtain the velocity field, the photograph can be scanned on a point-by-point basis, which yields measurements of the local displacement (i.e., velocity), or with a whole field filtering technique, which yields isovelocity contours. An example of this latter method is given by Meynart, (1980). Recently, an anamorphic optical system has been proposed by Collicott & Hesselink (1985). This method performs a 1-D Fourier transform in the x-direction for measuring the x-velocity component, and images the speckle pattern in the y-direction. This results in curved fringes which have a local spacing inversely proportional to the x-velocity at that point. Simultaneous multiple point measurements are obtained by imaging in the y-direction. Thus, it is possible to measure a velocity component along a selected line in the flow.

3. History of Particle Image Velocimetry

The terms Laser Speckle Velocimetry and Particle Image Velocimetry (or sometimes Particle Image Displacement Velocimetry) are often used interchangeably. However, these terms reflect an important distinction, related to the particle density in the flow field. To understand these differences, it is first necessary to describe how the application of this technique to the measurement of fluid flows developed.

The term "speckle", or the speckle phenomenon refers to the granular appearance that diffusely reflecting and transmitting surfaces take on when illuminated by a laser beam. This grainy appearance is caused by constructive and destructive interference of coherent light (i.e., the laser beam) scattered from a surface element whose roughness is large compared with the wavelength of the laser. For example, when a sheet of white paper is placed in the path of a laser beam, the reflected light contains information on the roughness of the paper. In the field of holography this is sometimes referred to as speckle noise (e.g., Collier, Burckhardt, and Lin, 1971). Actually, it is not noise but rather unwanted information in the context of holography. It is this information that is utilized in the laser speckle context. The first applications that made use of the speckle phenomena were in the field of solid mechanics. It was originally used to measure in-plane displacement and strain of solids with diffusely scattering surfaces and has also been applied to surface roughness measurement, vibration, and deformation analysis. Several early applications of the laser speckle concept are described in Erf (1980) and Stetson (1975).

The technique as used for the measurement of displacements in solid mechanics is essentially as follows. A surface is first illuminated by a laser beam, as shown in Figure 2. When this surface is imaged through a lens onto a photographic plate, the interference of the scattered light wavelets gives rise to a speckle pattern. The speckle size is a statistical average of the distance between adjacent regions of maximum and minimum brightness and can be estimated (Erf, 1980) by the Rayleigh resolution criterion

$$d_s = (1.2)\lambda f_N(1+M) \qquad (1)$$

where d_s is the size of a speckle grain, λ is the wavelength of the illuminating laser, f_N is the f-number of the recording optics, and M is the

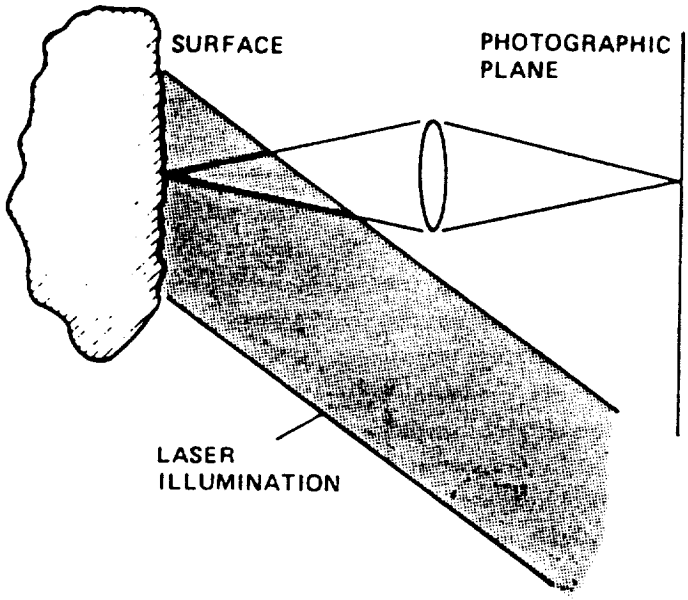

Figure 2. Laser Speckle Concept in Solid Mechanics

magnification. A doubly exposed photography of the speckle pattern is then recorded, once before and once after a lateral displacement is introduced. This photograph, or specklegram, contains two correlated grids which can be analyzed as a non-uniform diffraction grating. The technique can only be used when the displacement between exposures is greater than the speckle size, d_s, but not so great as to destroy correlation. Thus, the individual speckle size sets the lower measurable limit. Analysis of this specklegram was performed by generating Young's fringes from the specklegram transparency, as described in Section 4.2.

Although speckle photographs obtained in solid mechanics and fluid mechanics are similar, there are two fundamental differences. The first is that the fluid is illuminated by a sheet of laser light whose thickness is Δz. Therefore, scattering occurs from a volume distribution of particles rather than a surface distribution. Secondly, the number density of particles per unit volume (seeding concentration) can vary over a wide range of values. Strictly speaking, for a true speckle pattern to exist, the number of scattering particles must be so high that the images overlap and interfere to produce a random speckle pattern in the image plane. When the particle concentration is lower than this level (and reasons why this can often be an advantage will be discussed in a later section) discrete images of the particles will be photographed instead. This low particle concentration is referred to as Particle Image Velocimetry (PIV), reserving the term Laser Speckle Velocimetry (LSV) for the high particle concentration levels where a random speckle pattern is usually formed. Most of the early applications of this technique to fluid flows (e.g., Simpkins and Dudderar, 1978) used the LSV method, whereas for reasons to be described later, most of the more recent studies use the lower concentration PIV method.

4. Particle Image Analysis

4.1 Overview of Analysis Techniques

The most common methods of analysis are point-by-point techniques. In this type of analysis a small portion of the multiple-exposed photograph is examined, over which the velocity field is assumed constant. Several techniques have been developed to extract the flow field information. One approach consists of analyzing the position of the particles in the image plane and measuring directly the image pair spacings in the photographs. In this method the local particle displacements are measured, for example, by determining the two-dimensional correlation of the image field within the interrogation region. The spot is digitized in a NxN format (where N is the number of pixel rows or columns) and a two-dimensional correlation is performed. This results in a digital autocorrelation function with a maxima at the coordinates corresponding to the average displacement of the tracer particles. The major drawback of this method is that the computation of the autocorrelation function requires large data arrays and becomes extremely slow when N is large. A new processing method, developed and used by Yao and Adrian, (1984), reduces the general NxN element of a two-dimensional problem into two N element one-dimensional problems, by compressing the information in two orthogonal direction using integration techniques. In this method, called "orthogonal image compression", the 2-D image of an interrogation region is split, and optically compressed onto two orthogonally-aligned linear detector arrays. Particle images in the 2-D region appear as peaks in the 1-D distributions of each of the two array signals. The optimal method for determining the separation of the peaks, and thus the velocity, depends on the image density, defined as the mean number of particle image pairs in the interrogation region. If the image density is less than one, the peak separation is measured directly in each orthogonal direction. If the image density is greater than one, the peak separation is evaluated using 1-D spatial correlation. A recent study by Landreth, Adrian, and Yao, (1988) has indicated, however, that the correlation distributions given by this technique sometimes included random peaks in addition to the peaks created by the particle image pairs, resulting in incorrect measurements. These extraneous peaks seem to be due to random image pairings. Modifications to this method to prevent this possibility are currently being investigated.

4.2 Analysis of Young's Fringes

An alternate method for the measurement of the local displacement between the two images of the particle pair is by the use of Young's fringes. These fringes are obtained by illuminating a small portion of the specklegram, or multiple-exposed photograph, with a focused laser beam. The diffraction produced by coherent

illumination of the multiple images in the negative generates a fringe pattern in the Fourier plane of a lens, provided that the particle images correlate. This is shown schematically in Figure 3. These fringes have an orientation which is perpendicular to the direction of the local displacement and a spacing which is inversely proportional to the displacement. If Δ is the real translation of the object, then this is related to the distance between the particle images, s, by

$$\Delta = s/M \qquad (2)$$

The spacing between Young's fringes can be shown to be (e.g., Born and Wolf, 1980),

$$d_f = \lambda f_L/s \qquad (3)$$

where d_f is the fringe spacing and f_L is the focal length of the converging lens. Thus, the displacement of the images is given by

$$\Delta = \lambda f_L /M\, d_f \qquad (4)$$

This technique offers an important advantage over those that directly analyze the particle images in that it eliminates the difficulties associated with finding the individual image pairs on the photograph.

The basis of the Young's fringe method can be described as in the following. Consider the function D(r) describing the light intensity in the image plane of a photographic camera, where r(x,y) are the plane coordinates. Considering that there is an in-the-plane displacement dy of the scatterers, the image will be translated by Mdy between exposures, where M is the magnification of the camera lens, and the resulting intensity distribution of the specklegram is

$$D(x,y) + D(x,y + Mdy) = D(x,y) \otimes [\delta(x,y) + \delta(x,y + Mdy)] \qquad (5)$$

where δ (x,y) is the Dirac delta function centered on r(x,y), and considering that a translation can be represented as a convolution with a delta function. This total intensity is recorded on the photographic plate. After development, the transmittance, τ , of the negative is given by

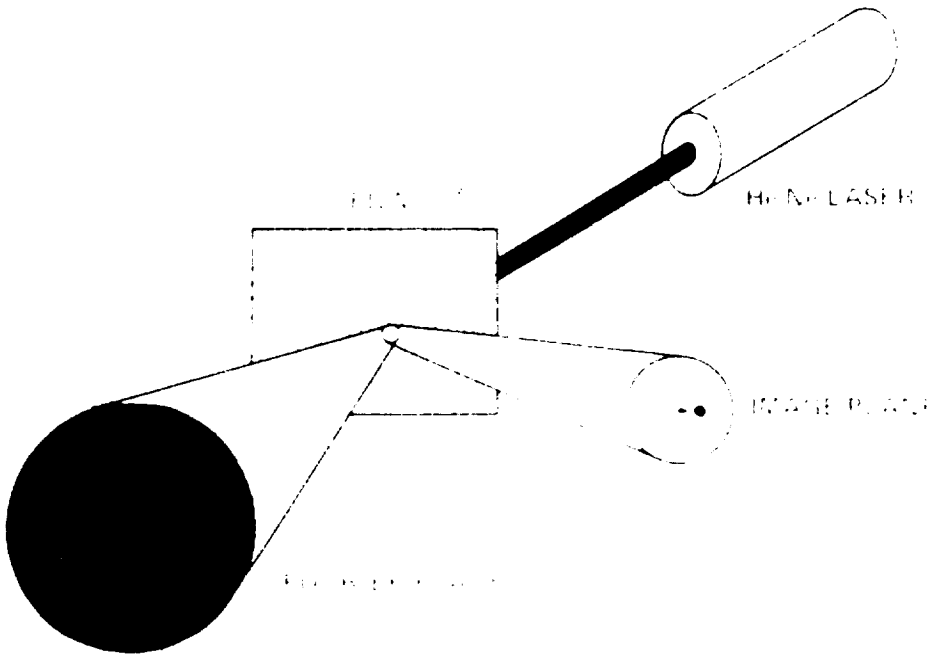

Figure 3. Schematic Diagram of Young's Fringe Formation for Specklegram Analysis

$$\tau(r) = a+bD(x,y) \otimes [\delta(x,y) + \delta(x,y+Mdy)] \quad (6)$$

where a and b are characteristic constants of the photographic emulsion. Local analysis of a small portion of the film negative with a probe laser beam will produce in the far field an optical two-dimensional Fourier transform of the transmittance distribution, with an intensity distribution given by

$$\tau(u,v) = a\ \delta(u,v) + b\ D(u,v)[1+\exp(i2\pi v\ Mdy)/\lambda_{il}] \quad (7)$$

where τ represents the Fourier transform of τ, u, and v are the angular coordinates of a point in the Fourier plane, and λ_{il} is the wavelength of the interrogating laser beam. The first term, $a\ \delta(u,v)$, on the right hand side of equation (7) represents the image of a point source, (i.e., the interrogating beam), when diffraction effects are neglected. This image is seen as a small bright spot in the center of the Fourier plane. The second term is composed of a fine speckle structure D, modulated by the expression

$$[1+\exp(i2\pi v\ Mdy)/\lambda_{il}] \quad (8)$$

The intensity distribution for the second term is obtained by multiplication with its complex conjugate, resulting in

$$|D(u,v)|^2[4\cos^2(2\pi v\ Mdy)/\lambda_{il}] \quad (9)$$

The diffuse background, given by $|D(u,v)|^2$ and called the "diffraction halo", is modulated by a set of Young's fringes whose spacing is given by equation (3). Knowing M, f_L, λ_{il}, and measuring d_f the displacement dy is easily found from equation (3). The direction of motion is perpendicular to the orientation of the fringes. There is a 180 deg. direction ambiguity in that the motion is known only as perpendicular to the fringes. A method to resolve this ambiguity is described in Section 5.8.

4.3 Limitations of the Young's Fringes Method

The formation of the fringe pattern that occurs when a local region of the specklegram is illuminated with a coherent laser beam requires that the displacement of the particle pairs within the interrogation region be correlated.

Identical shifting of all particle pairs will result in perfect correlation. Two factors reduce this correlation and can eliminate the fringe pattern. The first is when there is a slight out-of-plane motion of the particles, due to three-dimensional motions in the flow. The tolerance to out-of-plane motion is basically equivalent to the width of the illumination sheet and the depth of field of the recording optics. The time between exposures and the width of the illuminating sheet need to be carefully selected to avoid too many particles entering or leaving the sheet between exposures. The second factor is when the velocity varies across the interrogation region. This will cause the various particle image pairs to be displaced by different amounts. This will not occur when the diameter of the interrogation region is smaller than the smallest length scale of the flow being studied.

4.4 Data Processing

The Young's fringe pattern, produced by the techniques described in Section 4.2, are analyzed using a digital image analysis system, which typically consists of a host computer, a digital image processor, a frame digitizer, pipeline processor, and a video output controller to convert digital to analog information for display on a monitor. The system also usually includes a two-dimensional traversing mechanism and a controller for the purpose of automatically scanning the film transparencies. Analysis of the fringes can occur in either an interactive mode, which requires the assistance of an operator, or in an automated procedure.

The interactive method consists of first obtaining a 1-D periodic signal from the straight fringes. This is performed by determining the fringe angle relative to a predetermined reference line, followed by an averaging over the lines of the digitized picture as given by the following relation.

$$f(m) = \Sigma I[m+(n-255)\tan\alpha,n], \quad 0 \le m \le 511 \tag{10}$$

where $f(m)$ is the resulting periodic signal, $I(m,n)$ represents the digitized picture, and α, is the angle of the fringes with the reference n axis. In this equation it is assumed that the image is digitized with a 512x512 format with 256 shades of gray. The extraction of the frequency from this signal is straightforward. The Fourier transform of $f(m)$ displays a peak at the frequency proportional to the velocity component parallel to the m axis. However, due to low frequency modulation of the fringes, which is a consequence of the non-uniform light intensity distribution in the diffraction halo, it is sometimes difficult to identify this peak, especially if the fringes have a low frequency (i.e., few fringes). To remove this modulation, the fringe signal can be passed through a high pass filter prior to processing.

The advantage of this one-dimensional averaging technique is rapidity, in that only one line of the fringe pattern needs to be digitized. The computation, which includes the determination of the fringe angle by the operator and position updating of the film transparency scanning mechanism, can be completed in just a few seconds. The disadvantage of this method is the need for an external adjustment of the angle of the fringes by an operator. This inconvenience can be corrected by using the automated method.

The second method, which does not require an operator, consists of computing the velocity components along independent directions. The basis for this method is that each line of the fringe frame can be considered as a noisy periodic signal with variable phase. Then the automatic determination of a velocity component can be performed simply by averaging over a quantity independent of this phase. The autocorrelation for each line, or its Fourier transform for the power spectrum, satisfies this requirement. Using the autocorrelation, the m velocity component can be computed from the relation

$$g(u) = \Sigma[(\Sigma[I(m,n)I(m+u,n)]/\Sigma[I(m,n)]^2], \quad -511<u<511 \qquad (11)$$

where g(u) is the resulting periodic signal, based upon the autocorrelation of the intensity distribution. This algorithm has been implemented on a pipeline processor by Lourenco and Krothapalli, (1988) to compute the autocorrelation for all lines of a frame simultaneously. They found that, for an accurate estimate of both the velocity magnitude and direction, four such full image operations, giving four autocorrelation functions, were required. From these autocorrelation functions the velocity vector can be determined by selecting the values of the components which have been computed from autocorrelations having the highest signal-to-noise ratio, and visibility. The determination of the velocity vector typically takes on the order of two to five seconds.

The obvious advantage of this technique is that no external operator is required. However, a shortcoming of this technique is the difficulty in measuring the velocity when the fringe density is too low (typically less than three bright fringes). In this case, the velocity can still often be evaluated by the interactive, one-dimensional averaging method. Hence, these two methods are actually complementary.

5. Detailed Considerations

This section describes some of the parameters that can affect the use of particle image velocimetry. The impact of these parameters is discussed and, where possible, recommended values are given.

The technique relies on the ability to detect and record on a photographic plate the images of the tracer particles. This image is a function of the scattering power of the particles within the fluid, the amount of light in the illuminating sheet, the length of time the film is exposed, magnification of the recording optics, and film sensitivity at the wavelength of the illuminating laser light. The specific parameters playing a role in PIV include the following. Additional details are contained in Lourenco and Krothapalli, (1987) and Smith, Lourenco, and Krothapalli, (1986).

Light source;	strength and duration of pulses
Tracer particle;	type, dimension, and concentration
Exposure parameters;	duration, time between exposures, and number of exposures
Film parameters;	sensitivity, grain size, and resolution
Recording optics;	magnification and lens aperture

These parameters are strongly interrelated and depend upon such factors as the type of fluid, velocity range and length scales of the flow being studied, and the required spatial resolution in the results.

5.1 Light Source

The light recorded on the specklegram is that which has been scattered 90 deg. to the incoming laser light sheet. Extremely bright light sources are usually required because of the low efficiency of this scattering process. Although the particle detection increases proportionally with increasing power of the illuminating laser, it is important to keep the laser power requirement to a minimum, primarily because of the expense. The specific amount of laser light energy required is a function of tracer size and concentration, recording lens aperture and magnification, and film sensitivity. For a successful photographic recording of a particle image, the mean exposure of an individual particle image must be greater than the film sensitivity at the wavelength of the illuminating laser. This minimum sensitivity is sometimes referred to as the "gross fog" level (Adrian and Yao, 1985). In analytical terms this is expressed as

$$E = \int_{\Delta t} \tau dt > CE_0 \qquad (12)$$

where E is the mean exposure of an individual particle image, τ is the average intensity of light scattered by a particle, E_0 is the film fog level, and C is a constant between 1 and 10. The fog level is defined as the exposure level below which the transmissivity of the film is independent of the incident intensity, as shown in Figure 4.

The mean intensity of the light, τ, of the light scattered by a single particle can be expressed as

$$\tau = (4/\pi\kappa^2 d_i^2)\, I_0 \int_\omega \sigma^2 d\omega \qquad (13)$$

where κ is the wavenumber of the illuminating laser light, d_i is the nominal diameter of the particle, including diffraction, I_0 is the intensity of the illuminating sheet, σ is the Mie parameter, and ω is the solid angle subtended by the camera lens. The effective dimension of the particle image, d_i, can in turn be expressed as

$$d_i = \{ M^2 d_p^2 + d_e^2 \}^{1/2} \qquad (14)$$

where d_p is the actual particle diameter, and d_e is the diffraction-limited spot diameter of the particle image, given by

$$d_e = 2.44\, (1 + M)\, f_\# \lambda \qquad (15)$$

Equation (14) is an approximate relation representing the combined effects of magnification and image blurring in determining the final image diameter. When a pulsed laser is used, and assuming that the particle is stationary during exposure, the laser power required is determined from equation (12).

$$I_0 > \{ CE_0 (\pi\kappa^2 d_i^2) \} / 4 \int \sigma^2 d\omega \qquad (16)$$

The recommended value for the constant C in equation (16) is between three and

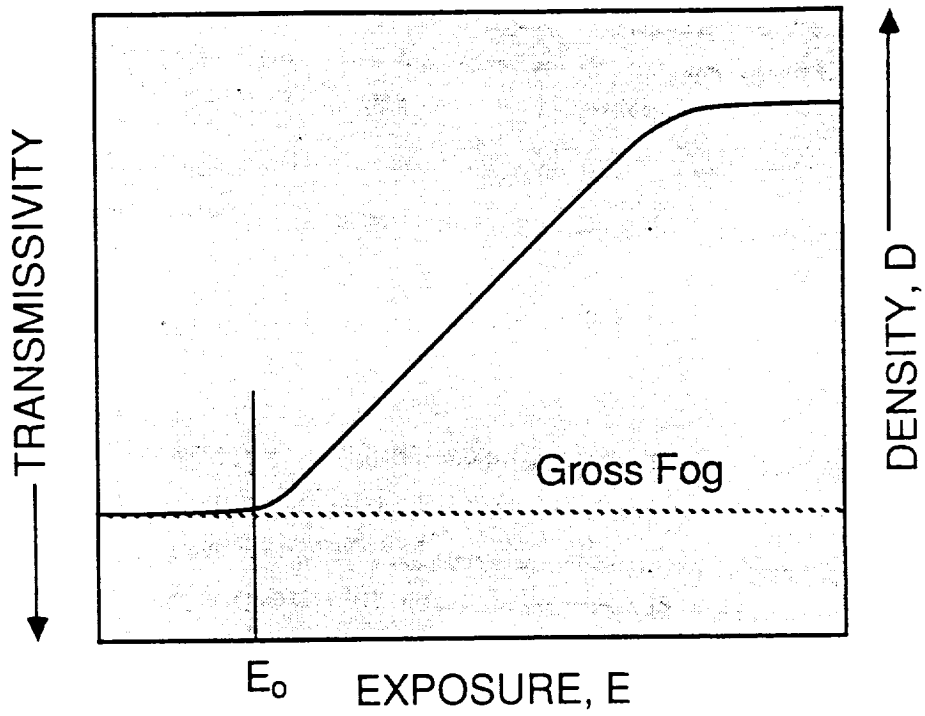

Figure 4. Density-Exposure Curve for a Film

five to account for the film reciprocity effects caused by very short exposures. Similar calculations for a CW laser are discussed by Lourenco, (1986).

5.2 Tracer Particles

The basic assumption in all techniques that use tracer particles added to the flow, whether it's LV, PIV, or some other technique, is that the motion of the particle accurately follows the motion of the fluid. These requirements are usually met by tracers used in LV applications. In air flows for instance, oil smoke produces a relatively uniform seeding. The minimum detectable particle diameter is a function of the recording optics and the laser input energy. Particles ranging from 0.5-10 μm are fairly typical. It should be noted that, for particles of this size, the diameter of the recorded image is relatively insensitive to the actual particle diameter. In this range of particle sizes, the image size is dominated by diffraction effects from the photographic lens.

5.3 Particle Concentration

The Laser Speckle mode of operation relies upon identical, laterally shifted speckle patterns. For these speckle patterns to exist, the number of scattering sites per unit volume must be high enough that many images overlap with random phase in the image plane. With lower concentrations the mode of operation changes from the speckle mode to the particle image mode (PIV) where the pattern consists of discrete images of particles. Velocities determined from the LSV mode suffer inaccuracies associated with the randomness of the speckles, but the velocity can be determined at any point in the flow. In the PIV mode, regions of the flow field may be left out due to poor seeding (sometimes referred to as signal drop-out) but the velocity can be measured without the inaccuracies of the speckle mode.

Slight out-of-plane motion of the particles, due to three-dimensional motions in the flow, will result in speckle patterns that are not entirely similar. As a consequence, the correlation between patterns decreases and the fringe pattern is suppressed of eliminated. This poses a severe limitation in the use of the laser speckle mode for the study of turbulent flows, or flows with a significant velocity component in the direction perpendicular to the laser sheet. However, the fringe quality is less dependent on out-of-plane motion in the PIV mode of operation. In this case the tolerance to out-of-plane motion is roughly equivalent to the width of the illuminating sheet and the depth of field of the recording optics.

There are practical bounds to the particle concentration in both modes of operation. In the PIV mode the upper boundary is set simply at that value above

which a speckle pattern is formed, as shown in Figure 5. If C_p is the particle concentration and Δz the width of the laser sheet, the maximum concentration is given by

$$\{1/(\Delta z C_p)\}^{1/2} >> d_i/M \qquad (17)$$

where d_i is the image diameter, given in equation (14).

The lower end in the PIV mode can be determined by the criterion that, in order to have a valid experiment, a minimum number of particle image pairs must be present in the area being scanned by the interrogation beam. The case of a single particle image pair is ideal because it yields fringes with optimum signal-to-noise ratio. However, this situation can only be achieved by lightly seeding the flow, which gives rise to signal drop-out. An interesting case occurs when two particle pairs are present in the interrogation area. The resulting diffraction pattern includes multiple equally intense fringe patterns due to cross interference of non-corresponding image pairs. In this situation, shown in Figure 6, the local displacement cannot be resolved. As the number of particle image pairs in the interrogation area increases, the cross interference fringes become weaker in comparison with the main fringe pattern, which reflects the local displacement. These cross-interference fringes are sometimes called "background speckle noise". Experience shows that, for reasonable fringe quality, at least four particle image pairs should be present in the interrogation area.

At the high end of the particle concentration scale, the LSV mode, the particle concentration is governed by convenience, economics, and flow distortion. Attempting to obtain these high particle concentrations in large scale flows or in high speed flows, such as in a wind tunnel, can become exceedingly difficult, as well as expensive as the actual number of particles increases. Finally, the high concentration of particles required by the LSV mode may influence or distort the flow field being studied. For these reasons, the PIV mode is normally used.

5.4 Exposure Parameters

The exposure parameters are chosen in accordance with the maximum expected velocity in the flow field and the required spatial resolution. The spatial resolution, which in turn is equal to the cross-sectional area of the interrogating laser beam, is dictated by the scales associated with the fluid motion. So as not to

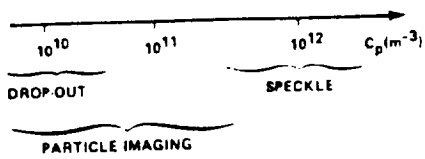

Figure 5. Mode of Operation vs. Particle Concentration

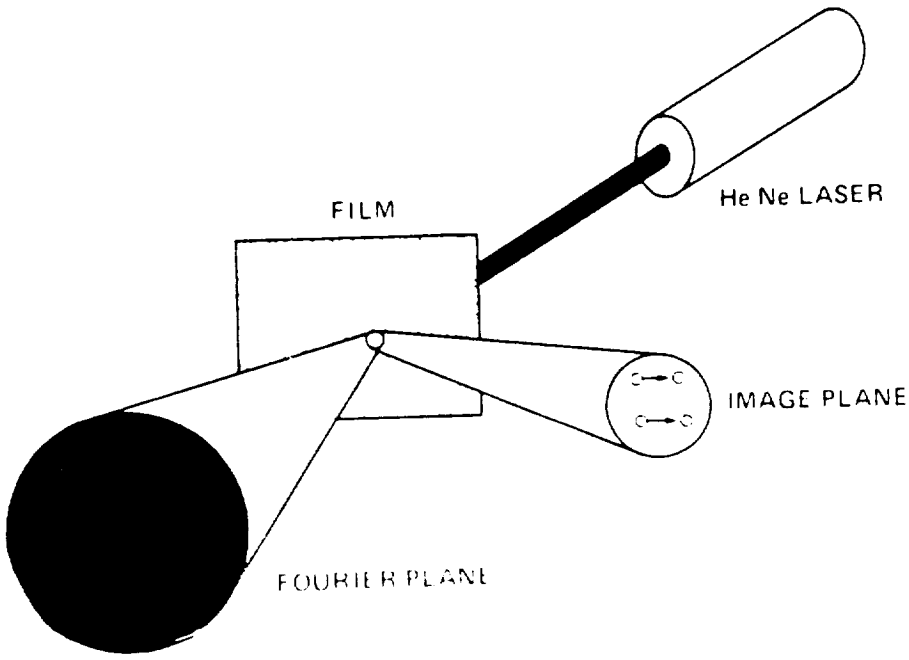

Figure 6. Cross-interference Fringe Pattern Generated by Two Particle Pairs

lose any information, the spatial resolution should be less than the smallest scale in the flow being studied.

The time between exposures, T, is determined by the maximum permissible displacement of a particle such that a correlation is obtained when the negative is analyzed locally with a probe laser beam. A necessary condition to obtain a fringe pattern is that the distance between adjacent particle images be less than a fraction of the analyzing beam diameter. In practice, the maximum permissible displacement that can be detected corresponds to the case when the fringe spacing, d_f, is larger than the diffraction limited spot diameter, d_l, of the interrogating optics. In analytical terms,

$$d_f = \lambda_a f_L / MTV_{max} > d_l = 4 \lambda_a f_L / \pi D \qquad (18)$$

The time between exposures can then be expressed as

$$T = (0.5)D/MV_{max} \qquad (19)$$

For practical purposes the value of (0.5) is used instead of the mathematically correct ($\pi/4$), as given in equation (18). This points up another advantage of this technique, in that the velocity sensitivity range can easily be shifted by altering the pulse separation, T.

For very short exposures the recorded particle images are identical to the diffraction limited particle images, as the particles appear to be stationary during the exposure. When the exposure time is increased, the recorded images becomes streaks whose length is directly proportional to the exposure time. The diffracted light in the spectrum is concentrated in a band whose width is inversely proportional to the streak length. For optimum exposure, Lourenco (1984) has shown that the exposure time, Δt, should be

$$\Delta t = d_i / MV_{max} \qquad (20)$$

where d_i is the particle image diameter.

5.5 Film Parameters

The technique relies on the ability to detect and record on photographic media the

images of the seeding particles. This is a function of the scattering power of the particles within the fluid, the amount of light in the illuminating sheet, camera lens and film sensitivity at the wavelength of the illuminating laser light. Although the particle detection increases proportionally with increasing power of the illuminating laser, it is of great importance to keep the laser power requirement to its minimum for economy.

To compensate for the many cases when limited laser power is available for illumination, the film used to record the particle images should have good sensitivity, but without sacrificing film resolution. Unfortunately, for commercially available photographic films, speed and resolving power are inversely related. Hence, choices range between high speed, low resolving power and low speed, high resolving power. For most practical applications good precision is necessary, so the advantage lies with the high resolution films (with about 300 line-pairs/mm). Of probably more importance, however, is the film grain. When illuminating the film negative to produce Young's fringes, the film's unexposed grains can introduce amplitude and/or phase changes into the wavefront of the analyzing laser beam, thus creating additional noise. This noise has a frequency content which is in the same general range as the fringes. Therefore, its elimination is difficult either by optical or digital filtering. Lourenco and Whiffen (1984) reduced this noise source by producing a positive copy through contact printing, on a very high resolution fine grain film. The positive copy was analyzed in the same manner using the probe laser beam. Problems arising from film grain will always be present, especially in applications where fast film is used to cope with low power density of the illuminating sheet. However, in general, the grain size should be much smaller than the diameter of the particle image to avoid this unwanted noise.

5.6 Recording Optics

As mentioned previously, the minimum detectable particle diameter is a function of the f-number of the recording optics. In fact, the f-number can have a significant effect on the mean exposure of an individual particle image. When the particle diameter is small compared with the diffraction-limited spot diameter, d_e, then d_i, the dimension of the particle image including diffraction, is independent of the actual particle diameter and instead is proportional to the f-number. The minimum detectable particle diameter can be shown to increase sharply for apertures smaller than f-11. Of course, any size particle can be detected provided the concentration is high enough. However, there are many reasons, described in other sections, for not increasing the concentration.

5.7 Dynamic Range

The dynamic range of the technique refers to its ability to resolve large velocity gradients in the flow field. It is defined as the largest velocity difference that can be detected. The low end of the dynamic range is determined by the requirement that the spacing between successive particle images be well resolved. That is, simply that they do not overlap. In analytical form,

$$l_s = d_i + V_{min}\,\Delta t \; < \; TV_{min} \qquad (21)$$

where l_s is the spacing between successive particle images. It was shown in the previous section that T, the time between exposures, is related to the maximum velocity V_{max} as

$$T = (0.5)\,D / MV_{max} \qquad (19)$$

For a pulsed laser and low speed flows it is sufficient to assume that $\Delta t = 0$. Thus, combining these Equations (21) and (19),

$$V_{min} = 2M\,d_i\,V_{max} / D \qquad (22)$$

The velocity dynamic range is then defined as the normalized velocity difference,

$$\Delta V = (V_{max} - V_{min}) / V_{min} \qquad (23)$$

and is written as

$$\Delta V = (D / 2M\,d_i) - 1 \qquad (24)$$

for a pulsed laser. Considering typical values of d_i = 0.3 mm, D = 5 mm, and M = 1, a dynamic range of 7.5 can be expected. A relation similar to equation (24) can be obtained for a CW laser, using $\Delta t = d_i / V_{max}$. Following the same line of reasoning,

$$\Delta V = (D - 2\,d_i) / (2\,M\,d_i) - 1 \qquad (25)$$

for a CW laser. A powerful advantage of this technique is evident in these equations. That is, by adjusting the magnification M in recording the specklegrams, the system sensitivity can be altered to accommodate the amount of motion anticipated in the experiment.

5.8 Direction Ambiguity

One disadvantage of using a multiple-exposure photograph to extract velocity data is the 180 deg. ambiguity in determining the direction of the velocity vector. That is, given identical conditions in recording each of the two exposures, there is no property identifying the order in which the two images of the particle were recorded. Measuring the separation of the particle image pair provides the magnitude of the velocity at that point, but is insufficient to give the direction of the velocity vector field. Thus, a given displacement will indicate a velocity of +/- U, with the sign being ambiguous. Many flow fields of interest (such as wakes and separated flows) contain regions of reversed flow and the direction may not be known a priori. Thus, a means to remove this ambiguity would be very useful.

A method to resolve both this ambiguity of the velocity vector, as well as to improve the dynamic range of the measurements, has been developed by Adrian, (1986) and Lourenco, et al (1986). This method is termed "spatial image shifting" or "velocity bias technique". The method consists conceptually of recording the flow field in a moving reference frame, and thus superposing a known velocity bias to the actual flow velocity. This is accomplished by shifting the image by a known displacement between the two exposures. The image can be shifted physically using a moving camera, or by optical means using rotating or scanning mirrors. This effect is demonstrated in Figure 7. Consider a flow field with regions of reversed flow, and with velocities ranging up to a value V. Four such velocities, one in each of the four quadrants, are shown in the figure. Using standard PIV recording techniques, it would not be possible to resolve between velocities lying in the first (or second) quadrant from those lying in the third (or fourth) quadrant. Now impose a velocity V*, much larger than V, as in Figure 7. The four velocity vectors are now transformed into four distinctly different vectors, depending upon their direction. The correct velocity, with its direction, can now be easily obtained upon removal of the velocity bias.

The method currently employed uses a scanning mirror to displace the image during the exposure with a predetermined velocity. A schematic of the scanning mirror arrangement is shown in Figure 8. Consider two particle pairs A B and C D, having equal displacements in opposite directions in the object plane. By introducing a mirror placed at 45 deg. between the camera lens and the object

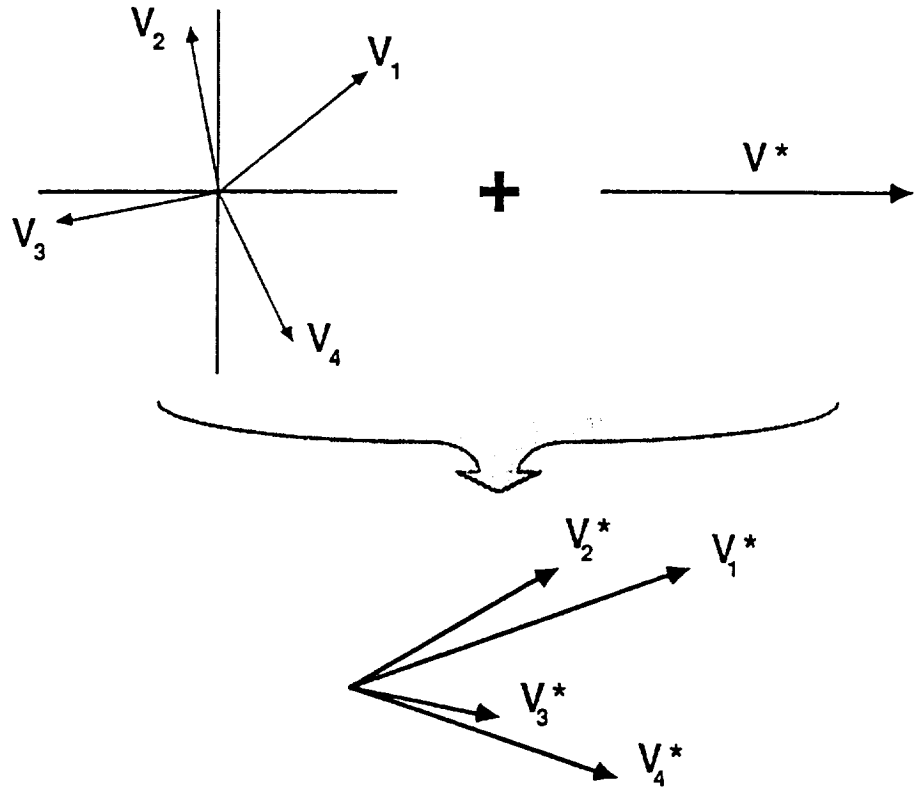

Figure 7. Removal of Direction Ambiguity Using Velocity Bias

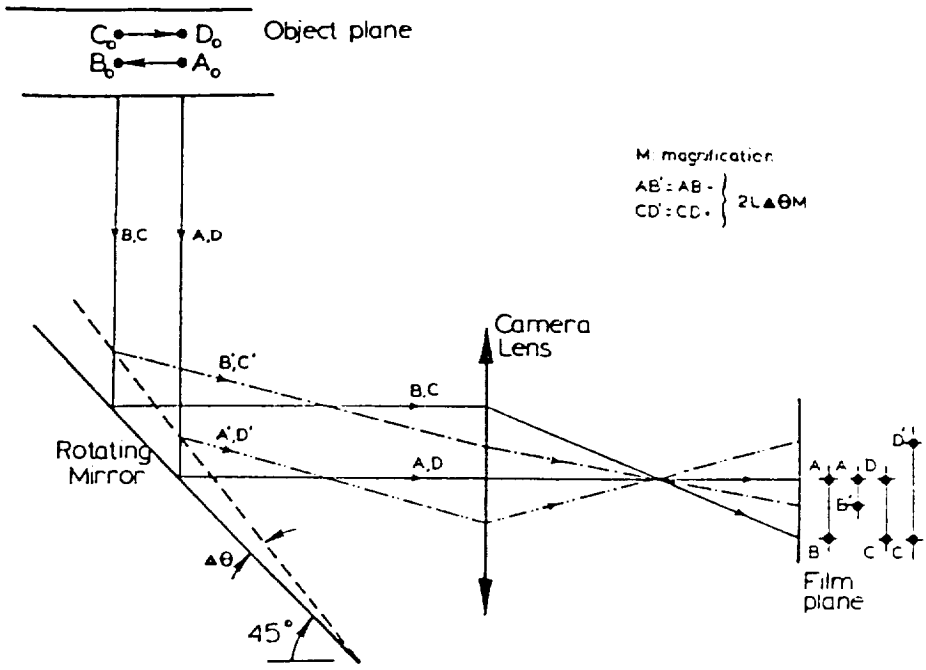

Figure 8. Scanning Mirror Arrangement for Imposing Velocity Bias

plane, the corresponding displacements appear in the film plane as AB and CD with equal magnitudes. When the mirror is rotated by an angle of $\Delta\theta$ between exposures, the displacements corresponding to A B and C D appear in the film plane as AB' and CD', with different magnitudes, resolving the direction ambiguity.

Figure 9a is a double-exposure photograph of the flow past in impulsively started airfoil captured at a stage of its development corresponding to a non-dimensional time of $t^* = tU/c$, where t is the time from the start of the motion, U is the free-stream velocity, and c is the airfoil chord. This figure depicts a complex flow field and exhibits large regions of flow reversal. Analysis of this photograph would yield velocity vector information only within the restriction of the 180 deg. direction ambiguity. In addition, there would also be regions of drop-out where the flow velocity is less than the lower velocity range limit of this technique. Using the velocity bias technique, with a bias velocity equal to two times the free stream velocity, gives the biased images shown in Figure 9b. The velocity field obtained by analyzing Figure 9b is shown in Figure 10a. The actual velocity field, in the reference frame of the airfoil, is given in Figure 10b, upon removal of the velocity bias.

5.9 Overall Accuracy of the Technique

It has been pointed out that out-of-plane motion (i.e., three-dimensional motion) is a severe limitation to this technique in the application to fluid flow. The reason for this limitation is that out-of-plane motion by the tracer particles results in patterns that are poorly correlated. Consider the imaging system shown in Figure 11, with the particle in position P_0 within the laser sheet. The particle will more to a new position R_0 between exposures due to the fluid motion, including an out-of-plane motion dz. In the image plane the corresponding positions are P_L and R_L. The coordinates of these latter two locations are, neglecting second-order and higher terms for simplicity,

$$P_L; \{-M_x, -M_y, (d_0 + d_L)\}$$

$$R_L; \{-M(x + dx)(1 + dz/ d_L), -M(y + dy)(1 + dz/ d_L), (d_0 + d_L)\} \qquad (26)$$

The displacement between these two locations, $P_L R_L$, determined by the method of Young's fringes, is given by

Figure 9a. Double-Exposed Photograph of Airfoil Impulsively Started from Rest; Unbiased Image

Figure 9b. Double-Exposed Photograph of Airfoil Impulsively Started from Rest; Biased Image

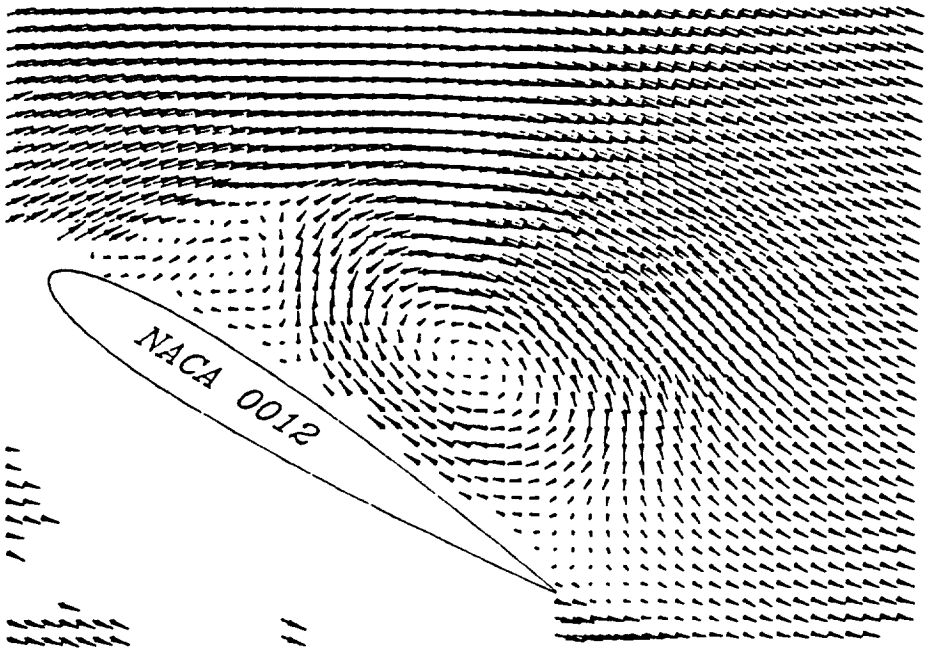

Figure 10a. Instantaneous Velocity Field of Airfoil Impulsively Started from Rest; Before Removal of Velocity Bias

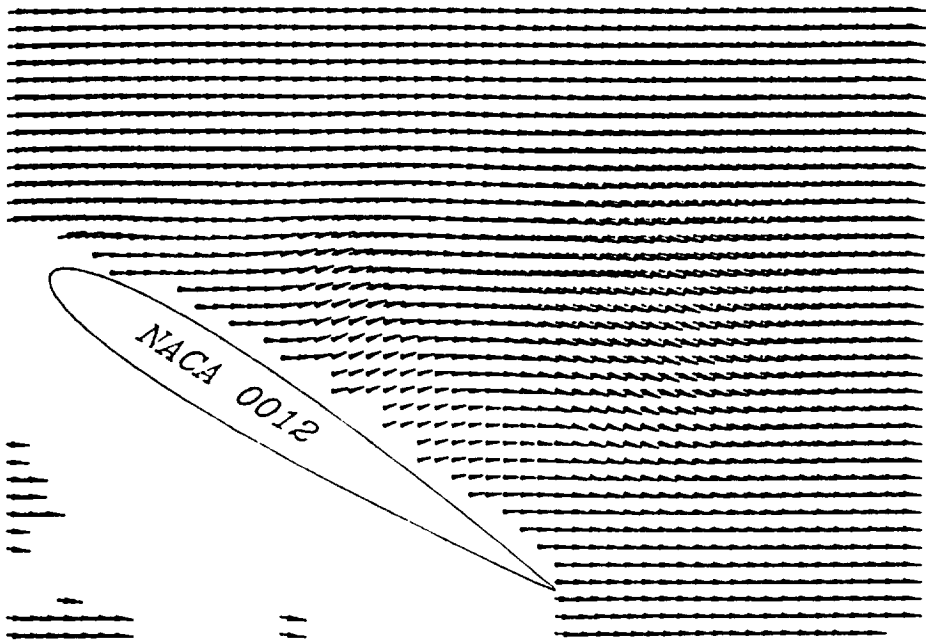

Figure 10b. Instantaneous Velocity Field of Airfoil Impulsively Started from Rest; After Removal of the Velocity Bias

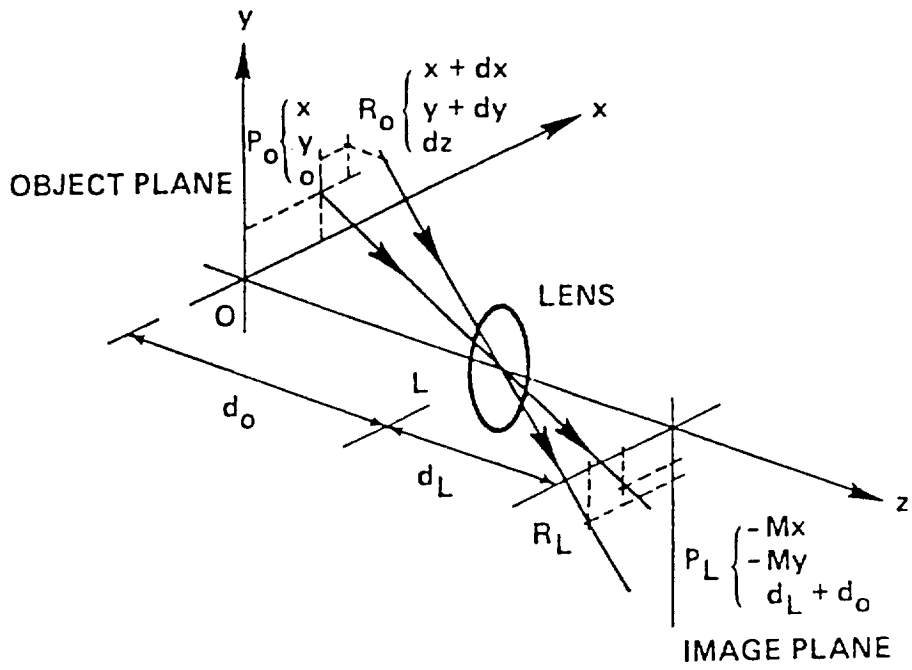

Figure 11. Schematic of Imaging System Estimating the Effect of Out-Of-Plane Motion

$$dx_m = M\,dx\,(1 + x\,dz/dx\,d_L), \quad dy_m = M\,dy\,(1 + y\,dz/dy\,d_L) \qquad (27)$$

Thus, the measured displacement components, referred to the object plane, become

$$dx_0 = dx + x\,dz/d_L, \qquad dy_0 = dy + y\,dz/d_L \qquad (28)$$

The contribution of the out-of-plane displacement to the measured displacement is given by the two parasite terms, $x\,dz/d_L$ and $y\,dz/d_L$. The error produced by three-dimensional motion is a function of the distance from the optical axis. While negligible near the optical axis, it increases linearly, and may become important, farther away. The importance of the out-of-plane motion therefore becomes particularly important when using short focal lengths and wide angle objectives.

The overall accuracy of the technique can be evaluated by studying the uniform flow field created by towing a camera at constant speed past a quiescent flow. Several multiple-exposure photographs were taken, with differing times between exposures, thus resulting in photographs with particle pairs at different known distances. The range of time between exposures, as well as the distance between corresponding particle images in the film plane are presented in Table 1. A large number of points (100) of these five photographs were analyzed using the methods described previously. Uncertainties in the experiment include errors introduced during the recording of the multiple-exposure photograph, such as the ones introduced by distortion of the scene being recorded by the camera lens, limited film resolution, and inaccuracies due to the processing algorithms.

In the absence of a systematic bias, the standard deviation of the measured velocity distribution is an estimate of the mean measurement error. Analysis of the film transparencies using the two techniques (the interactive, one-dimensional averaging method and the automatic autocorrelation method) yields the same mean value with a nearly equal standard deviation (Table 1). The values in Table 1 indicate that using these methods, inaccuracies of the order of 1-2 % are expected. It is believed that these inaccuracies are due to a combination of the limited resolving power of film used for recording (only about 100 lines/mm) and the limited response of the camera lens. Another source of error which is not accounted for in this analysis is the one due to the spurious contributions on the in-plane displacement recording by the out-of-plane motions (Lourenco & Whiffen, 1984, Lourenco, 1986).

Table 1. Overall Accuracy of the Technique

Time Between Exposures, msec	Fringe Frequency	RMS Fringe Frequency	Measured Distance, μM
22.2	33.447	0.257	194
25.0	37.045	0.208	218
28.6	42.950	0.381	249
33.3	49.037	0.710	291
40.0	60.693	1.190	350

6. Examples

6.1 Flow Behind a Circular Cylinder

The time-space development of the near wake flow behind a circular cylinder impulsively accelerated from rest to a constant velocity is studied in this first example. This flow is excellent as a first example because it contains large-scale vortical motions and has extreme velocity gradients. Also it is a well-studied flow and there are several theoretical analyses.

A classic flow visualization study of this flow was performed by Prandtl (1927) and reveals several interesting flow features. Soon after the motion begins, the boundary layer separates and vorticity is convected away from the rear of the cylinder. Two symmetric eddies are formed behind the cylinder, each containing vorticity of opposite sign. The two separating streamlines that surround these eddies join downstream of the eddies and form a closed vortex region. The size of this region grows with time and eventually becomes larger than the cylinder itself. As time increases still further, perturbations cause the standing vortices to develop asymmetric oscillations. Eventually, some of the vorticity in the larger eddy breaks away and moves downstream. The process repeats itself with the other eddy and the flow develops into the familiar Karman vortex street.

The experiment was conducted by towing circular cylinder, 25.4 mm in diameter through a towing tank measuring 300x200x600 mm. The towing carriage is driven by a variable DC motor, and the towing velocity was 22 mm/sec. The Reynolds number, based on cylinder diameter, was 550. The fluid used in the experiment was water seeded with 4 micron metallic-coated particles. For the illumination, a laser beam from a 5 Watt Argon-Ion laser is steered and focused to a diameter of 3 mm using an inverse telescope lens arrangement. A cylindrical lens, with a focal length of -6.34 mm, is used to diverge the focused beam in one dimension, creating a light sheet. The laser sheet was 70 mm wide and the illuminated the mid-span section of the cylinder. For the multiple exposure, the CW laser beam was modulated using a Bragg cell. In this experiment the laser power density, I_0, of the sheet was 0.27 W/mm^2. A 35 mm camera, attached to the towing carriage, was used to record the flow field. The frequency at which the multiple exposures were taken was 1.7 Hz. The aperture of the lens, with a focal length of 50 mm and a space of 12 mm, was set at F#5.6 and the resulting magnification factor was 0.40. The exposure time, t, and the time between exposure, T, were chosen by the criteria described in Section 5 and are 3 msec and 30 msec, respectively. These two parameters, along with the

diameter of the analyzing beam and the particle image diameter, determine the dynamic range of the velocity (see Section 5). For this experiment, the dynamic range was roughly 6.

The flow was captured at several stages of its development, corresponding to t^*, where $t^* = tU/D$, the non-dimensional time, t is the time from the start of the motion, U is the free stream velocity, and D is the cylinder diameter. Figure 12a-d show typical multiple-exposure photographs of this flow field. In Figure 12a, at $t^* = 2.2$, the two symmetric eddies are clearly seen in the wake of the cylinder and the closed vortex region is roughly the same size as the cylinder diameter. At a later time, $t^* = 3.2$, (Figure 12b) the eddies are still symmetrical but has grown much larger. At a still later time, $t^* = 4.2$, (Figure 12c) the asymmetry is just beginning. Finally, at $t^* = 5.2$, (Figure 12d) the flow field is completely asymmetric and vorticity from the upper eddy is about to break away and move downstream.

The velocity data are acquired in a square mesh by digital processing of the Young's fringes, produced by point-by-point scanning of the positive contact copy of the photograph (Lourenco, 1986). The scanning step size and the dimension of the interrogating laser beam are both 0.5 mm, which, with the magnification of 0.40 corresponds to a spatial resolution of about 1.25 mm in the object plane. This is about 1/20 of the diameter of the cylinder. The fringes were processed using the methods described in Section 4. The resultant two-dimensional velocity fields, corresponding to Figures 12a-d, are shown in Figures 13a-d are a good representation of the expected flow pattern. The length of each vector in the Figure 13 is proportional to the local velocity at that point.

Because of the high spatial resolution of these data, vorticity contours can be derived by taking spatial derivatives of the velocity data. Letting each grid location be labeled with indices (i,j), the vorticity component at location (i,j) is given by

$$\Omega_{i,j} = 1/2\{(V_{i+1,j} - V_{i-1,j})/2\Delta X - (U_{i,j+1} - U_{i,j-1})/2\Delta Y\} \qquad (29)$$

where $\Omega_{i,j}$ is the vorticity at point (i,j), U and V are the longitudinal and lateral velocities, and Δx and Δy are the mesh intervals in the streamwise and cross-stream directions, respectively. Figure 14a-d show the smoothed vorticity contours, normalized with respect to the free steam velocity and the cylinder diameter. To aid in the understanding of this flow, the value of vorticity can be

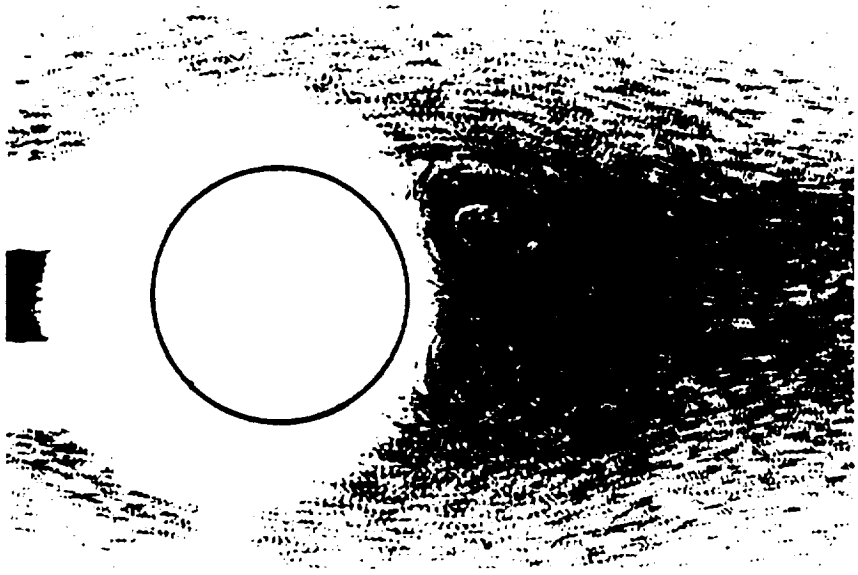

(a)

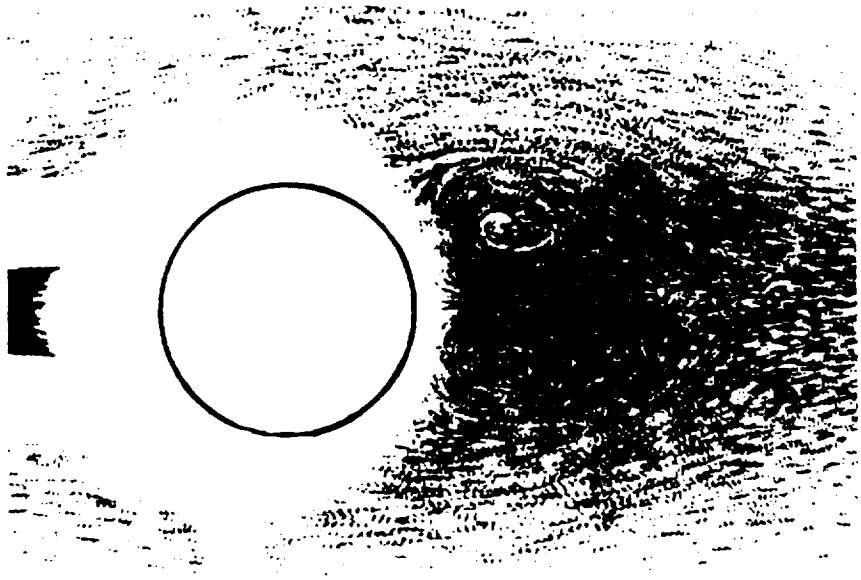

(b)

Figure 12. Multiple-Exposed Photographs of the Wake Flow Field Behind a Circular Cylinder; a) $t^* = 2.2$; b) $t^* = 3.2$; c) $t^* = 4.2$; d) $t^* = 5.2$

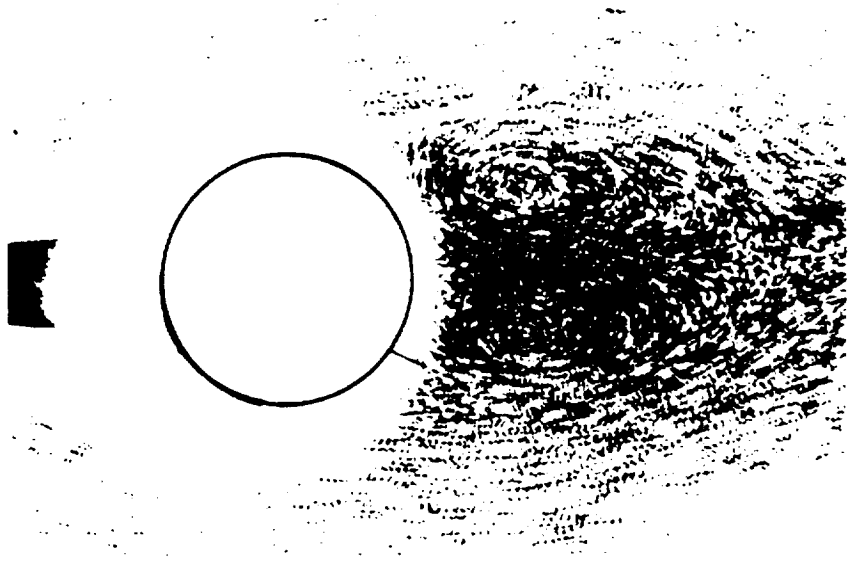

c)

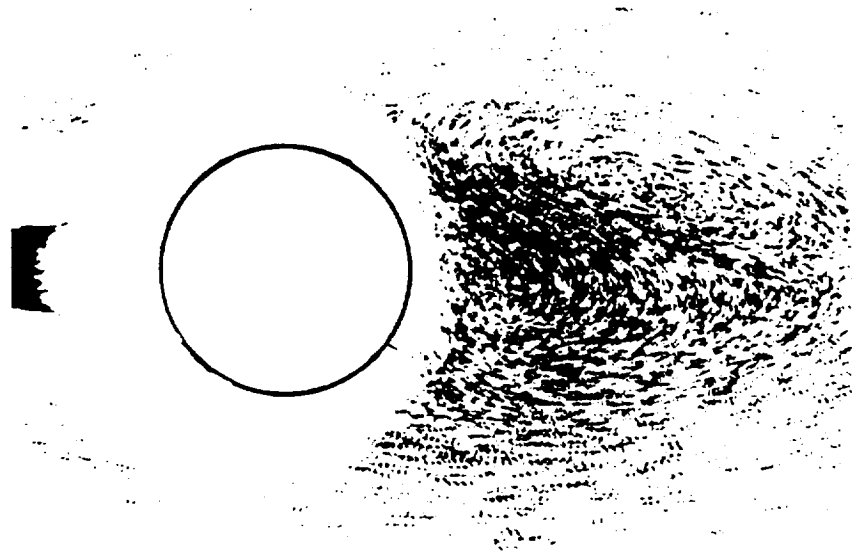

(d)

Figure 12. Multiple-Exposed Photographs of the Wake Flow Field Behind a Circular Cylinder (Concluded); a) $t^* = 2.2$; b) $t^* = 3.2$; c) $t^* = 4.2$; d) $t^* = 5.2$

Figure 13. Instantaneous Velocity Field of the Wake Flow Field Behind a Circular Cylinder; a) $t^* = 2.2$; b) $t^* = 3.2$; c) $t^* = 4.2$; d) $t^* = 5.2$

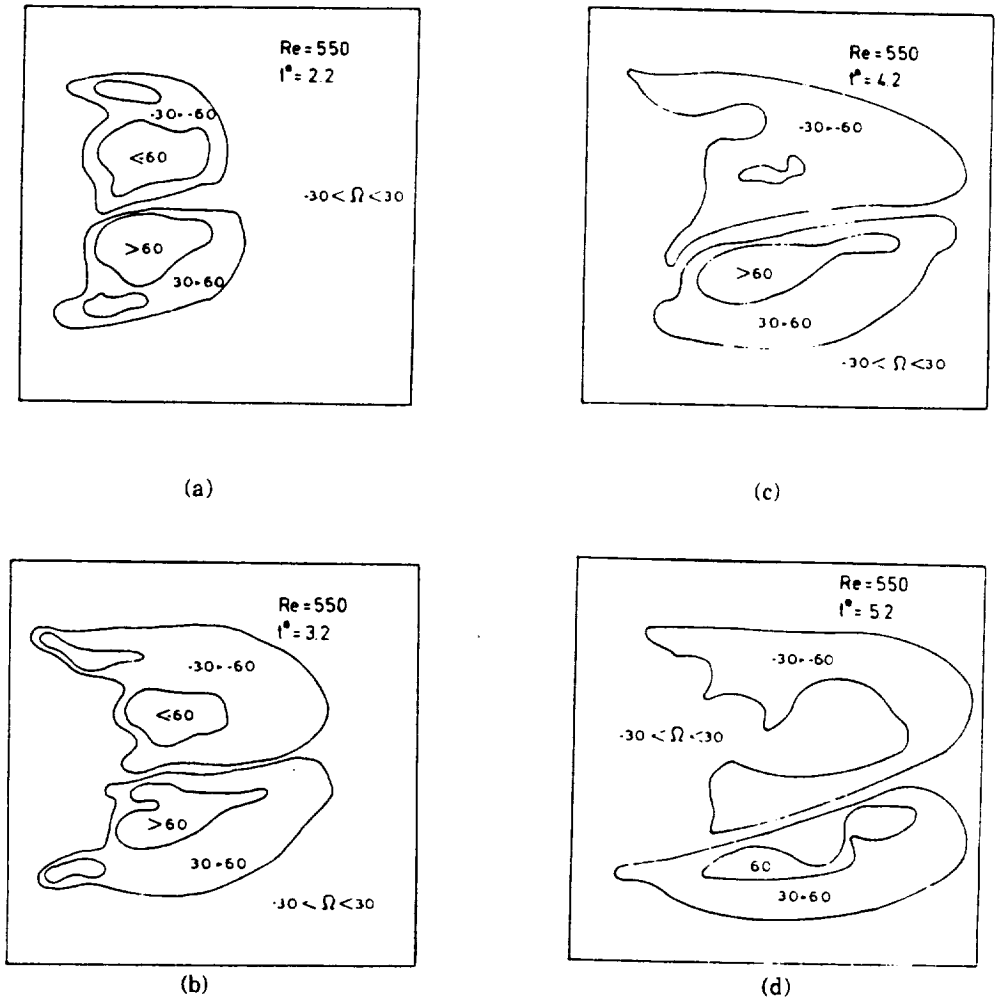

Figure 14. Constant Vorticity Contours of the Wake Flow Field Behind a Circular Cylinder; a) $t^* = 2.2$; b) $t^* = 3.2$; c) $t^* = 4.2$; d) $t^* = 5.2$

superposed on the velocity data of Figure 13. This is shown in Figure 15a-d, where the vorticity is displayed by color coding each velocity vector. The color code represents the vorticity level, the magnitude of which is given by the color bar on the top of each figure. The red and blue colors represent the peak positive and negative vorticity regions, respectively.

Analysis of these figures reveals some interesting features. Two primary regions of high vorticity form at the rear of the cylinder, corresponding to the startup vortices, while two secondary high vorticity regions are observed further outward. This is especially clear in the vorticity contours shown in Figure 14. The primary vorticity regions may possibly correspond to the "vorticity peak" reported by Bouard and Coutanceau (1980), whereas the secondary regions may be related to the breakup of the feeding sheet as suggested by the flow visualization of Tietjens (1970). Also, it is interesting to observe that the vorticity field (Figure 14) displays earlier evidence of asymmetry than the velocity field (Figure 13).

Using the velocity data of Figure 13, global wake characteristics can also be determined. One example is the growth in the size of the closed vortex region, or wake bubble, with time. Figure 16 displays the development of the wake length, measured in terms of the distance between the cylinder surface and the saddle point (zero velocity) where the two counter-rotating wake vortices join. These values, which are plotted in terms of the non-dimensional time, t^*, compare well with available experimental data by Honji & Taneda (1969) and numerical predictions by Loc (1980) and van Dommelen (1981). It was observed that the distance between the two twin vortices remained constant at a value of about 0.55D, where D is the cylinder diameter, throughout the experiment. This is also in good agreement with the observations reported by Honji & Taneda (1969).

6.2 Flow Past an Airfoil at Angle of Attack

The time-space development of the unsteady separated flow generated by an NACA 0012 airfoil at an angle of attack of 30 deg. and started impulsively from rest is studied in this section. The flow is created by towing the airfoil in the same towing tank as described in the previous section. The airfoil chord is 60 mm and was towed with a velocity of 22 mm/sec. The corresponding Reynolds number was 1400. In order to record the time development of the flow field, the camera was attached to the towing carriage and the frequency which the multiple exposures were taken was set at 2 Hz. Typical multiple exposure photographs of this flow are shown in Figure 17. The photographic arrangement was purposely adjusted to enhance the view of the flow field on the upper surface of the airfoil rather than to show the entire flow around the airfoil. Consequently, the details of the flow

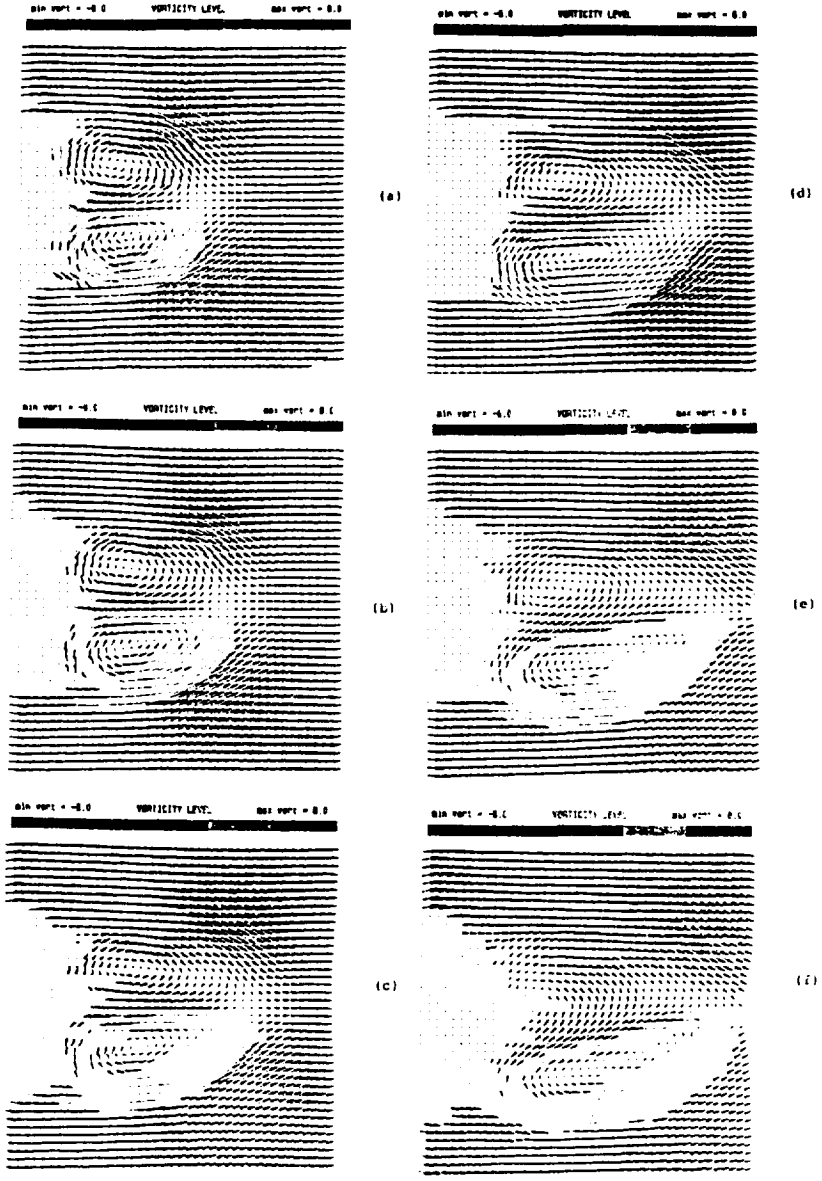

Figure 15. Superposition of Velocity and Vorticity Fields for the Circular Cylinder Wake Flow; a) $t^* = 2.2$; b) $t^* = 2.7$; c) $t^* = 3.2$; d) $t^* = 3.7$; e) $t^* = 4.2$; f) $t^* = 4.7$

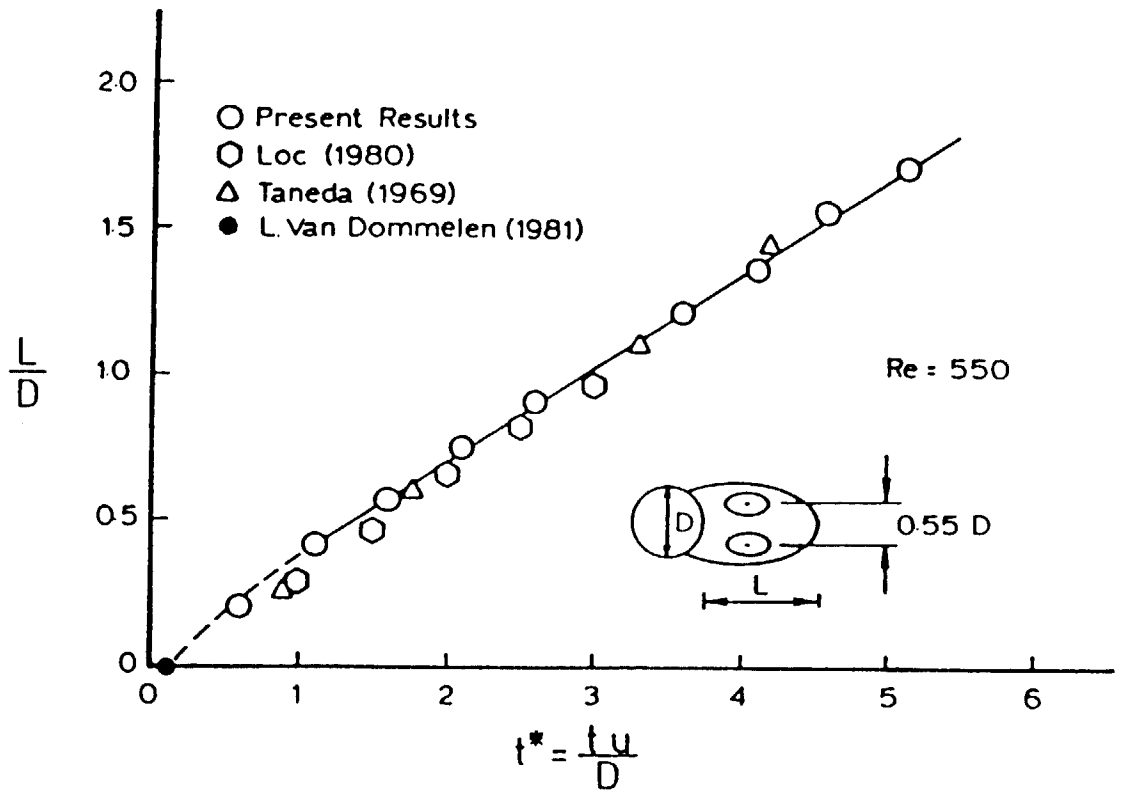

Figure 16. Development of Cylinder Wake Size with Time

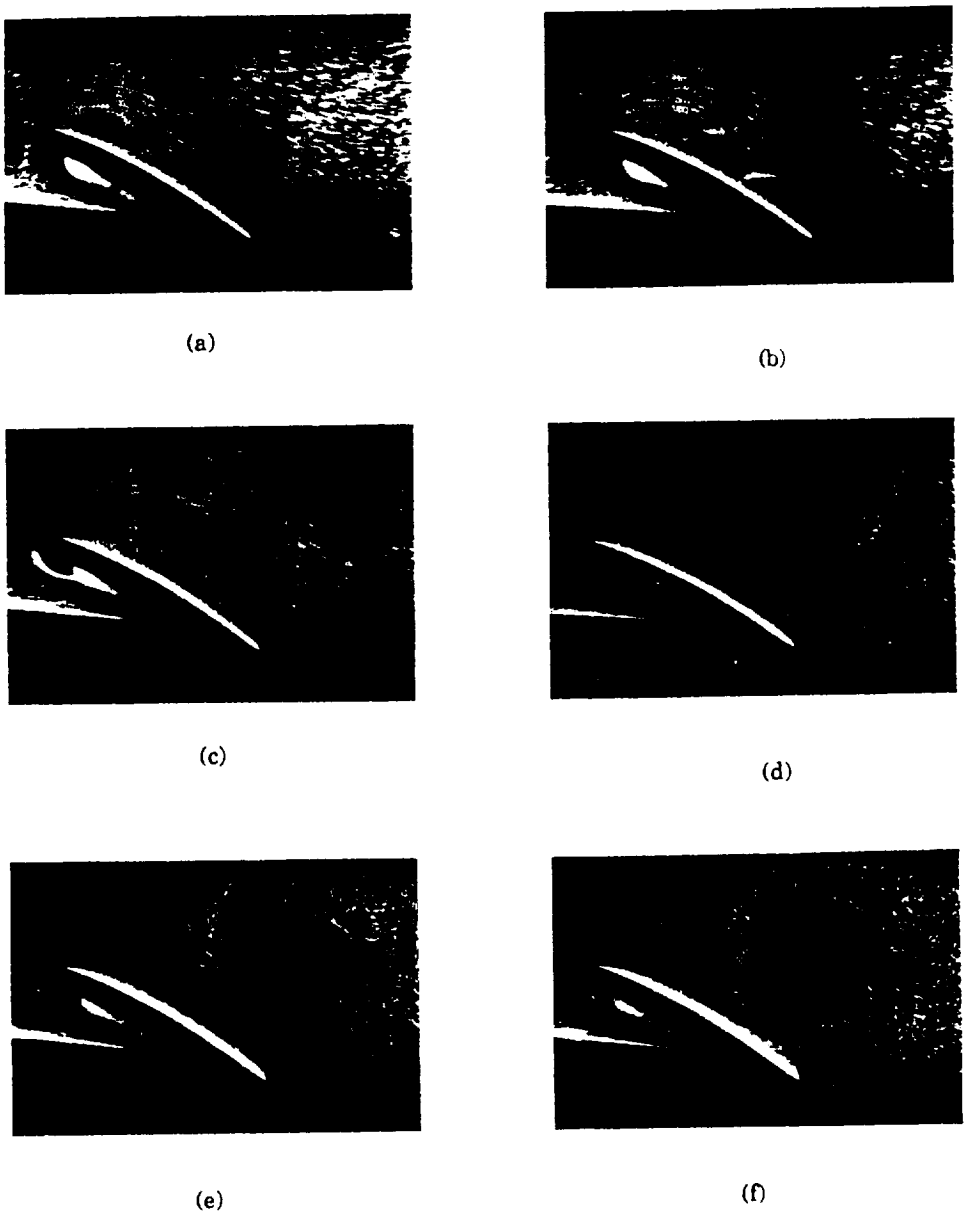

Figure 17. Multiple Exposure Photographs of the Flow Over an Airfoil at Angle of Attack; a) $t^* = 0.68$; b) $t^* = 1.02$; c) $t^* = 2.02$; d) $t^* = 3.02$; e) $t^* = 4.02$; f) $t^* = 4.85$

under the airfoil cannot be seen clearly in these photographs. These photographs display the flow field from the leading edge of the airfoil to a downstream location of about 1-1/2 chords. The quadruple exposures shown here increase the SNR (signal-to-noise ratio) as well as the fringe visibility and provide an excellent flow visualization.

When the airfoil is at angles of attack of ten deg. or less, the flow is well behaved and attached over the entire impulsive process. However, at larger angles of attack ($\alpha \geq 20$ deg.), the flow separates on the upper surface of the airfoil and generates large scale vortices. The photographs shown in Figure 17 reveal that when the airfoil is first started, a vortex at the trailing edge, commonly referred to as the "starting" vortex, is generated and is carried away from the body. Concomitant with this is the generation of a separation bubble at the leading edge of the airfoil. At a later time, the separation bubble grows into an isolated primary vortex with secondary vortices following behind it. A similar type of vortex structure was also observed in the flow behind a circular cylinder. This multiple vortex structure continues to grow together and move along the upper surface until it reaches the trailing edge. At this point the primary vortex induces a vortex at the trailing edge. At a later time the primary vortex abruptly moves away from the surface of the airfoil leaving behind a vortex-sheet-like structure. This vortex sheet rolls up into distinct vortices and they grow in size with time. During this process the trailing edge vortex also grows, creating a very complex flow field. Close to the surface of the airfoil a small vortex remains present for $t^* > 3.0$. This vortex has the same sign as the trailing edge vortex. A similar vortex structure was observed by Ho (1986), who call it an "induced vortex" and associates it with the unsteady separation phenomenon.

Typical measurements of the instantaneous velocity field are shown in Figure 18. The data are presented in a body-fixed reference frame. The starting vortex and the initial separation bubble at the leading edge can be seen clearly at $t^* = 0.68$. At $t^* = 2.02$ the primary vortex with the secondary vortices behind it can be seen. The trailing edge vortex has just formed and is starting to move downstream at $t^* = 3.02$. Also, at $t^* > 3$, the vortex sheet structure described in the previous paragraph can be seen. This structure may be attributed to the interference of tip vortices generated at the tips of the wing.

Two-dimensional computational results from random-walk vortex simulations of the full Navier-Stokes equations are shown in Figure 19. The angle of attack and the Reynolds number are the same as those in the experiment. The streamline pattern, along with vorticity, which is represented in bit-mapped graphics as half

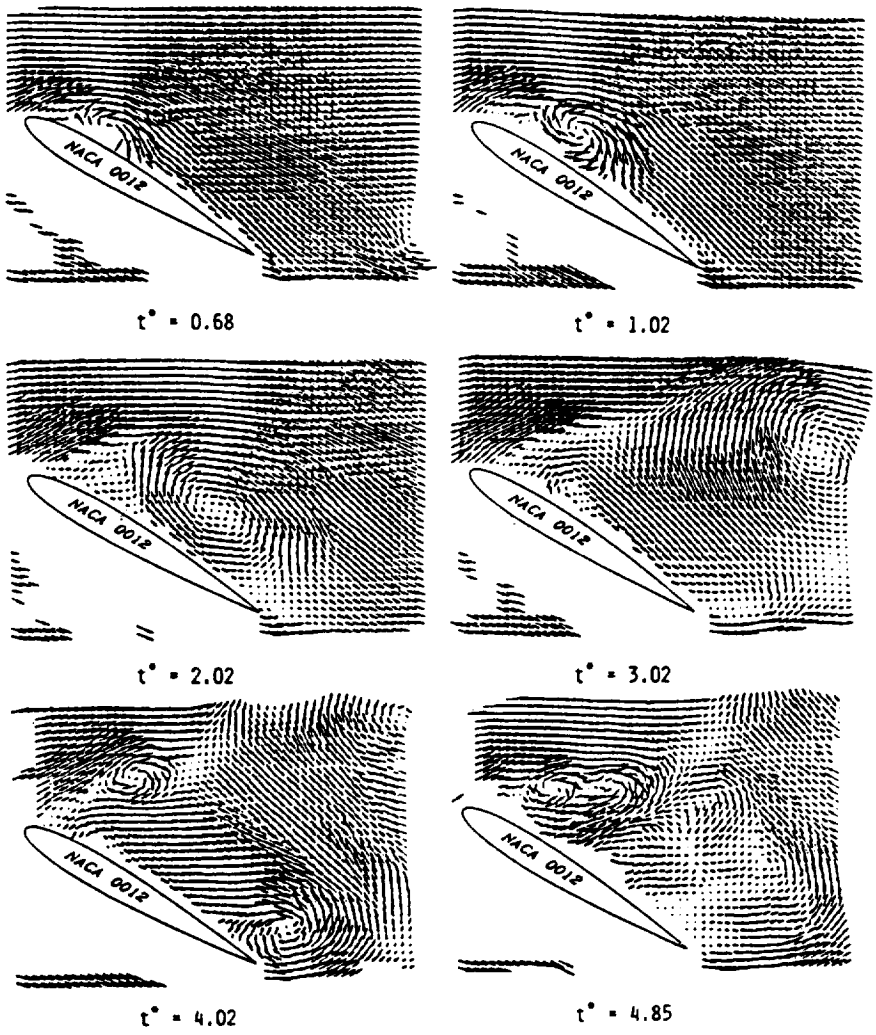

Figure 18. Instantaneous Velocity Field of the Flow Over an Airfoil at Angle of Attack; a) $t^* = 0.68$; b) $t^* = 1.02$; c) $t^* = 2.02$; d) $t^* = 3.02$; e) $t^* = 4.02$; f) $t^* = 4.85$

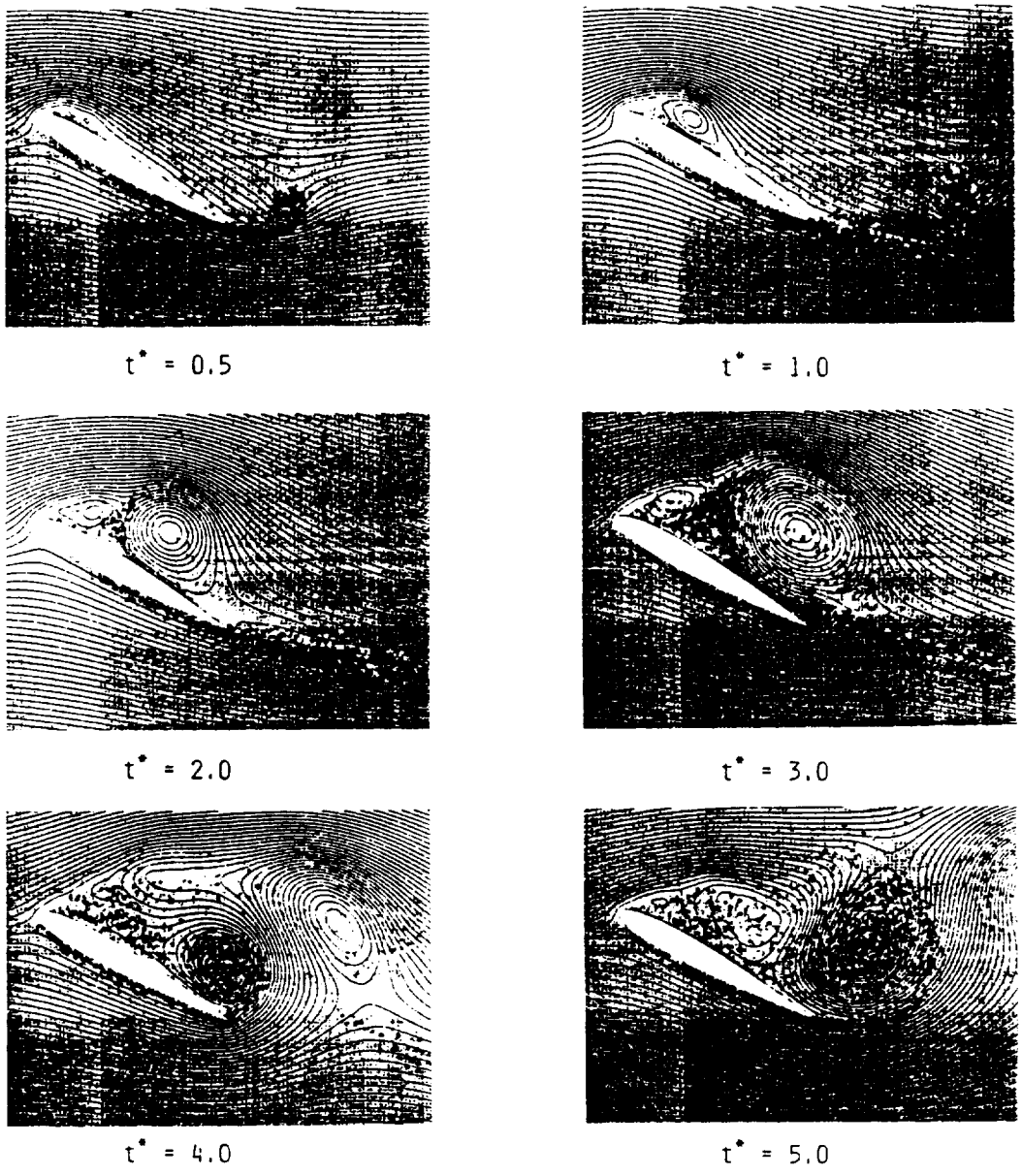

Figure 19. Two-Dimensional Computational Results of the Flow Field Over an Airfoil at Angle of Attack; a) $t^* = 0.5$; b) $t^* = 1.0$; c) $t^* = 2.0$; d) $t^* = 3.0$; e) $t^* = 4.0$; f) $t^* = 5.0$

tones are shown in the figure. Except for the effect of the finite aspect ratio of the airfoil, the streamline patterns look very similar to the patterns observed in Figure 17. To further evaluate these results, the locus of the primary vortex as it develops in time is shown in Figure 20. The computational results agree well with the experiment for $t^* \leq 2$. Beyond this time, it is expected that the experimental flow field was influenced by the tip vortices, making the flow three dimensional. The coefficients of lift and drag as obtained from the computations are shown in Figure 21. As expected, the coefficient of lift increases with t^* up to a point where the primary vortex is attached to the upper surface. For later times, where the primary vortex leaves the upper surface, the coefficient of lift drops significantly.

6.3 Three-Dimensional Turbulent Jet Flow

The flow field considered is a three-dimensional incompressible jet of air issuing from a rectangular nozzle of aspect ratio 4. The structure and development of such a jet is markedly different from those issuing from two-dimensional or axisymmetric nozzles, the focus of most previous investigations on turbulent jets (e.g., Krothapalli, Baganoff, and Karamcheti, 1981). With renewed interest on thrust vectoring and mixing devices, emphasis is now shifting to the study of three-dimensional nozzles. The structure and development of these jets contain many interesting features and are yet to be thoroughly understood. One such feature is the "cross-over" phenomenon, which is generally characterized by the switching of the major and minor axes downstream of the nozzle exit. Recent experiments, conducted by Ho and Gutmark, (1987) on low aspect ratio elliptic jets suggest that an initial instability process, which is accompanied by large vortices, may influence the position of the cross-over point, and thus the development of the jet. The example described here examined the structure and growth of the mixing layer region of the jet. Additional details may be found in Lourenco and Krothapalli, (1988) and Lourenco, Krothapalli, and Smith (1988).

A simple low speed air supply system was used to provide the airflow to a cylindrical settling chamber 27 cm in length and 10 cm in diameter. A honeycomb and a series of screens at the inlet of the nozzle are used to further reduce flow disturbances. The cross section of the contraction changes from a circular cross section, 10 cm in diameter, to a rectangular cross section, 3 cm by 0.75 cm. The contraction contours in the two central planes were fifth-order polynomials. Seeding of the jet was accomplished by using a theatrical-type smoke generator, which produces smoke particles in the sub-micron range. Smoke and ambient air were mixed in a large settling tank and then supplied to

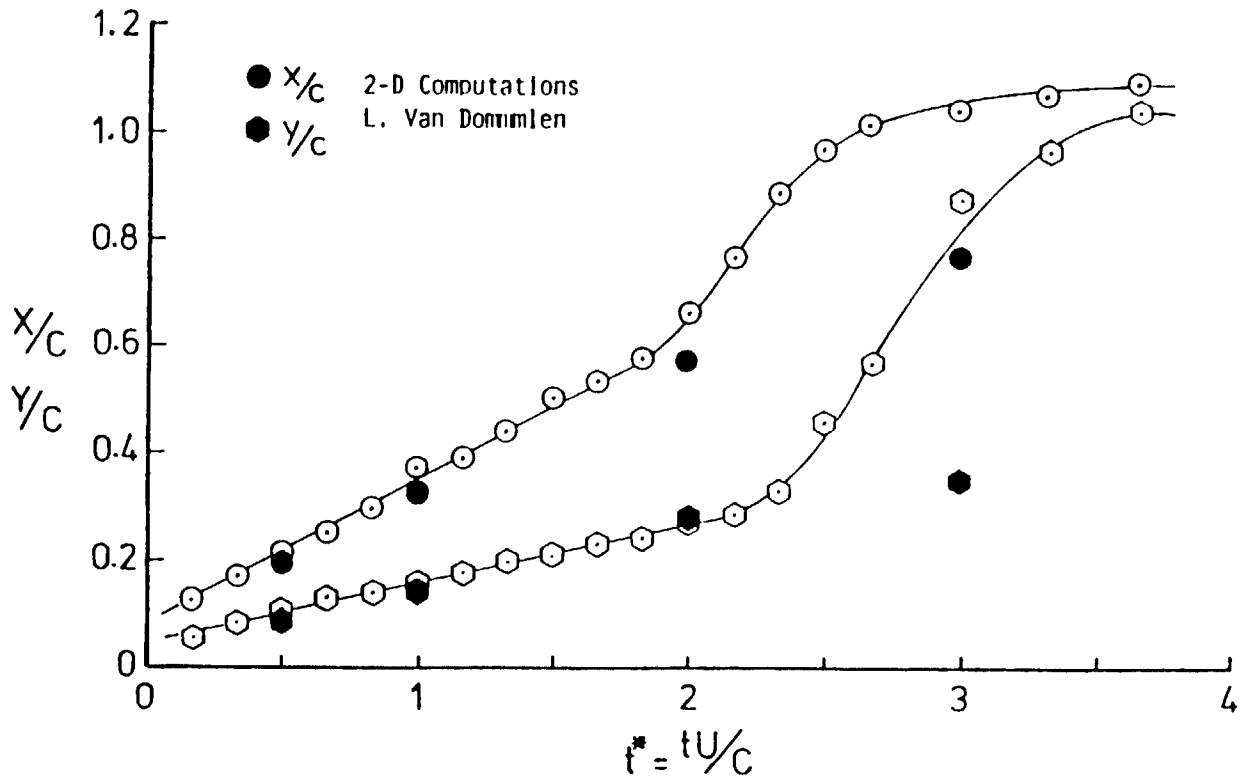

Figure 20. The Variation of the Primary Vortex Location with Time

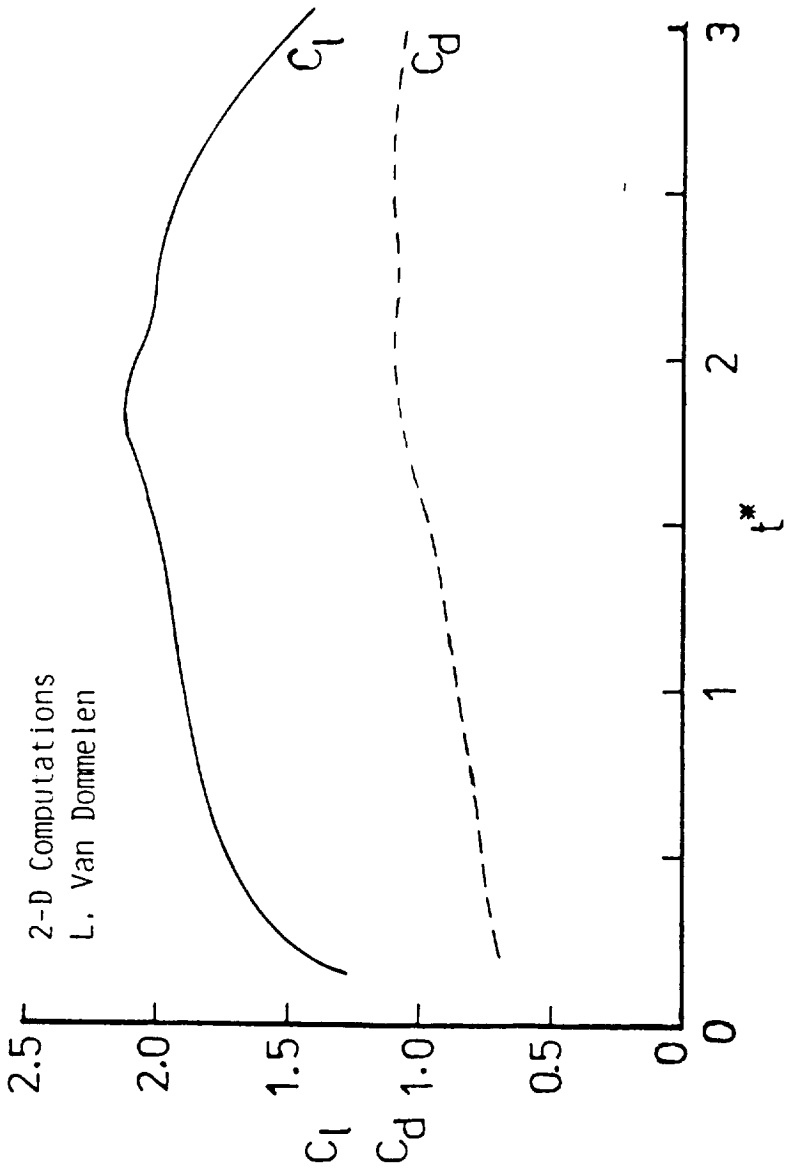

Figure 21. Computed Lift and Drag Variation with Time

the settling chamber of the jet using a small axial fan. A second smoke generator of the same type was used to seed the outside ambient flow surrounding the jet. A schematic of the arrangement is shown in Figure 22. The mean velocity at the exit of the jet was 4.5 m/sec. This resulted in a Reynolds number of 3600, based on the hydraulic diameter (four times the nozzle area divided by the perimeter). Basing the Reynolds number on the jet width (0.75 cm) gives a value of 2250, which may be more appropriate when discussing the stability of the jet. The mean velocity profile at the exit plane of the nozzle was flat with a laminar boundary layer at the walls.

The laser light sheet was created with a frequency doubled, double-pulse Nd:Yag laser, with a similar inverse telescope lens/cylindrical lens arrangement as described in Section 6.1. The laser sheet was 60 mm wide and illuminated the central plane through the small dimension of the nozzle (i.e., the X-Y plane in Figure 22). Two laser pulses with a duration of 10 nsec and a separation of 50 microsec were used to create the specklegram. The pulse separation of 50 microsec is much smaller than any relevant time scale of the flow field and thus the double exposure photograph truly represents a flow field at a given instant of time. The velocity bias technique, described in Section 5, was used to resolve the ambiguity of the velocity vector. A 35 mm camera was used to record the specklegram, using Kodak TMAX 400 ASA film, which has good sensitivity at the frequency of the illuminating laser light. The magnification was 0.50.

Typical double-exposure photographs of the jet, taken at two different times, are shown in Figure 23. These pictures display the flow field from the nozzle exit to about eight jet widths downstream. The photographs were taken using the velocity shift technique described in Section 5 and with external seeding of the ambient medium. From these results, along with other pictures, several observations can be made. The jet consists of three regions: the region in which the initial shear layer is unstable and rolls up into discrete vortices; an interaction region in which the vortices pair with each other; and a region in which the vortices break up into random, three-dimensional motion. In spite of the relatively large aspect ratio of the nozzle exit (AR = 4), the rectangular jet organizes itself into a structure similar to that of an axisymmetric jet, as shown by Bouchard and Reynolds, (1982). The pairing process is also quite similar. In this process, the trailing vortex catches up with the leading vortex, decreases in size and passes through the leading vortex, which has slowed down and grown in size. The vortex cores rotate around each other and ultimately merge, producing a single vortex. A number of vortex pairings can occur before vortex breakdown occurs. Figure 23b shows such a vortex pairing in progress. The physical

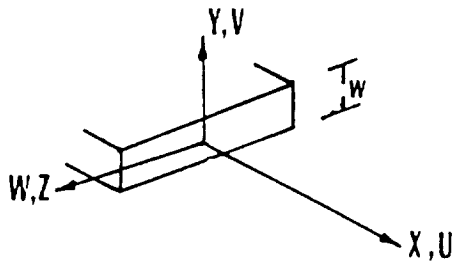

Figure 22. Schematic of Three-Dimensional Jet Experiment

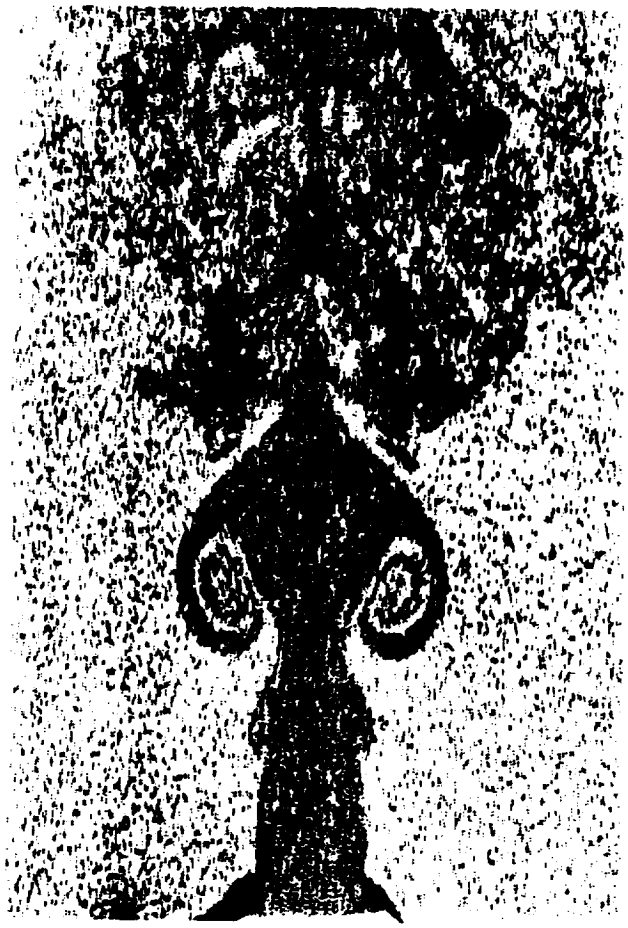

(a)

Figure 23. Instantaneous Double-Exposed Photographs of the Central Plane of the Jet

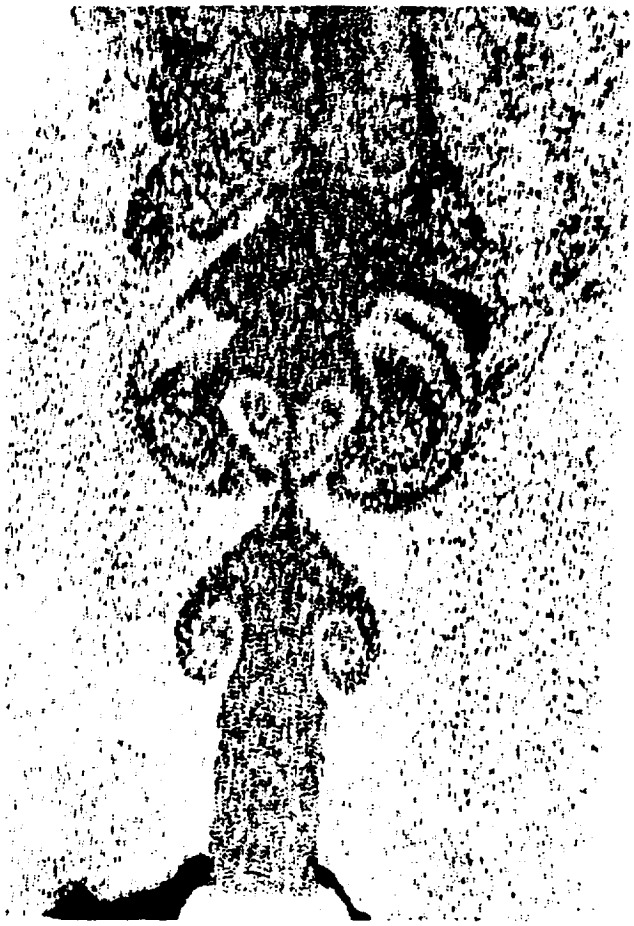

(b)

Figure 23. Instantaneous Double-Exposed Photographs of the Central Plane of the Jet (Concluded)

regions where these phenomena takes place overlap and depends on the phase of the development of the jet. The jet Strouhal number, St (non-dimensional passage frequency of the vortices prior to pairing), is given by St = fw/U, where f is the passage frequency, w the nozzle width, and U is the mean exit velocity of the jet. For this experiment, St is estimated to be about 0.7. This Strouhal number is close to that measured for an axisymmetric jet by Becker and Massaro, (1968), at a comparable Reynolds number. Examination of several photographs suggests that the vortex breakdown enhances the mixing in the plane of the small dimension of the nozzle. No increase in mixing was observed in the central plane containing the long dimension of the nozzle.

The instantaneous velocity field, for two typical phases of the development of the jet, are shown in Figure 24. In this figure the velocity is given in the laboratory reference frame; that is, the velocity bias has been removed. The length of each vector is directly proportional to the magnitude of the velocity. Because the velocity gradients are largest in the transverse direction, the velocity data were acquired using a rectangular mesh with a mesh spacing of 2 mm in the jet axial direction and 0.5 mm in the jet transverse direction. The velocity fields displayed in Figure 24 describe in great detail all of the aforementioned regions of the jet flow field, from the initial shear layers to regions with highly three-dimensional motion. Such an accurate and detailed representation of the flow field was a consequence of the use of the velocity bias technique together with judicious management of the seeding.

Examination of these velocity fields further reinforces the previous analysis made on the basis of the flow visualization pictures. The jet structure is further enhanced by presenting the velocity field in a reference frame with a convection velocity of the vortical structure, estimated at about 70 percent of the jet exit velocity, as shown in Figure 25. In this reference frame, the large scale vortical structures are clearly observed which shows the nature of the symmetric instability. The instantaneous velocity profiles provide a unique means to quantify the extent of the jet unsteadiness, the existence of the coherent motions, their interactions, and subsequent generation of the random three-dimensional motions. As an example, Figure 26 shows the instantaneous distribution of the axial centerline velocity along the jet axis obtained from the data of Figure 24. As expected, the centerline velocity distribution is phase dependent and does not display a monotonic behavior as commonly observed in mean velocity distributions. The peaks and valleys in this phase-dependent distribution are a consequence of the vortex dynamics. Thus, a complete understanding of the structure and development of the jet must include a detailed study of the time evolution of the whole flow field.

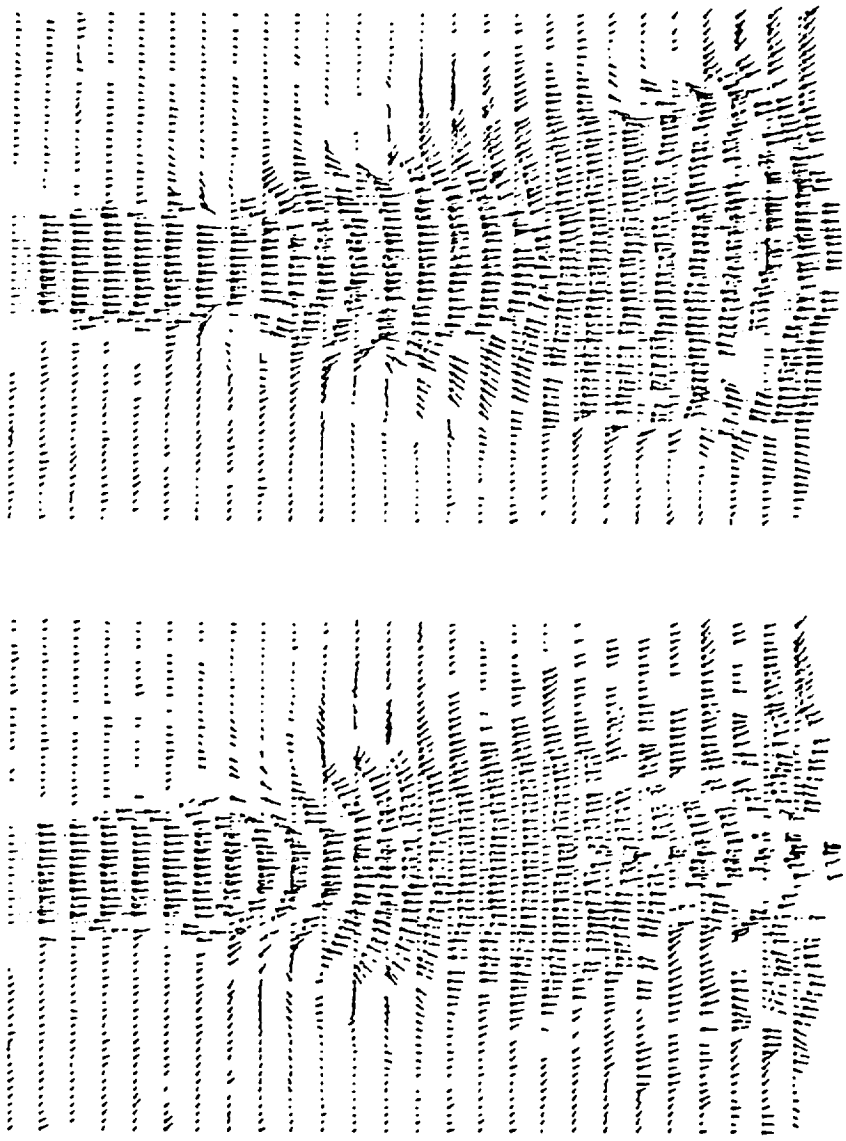

Figure 24. Instantaneous Two-Dimensional Velocity Field in the Central Plane of the Jet

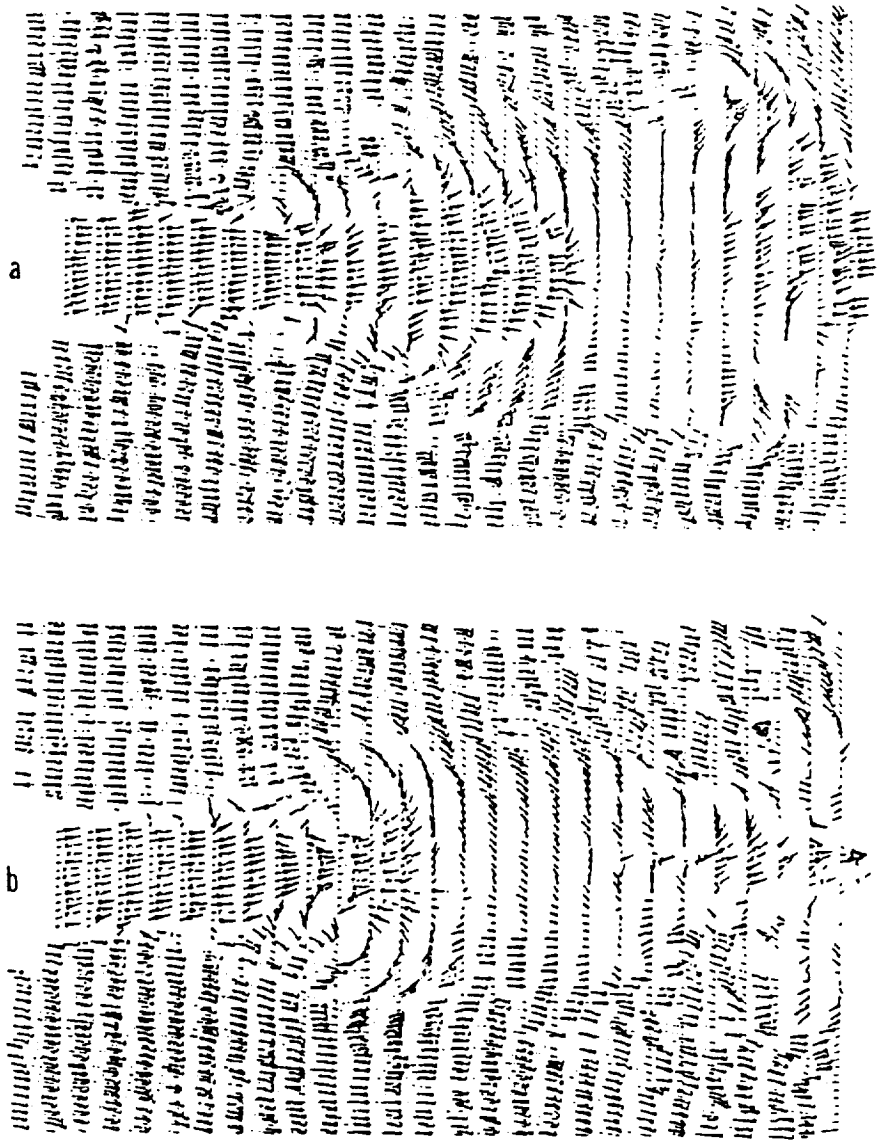

Figure 25. Instantaneous Two-Dimensional Velocity Field Shown in the Reference Frame with a Convection Velocity of the Vortical Structures.

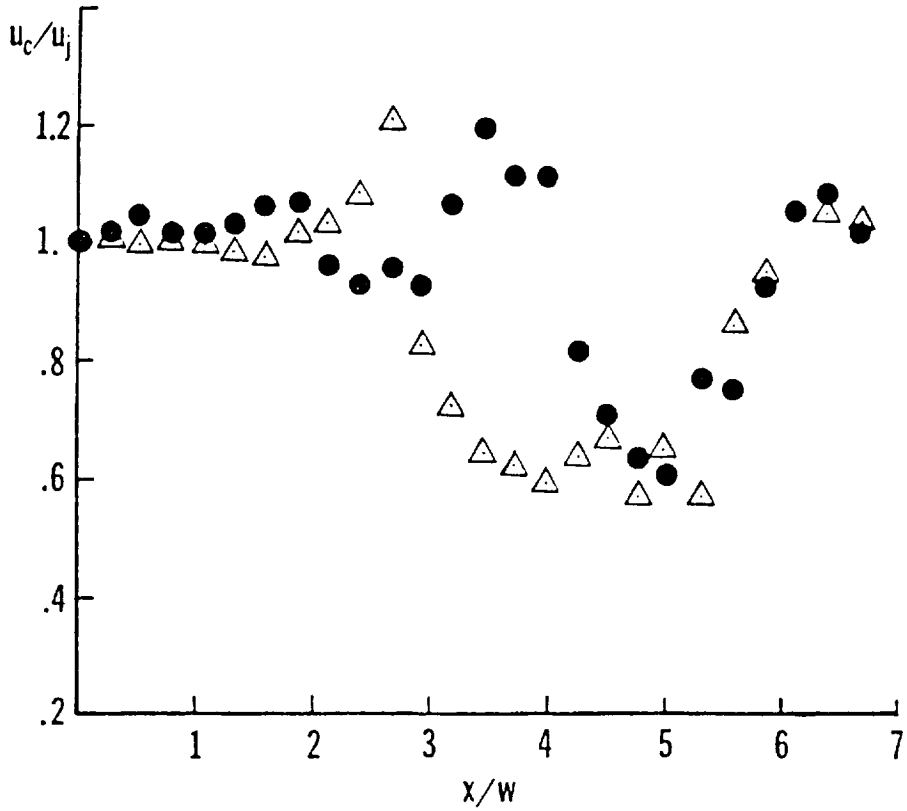

Figure 26. Variation of the Instantaneous Centerline Axial Velocity with Downstream Distance for the Two Cases Shown in Figure 25; •) Figure 25a, Δ) Figure 25b.

7. Recent Developments

7.1 High-Speed Measurements

A recent study by Kompenhans and Hocker, (1988) has demonstrated conclusively that PIV can be successfully applied to the study of high-speed flows. In their experiment, a pair of Nd:Yag lasers were combined by means of polarizing prisms. The schematic of this system is shown in Figure 27. Utilizing a digital clock to control the exact time delay between the two pulses, they studied the flow of a circular jet at exit Mach numbers ranging from 0.1 to almost 1. The seeding particles, created by injecting pressurized air into olive oil, were of the order of 1 μm in diameter. The flow facility consisted of a 15 mm diameter circular air jet, at ambient temperature. The Reynolds number, based on jet diameter, ranged from $4x10^4$ to $3x10^5$. Both the jet flow and the ambient air outside the jet were seeded in order that the particle concentration in the shear layer region, where ambient air is entrained into the jet, was sufficiently high to yield good results. The multiple-exposure photographs were analyzed using the Young's fringes technique.

7.2 Three-Dimensional Measurements

Until recently, applications of PIV have been limited to two-dimensional flows. The physical limitation of the system is that the particle must be in the illuminated sheet during both exposures. Any out-of-plane motion of particles into or out of this sheet reduces the particle correlation and can result in a loss of the signal. However, many flows of interest are three-dimensional and ways of extending PIV to the study of such flows are of obvious interest. One such method, pioneered by Riethmuller and his colleagues at the von Karman Institute (VKI), is described in this section, which summarizes the work presented by Gauthier and Riethmuller (1988).

The VKI method is a stereoscopic scheme in which the flow in the illuminated plane is viewed from two different directions simultaneously. Thus, with this technique measurements over a single plane are still made, but all three components of velocity are obtained. The constraint is that the time delay between exposures must be chosen such that the maximum particle motion normal to the illuminated plane is much less than the thickness of the sheet. With this scheme it is often necessary to add a velocity bias to the particle images to keep them in the range of the analysis system.

In the stereoscopic method the flow is the flow is viewed from two different

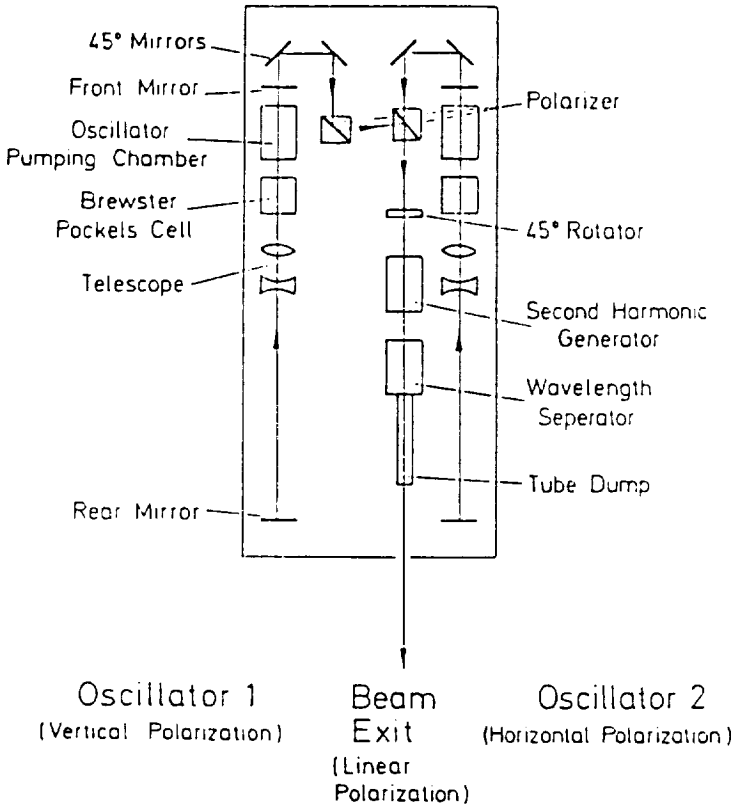

Figure 27. General Layout of the Double Pulse Laser System used by Kompenhans and Hocker, (1988)

directions and the three velocity components are obtained from their projections and the geometrical characteristics of the optical system. Two different stereoscopic systems have been tried thus far by the VKI group. The first is called an angular displacement method and is one in which the optical axes are not perpendicular to the illuminated sheet but are inclined at an angle β to the normal to the sheet, as shown in Figure 28. To estimate the error in measuring the displacement, Gauthier and Riethmuller considered a displacement of 250 μm at an angle of θ to the illuminated plane, a magnification of 0.4 and a resolution of 2.5 μm. Results are shown in Figure 29. The error is minimized when the optical axes are at an angle of 45 deg. to the illuminated plane, and for small values of θ (which can be obtained by superposing a velocity bias to the flow if necessary).

The second stereoscopic scheme is referred to as the translation method and is shown schematically in Figure 30. In this technique the optical axis of each camera is perpendicular to the illuminated sheet and the distance between the two axes provides the stereoscopic effects. The error associated with this method is shown in Figure 31 for the same conditions as in Figure 29. Although the error decreases with increasing distance between the two optical axes, so does the overlap or common area recorded by the two cameras.

Gauthier and Riethmuller applied each of these methods to a simulated 3-D flow by measuring the uniform flow in a rectangular duct (25x40 mm) with a laser sheet at an angle of 20 deg. to the duct axis, as shown in Figure 32. The velocity was 5 m/s (no velocity bias was used), the magnification was 0.5, and the time between exposures was 50 μs. The scatter in the out-of-plane displacement for the two methods is shown in Figure 33. There is a large scatter of 32 deg. in the measurements using the translation method, and a scatter of 8 deg. with the angular displacement method. These results confirm the predicted errors in Figures 29 and 31, which indicated better accuracy for the angular displacement method. These basic experiments demonstrate the applicability of PIV for the instantaneous measurements of the three components of velocity in a plane of a fluid flow.

7.3 Suggestions for Future Work

Although some success in demonstrating the applicability of this technique on high-speed flows and three-dimensional flows has been demonstrated, much work remains to be done. For example, application of PIV to the study of

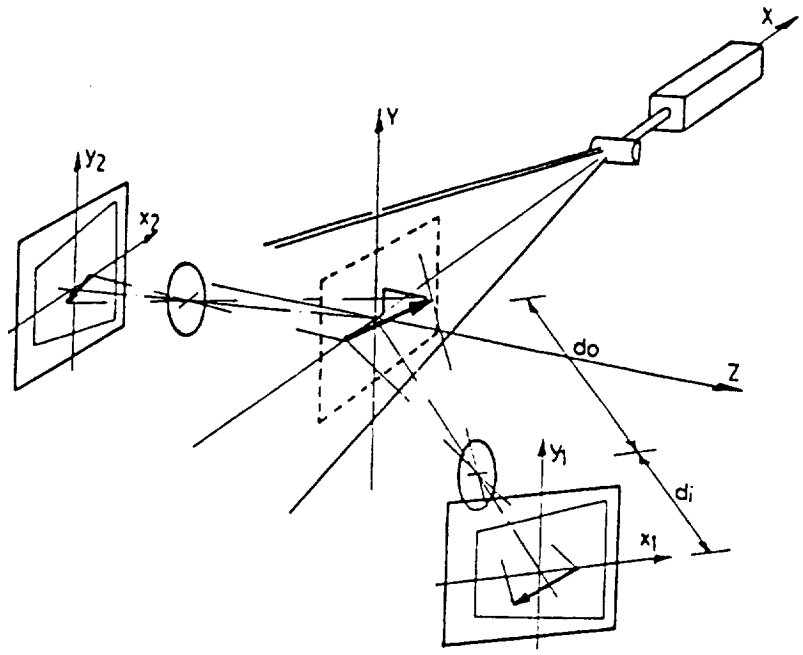

Figure 28. Stereoscopic Angular Displacement Method, from Gauthier and Riethmuller, (1988)

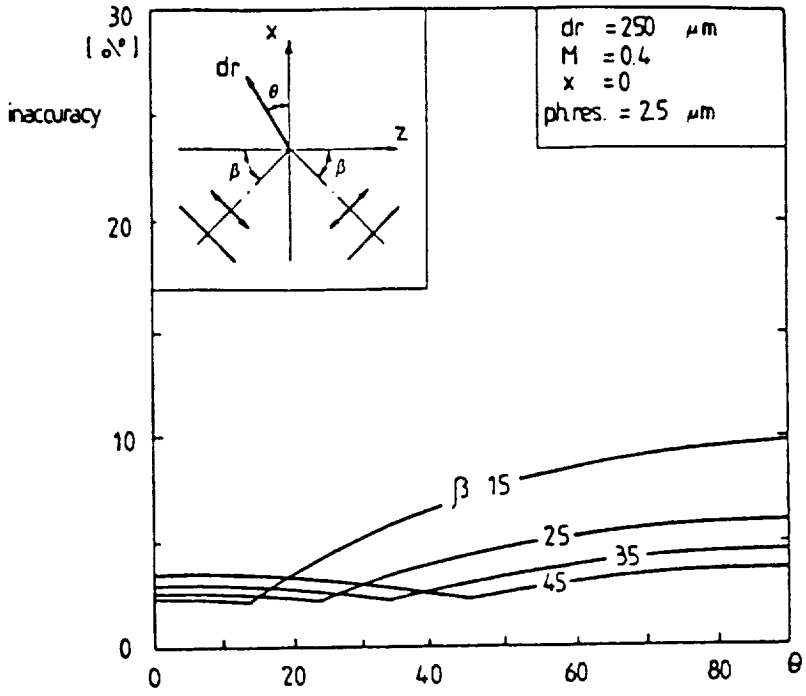

Figure 29. Inaccuracy of the Angular Displacement Method, from Gauthier and Riethmuller, (1988)

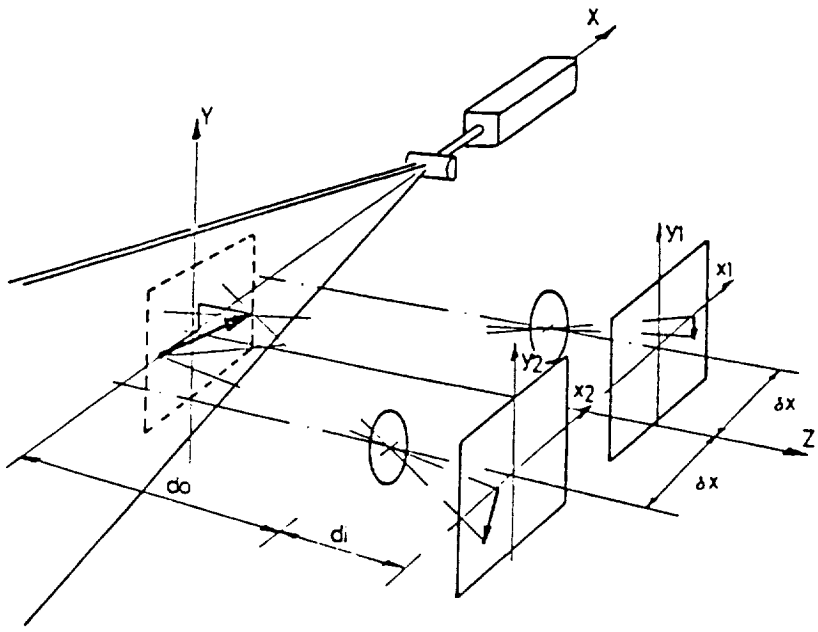

Figure 30. Stereoscopic Translation Method, from Gauthier and Riethmuller, (1988)

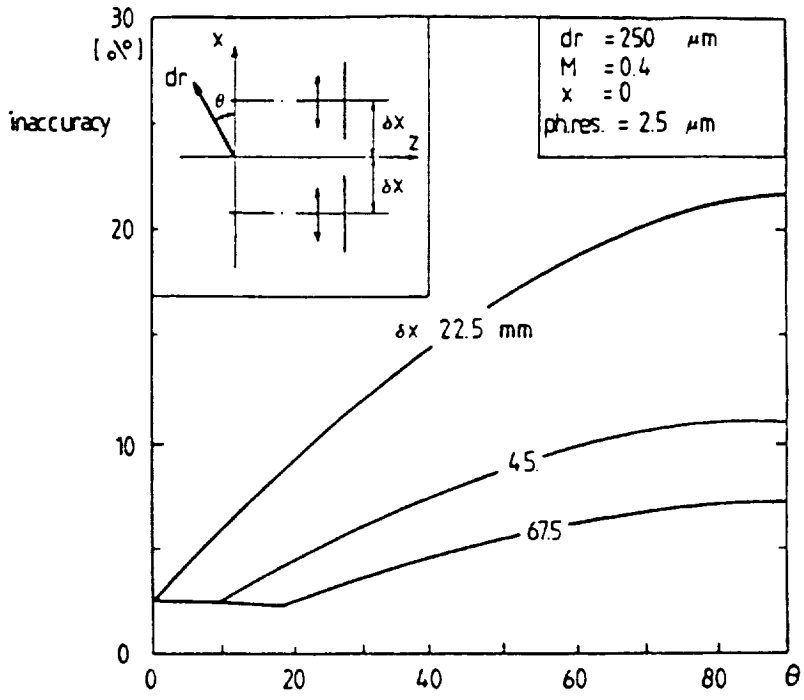

Figure 31. Inaccuracy of the Translation Method, from Gauthier and Riethmuller, (1988)

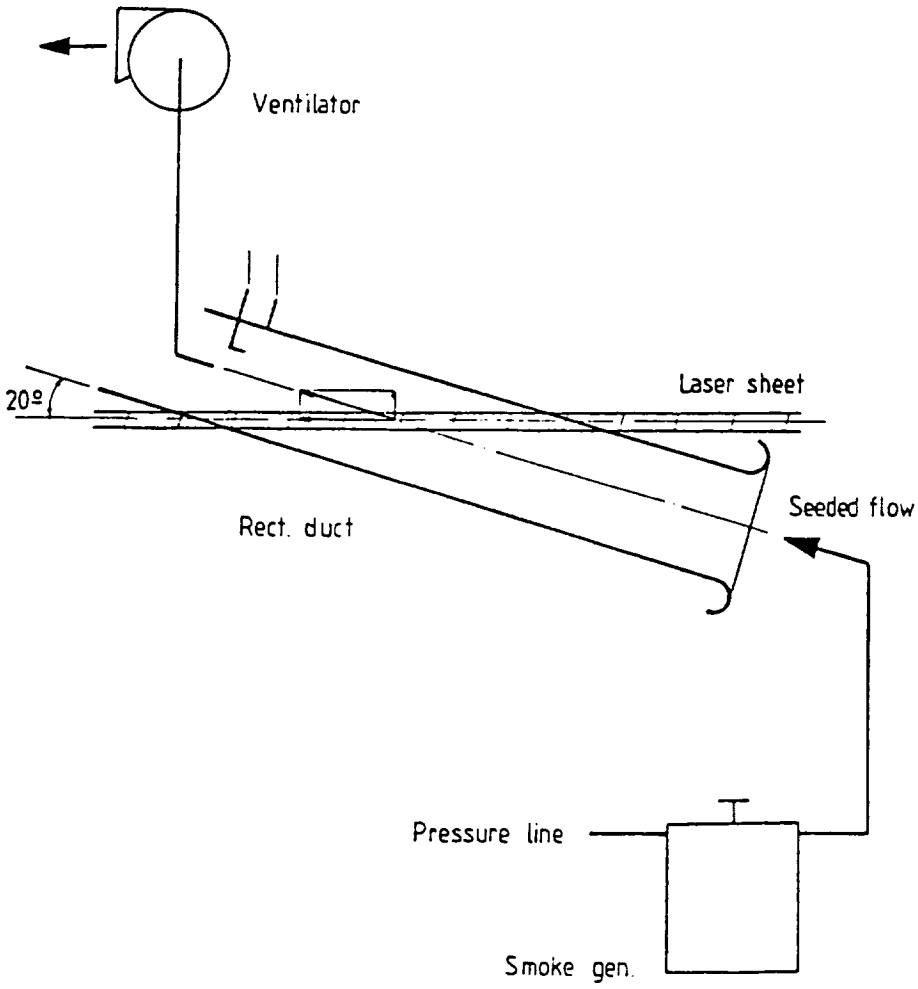

Figure 32. Experimental Setup for Uniform Out-of-Plane Motion, from Gauthier and Riethmuller, (1988)

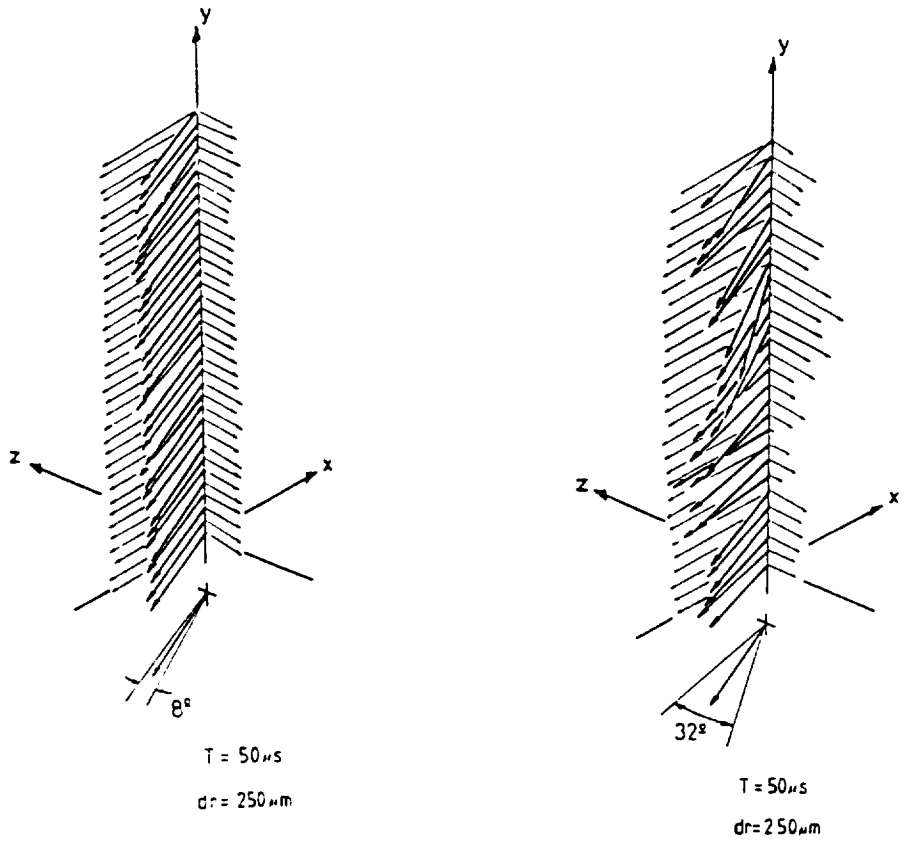

Figure 33. Scatter in Out-of-Plane Displacement Measurements, from Gauthier and Riethmuller, (1988); a) Angular Displacement Method, b) Translation Method

three-dimensional flows with large velocity gradients, such as the tip vortex wake behind an aircraft wing, will require much study. Also, the relationship between the laser sheet thickness, the flow quantities (such as velocity, spatial resolution, time and length scales), and the processing techniques needs additional study. Finally, the use of PIV as a means to validate CFD (computational fluid dynamics) codes is a fruitful area for further work.

8. Conclusions

The concept of Particle Image Velocimetry has been described and shown to be applicable to the study of flows with vortical motions. At present, most of the work in this field has been towards developing the technique itself, and very little has been done in applying this technique to fluid flows of research interest. Most of the work to date has been limited to low speed, primarily two-dimensional flows, although some research has been done to extend the technique to higher speeds and all three dimensions. The use of dual systems (i.e., two lasers to study high speed flows and two recording systems to study three-dimensional flows) looks especially promising. These activities should be continued. One area that has received very little attention to date is an effort to increase the size of the viewing area. Most research has been done on small, laboratory-type experiments and a field in which PIV would prove especially useful is the study of wind tunnel flows. A means to measure three-dimensional, unsteady, vortical flow fields in wind tunnels at high speed and high Reynolds number and on a regular basis would increase the productivity of these facilities by several orders of magnitude.

9. References

Adrian, R.J.;"An Image Shifting Technique to Resolve Directional Ambiguity in Double-Pulsed Laser Velocimetry", Appl. Opt., vol 25, pp 3855-3858, 1986.

Becker,H.A. and Massaro,T.A.;"Vortex Evolution in a Round Jet", J. Fluid Mech., vol 31, pp 435-448, 1968.

Born,M. and Wolf,E.;Principles of Optics, Pergamon Press, 1980.

Bouard,R. and Coutanceau,M.;"The Early State of Development of the Wake Behind an Impulsively Started Cylinder for $40<Re<10^4$", J. Fluid Mech., vol. 101, pp 583-607, 1980.

Bouchard,E.E. and Reynolds,W.C.;"The Structure and Growth of the Mixing Layer Region of a Round Jet", Rept. TF-17, Thermosciences Division, Dept. of Mech. Engrg., Stanford Univ., 1982.

Collicott, S.H. and Hesselink, L.;"Anamorphic Optical Processing of Laser Speckle Anemometer Data", Bull. Amer. Phys. Soc., vol 30, pg 1728, 1985.

Collier, R.J., Burckhardt, C.B., and Lin, L.H.;Optical Holography, Academic Press, New York, 1971.

Dimotakis, P.E., Debussy, F.D., and Koochesfahani, M.M.;"Particle Streak Velocity Field Measurements in a Two-Dimensional Mixing Layer", Phys. Fluids, vol 24, pp 995-999, 1981.

Elkins, R.E.,III, Jackman, G.R., Johnson, R.R., Lindgren, E.R., and Yoo, J.K.;"Evaluation of Stereoscopic Trace Particle Records of Turbulent Flow Fields", Rev. Sci. Instrum., vol 48, pp 738-746, 1977.

Erf, R.K.;"Application of Laser Speckle to Measurement", in Laser Applications, vol 4, ed. by Goodman, J.W. and Ross, M., Adademic Press, New York, 1980.

Frish, M.B. and Webb, W.W.;"Direct Measurement of Vorticity by Optical Probe", J. Fluid Mech., vol 197, pp 173-200, 1981.

Gauthier,V. and Riethmuller,M.L.;"Application of PIDV to Complex Flow:Measurement of the Third Component", VKI Lecture Series on Particle Image Displacement Velocimetry, Brussels, Mar. 1988.

Gharib, M., Dyne, B., Thomas, O., and Yap, C.;"Flow Velocity Measurements by Image Processing of Optically Modulated Traces", AGARD CP-413, 1987.

Ho,C.M.;"An Alternative Look at the Unsteady Separation Phenomenon", Recent Advances in Aerodynamics, ed. by A.Krothapalli and C.A.Smith, Springer-Verlag, pp 165-178, 1986.

Ho,C.M. and Gutmark,E.;"Vortex Induction and Mass Entrainment in a Small Aspect-Ratio Elliptic Jet", J. Fluid Mech., vol 170, pg. 383, 1987.

Honji,H. and Taneda,S.;"Unsteady Flow Past a Circular Cylinder", J. Phy. Soc. of Japan, vol 27, pp 1668-1677, 1969.

Kompenhans, J. and Hocker, R.;"Application of Particle Image Velocimetry to High Speed Flows", VKI Lecture Series on Particle Image Displacement Velocimetry, Brussels, Mar. 1988.

Krothapalli,A. Baganoff,D. and Karamcheti,K.;"On the Mixing of a Rectangular Jet", J. Fluid Mech., vol. 107, pg 201, 1981.

Landreth, C.C., Adrian, R.J., and Yao, C.-S.;"Double Pulsed Particle Image Velocimeter with Directional Resolution for Complex Flows", Experiments in Fluids, vol 6, pp 119-128, 1988.

Loc,T.P.;"Numerical Analysis of Unsteady Secondary Vortices Generated by an Impulsively Started Circular Cylinder", J. Fluid Mech., vol. 100, pp 111-128, 1980.

Lourenco, L.;"The Fundamentals and Application of Particle Image Displacement Velocimetry", von Karman Institute Lecture Series, Belgium, 1986.

Lourenco, L.;"Application of Laser Speckle and Particle Image Velocimetry in Flows with Velocity Reversal", Bull. Amer. Phy. Soc., vol 31, no 10, 1986.

Lourenco, L.M., Krothapalli, A., Buchlin, J.M., and Riethmuller, M.L.;"A Non-Invasive Experimental Technique for the Measurement of Unsteady Velocity and Vorticity Fields", Aerodynamic and Related Hydrodynamic Studies Using Water Facilities, AGARD CP-413, paper 23, Monterey, CA, 1986.

Lourenco, L.M. and Krothapalli,A.;"The Role of Photographic Parameters in Laser Speckle or Particle Image Displacement Velocimetry", Experiments in Fluids, vol 5, pg 29-32, 1987.

Lourenco, L.M. and Krothapalli,A;"Instantaneous Velocity Field Measurements of a Turbulent Rectangular Jet (AR = 4) Using Particle Image Displacement Velocimetry", AIAA paper 88-0498, 26th Aerospace Sciences Meeting, Reno, Jan. 1988.

Lourenco, L.M. and Krothapalli,A.;"Application of PIDV to the Study of the Temporal Evolution of the Flow Past a Circular Cylinder", Laser Anemometry in Fluid Mechanics-III, Ladoan-Institute Superior Tecnico, Lisbon, Portugal, pg 161, 1988.

Lourenco,L., Krothapalli,A., and Smith, C.A.;"On the Instability of a Rectangular Jet", Intl. Symp. on Laser Velocimetry, Lisbon, Portugal, July 1988.

Lourenco, L. and Whiffen, M.C.;"Laser Speckle Methods in Fluid Dynamics Applications", Proc. Intl. Symp. on Appl. of Laser Anemometry of Fluid Mechanics, Lisbon, 1984.

Meynart, R.;"Equal Velocity Fringes in a Rayleigh-Benard Flow by the Speckle Method", Appl. Opt., vol 19, pg 1385, 1980.

Prandtl, L., J. Roy. Aero. Soc., vol. 31, pg. 730, 1927.

Simpkins, P.G. and Dudderar, T.D.;"Laser Speckle Measurement of Transient Benard Convection", J. Fluid Mech., vol 89, pp 665-671, 1978.

Smith, C.A., Lourenco, L.M.M., and Krothapalli, A.;"The Development of Laser Speckle Velocimetry for the Measurement of Vortical Flow Fields", AIAA paper 86-0768-CP, 14th Aerodynamic Testing Conf., West Palm Beach, Mar. 1986.

Stetson, K.A.;"A Review of Speckle Photography and Interferometry", Opt. Engr., vol 14, pp 482-489, 1975.

Tietjens,O.;Stromungslehre, 1st Edition, vol. 2, Springer-Verlag, Berlin, pp 105-109, 1970.

Van Dommelen,L.L.;"Unsteady Boundary Layer Separation", Ph.D. Thesis, Cornell University, 1981.

Yao, C.-S. and Adrian, R.J.;"Orthogonal Compression and 1-D Analysis Technique for Measurement of 2-D Particle Displacements in Pulsed Laser Velocimetry", Appl. Opt., vol 23, pp 1687-1689, 1984.

APPENDIX II

By L. M. LOURENÇO AND A. KROTHAPALLI
THE FLORIDA STATE UNIVERSITY
FAMU/FSU College of Engineering
Dept. of Mechanical Engineering
Tallahassee, Florida 32306

APPLICATION OF PIDV TO THE STUDY OF THE TEMPORAL EVOLUTION OF THE FLOW PAST A CIRCULAR CYLINDER

From the book «Laser Anemometry in Fluid Mechanics»
Published by Ladoan — Instituto Superior Técnico
1096 Lisbon Codex - Portugal
1988

Application of PIDV to the study of the temporal evolution of the flow past a circular cylinder

By L. M. LOURENÇO AND A. KROTHAPALLI

THE FLORIDA STATE UNIVERSITY
FAMU/FSU College of Engineering
Dept. of Mechanical Engineering
Tallahassee, Florida 32306

A novel experimental technique is being developed for the field measurement of instantaneous velocity in unsteady or steady fluid flows. The main advantage of this technique is that the velocity field data is measured with sufficient accuracy so that the distribution of vorticity can be calculated with reasonable accuracy.

This technique which is ideally suited for the study of unsteady vortical flows, has been utilized to measure the time development of the near-wake flow field created behind a circular cylinder impulsively started from rest.

A detailed explanation of the basic principles of the technique as well as a discussion of some of the important parameters that affect its use are included in this paper.

1. Introduction

One of the most challenging problems in experimental fluid mechanics remains the measurement of unsteady vorticity field and associated physical variables such as velocity and pressure. Local measurements of the velocity field are now done routinely in many experiments. However, a great deal of flow fields of current interest, such as coherent structures in shear flows are highly unsteady. Hot-wire or laser doppler velocimeter data of such flows are difficult to interpret as both spatial and temporal information of the entire flow field are required, and these methods are commonly limited to simultaneous measurements at only a few spatial locations. Recently, a novel velocity measurement technique, commonly known as Laser Speckle or Particle Image Displacement Velocimetry has become available (Adrian & Yao (1985), Lourenço & Whiffen (1984), Meynart (1980), Simpkins & Dudderar (1978). This technique provides the simultaneous visualization of the two-dimensional streamline pattern in unsteady flows as well as the quantification of the velocity field over an entire plane. The advantage of this technique is that the velocity field can be measured over an entire plane of the flow field simultaneously, with accuracy and spatial resolution. From this, the instantaneous vorticity field can be easily obtained. This constitutes a great asset for the study of a variety of flows that evolve stochastically in both space and time. In this paper some of the results obtained

in a measurement of the time-space development of the near-wake of an impulsively started circular cylinder are presented. In addition, the basic principles of operation of LSV or PIDV are introduced and a discussion is made on some of the parameters that affect its utilization.

2. Principle of the technique

The application of LSV or PIDV to fluid flow measurement involves several steps. First, it is necessary to «create» a selected plane or surface within the flow field. This is accomplished by seeding the flow with small tracer particles, similarly to LDV applications, and illuminating it with a sheet of coherent light, as shown in figure 1. A pulsed laser such as a Ruby or a NdYag laser, or a CW

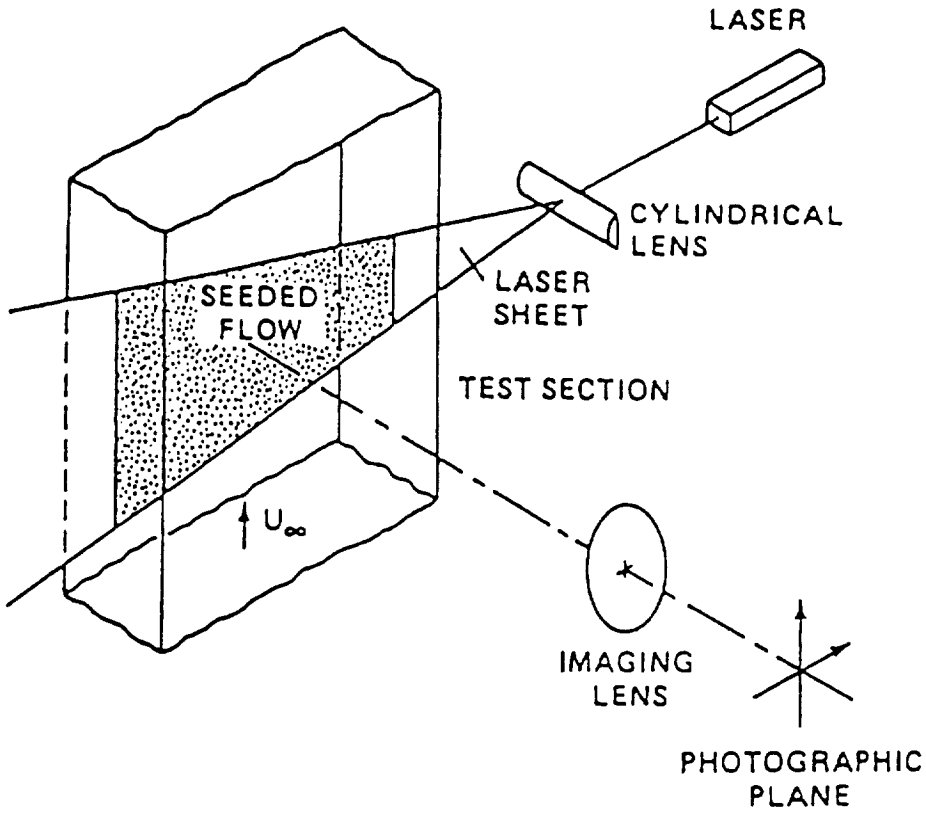

FIGURE 1. Schematic of the set up for photography.

laser with a shutter is normally used as the light source. The laser sheet is formed, for example, by focusing the laser beam first with a long focal length spherical lens, to obtain minimum thickness, and then diverging the beam in one dimension with a cylindrical lens. The light scattered by the seeding particles in the illuminated plane provides a moving pattern. When the seeding concentration is low, the pattern consists of resolved diffraction limited images of the particles. When their concentration increases, the images overlap and interfere to produce a random speckle pattern. A multiple exposure photograph records this moving pattern. The lower particle concentration is a mode of operation of

the technique referred to as Particle Image Displacement Velocimetry, reserving the term Laser Speckle Velocimetry for the high particle concentration levels where a random speckle pattern is actually formed. In a second step the local fluid velocity is derived from the ratio of the measured spacing between the images of the same tracer, or speckle grain, and the time between exposures.

Several methods exist to convert the information contained in the multiple-exposed photograph, or specklegram, to flow field data such as velocity or vorticity. The recorded image, whether formed by isolated disks, in the case of low particle concentration, or speckle grains for high particle concentration is a complicated random pattern. It would be very difficult to measure the local displacements by visual or computer-aided inspection. However, it is important to realize that the multiple exposure photograph results in a periodic random image from which the periodicity information can be retrieved using Fourier or Autocorrelation analysis. Basically, the multiple-exposed photographs or specklegrams can be analyzed either on a point-by-point basis, which yields measurements of the local displacements (velocity), (Adrian & Yao (1985), Lourenço & Whiffen (1984)) or with a whole field filtering technique, which yields isovelocity contours Meynart (1980). Recently an anamorphic optical system has been proposed Collicott & Hesselink (1985). This method performs a 1-D Fourier transform in the x-direction for measuring the x-velocity component, and images the speckle pattern in the y-direction. This results in curved fringes which have a local spacing inversely proportional to the x-velocity at that point. Simultaneous multiple point measurements are obtained by imaging in the y-direction. Thus it is possible to measure a velocity component along a selected line in the flow. The most current methods of analysis are point-bypoint techniques. The first one which is being developed and used by Yao & Adrian (1984), consists of measuring directly the image pair spacings in the photographs, using an autocorrelation technique. However, unlike the usual full 2-D autocorrelation or Fourier techniques which require a computation of large data arrays and are generally inefficient, this method reduces the general $N \times N$ element 2-D problem to two N element 1-D problem by compressing the information, in the photograph, in orthogonal directions using integration. The other method, which has been selected and implemented by the Fluid Mechanics Research Laboratory at the Florida State University, is the Young's fringes method Lourenço & Whiffen (1984). The local displacement is determined using an focused laser beam to interrogate a small area of the multiple exposed photograph transparency. The diffraction produced by coherent illumination of the multiple images in the negative generates Young's fringes, in the Fourier plane of a lens, provided that the particle images correlate. This is shown schematically in figure 2. These fringes have an orientation which is perpendicular to the direction of the local displacement and a spacing inversely proportional to the displacement. The use of Young's fringes eliminates the difficulties of finding the indviidual image pairs in the photograph. The basis of the Young's fringe method can be described as in the following.

Consider the function $D(\vec{r})$ describing the light intensity in the image plane of a photographic camera, where $\vec{r}(x, y)$ are the plane coordinates. Considering that there is an in-the-plane displacement dy of the scatterers, the image will be translated by Mdy, where M is the magnification of the camera lens, and the resulting intensity distribution is

$$D(x, y) + D(x, y + Mdy) = D(x, y) \otimes [\delta(x, y) + \delta(x, y + Mdy)] \qquad (1)$$

where $\delta(x, y)$ is the Dirac delta function centered on $\vec{r}(x, y)$, and considering that a translation can be represented as a convolution with a delta function.

The total intensity is recorded on photographic plate. After development the transmittance, τ, of the negative is given by

$$\tau(\vec{r}) = a + bD(x, y) \otimes [\delta(x, y) + \delta(x, y + Mdy)] \quad (2)$$

where a and b are characteristic constants of the photographic emulsion. Local analysis of the film negative with a probe laser beam, figure 2, produces in the

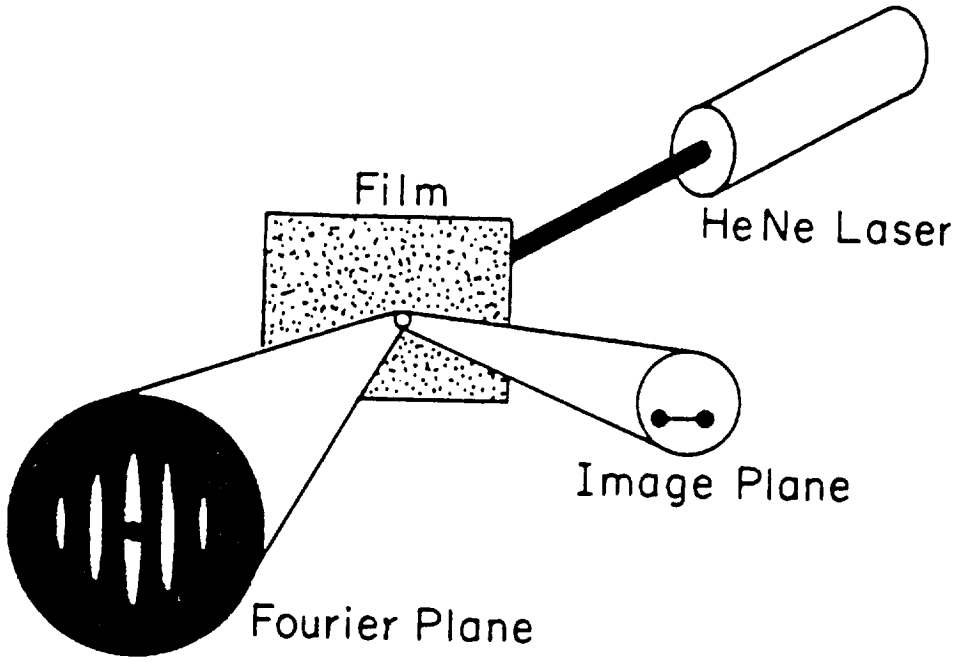

FIGURE 2. Schematic of the set up for obtaining Young's fringes.

far field an optical two-dimensional Fourier transform of the transmittance distribution, with an intensity distribution as follows:

$$\vec{\tau}(u, v) = a\delta(u, v) + b\vec{D}(u, v) \; [1 + \exp(i2\pi vMdy/\lambda_a] \quad (3)$$

where $\vec{\tau}$ represents the Fourier transform of τ, u and v are the angular coordinates of a point in the Fourier plane, λ_a is the wavelength of the interrogating laser light beam. The first term, $\delta(u, v)$ on the r.h.s. of equation represents the image of a point source, i.e. the interrogating beam, when diffraction effects are neglected. This image is seen as a small bright spot in the center of the Fourier plane. The second term is composed by a fine speckle structure $\tilde{D}$ modulated by

$$[1 + \exp(i2\pi vMdy/\lambda_a] \quad (4)$$

The intensity distribution for the second term is obtained by multiplication with its complex conjugate, resulting in

$$|\tilde{D}(u, v)|^2 \; [4\cos^2(\pi vMdy/\lambda_a)] \quad (5)$$

The diffuse background, $|\widetilde{D}|^2$, called «diffraction halo» is modulated by a set of Young's fringes whouse spacing is given by

$$d_F = \frac{\lambda_a f_L}{Mdy} \tag{6}$$

where f_L is the focal length of the converging lens. Knowing M, f_L, λ_a and measuring d_F the displacement dy is easily found from equation (6), with the direction of motion perpendicular to the orientation of the fringes.

By scanning the double exposed photograph one can resolve the two components of the velocity vector at every point of the field. This is a unique feature of this technique.

3. Limitations of the laser speckle mode

The Laser Speckle mode of operation relies upon identical, laterally shifted speckle patterns. Slight out-of-plane motion of the scatterers, due to three-dimensional motions in the flow, will result in speckle patterns that are not entirely similar. As a consequence, the correlation between patterns decreases and the fringe pattern, produced by local coherent illumination, is suppressed or eliminated. This poses a severe limitation in the use of the Laser Speckle mode for the study of turbulent flows or flows with a significant velocity component in the direction perpendicular to the laser sheet. However, the fringe quality is less dependent on the out-of-plane motion in the Particle Image mode of operation. In this case the tolerance to out-of-plane motion is roughly equivalent to the width of the illumination sheet and depth of field of the recording optics. For this reason we use almost exclusively the Particle Image mode of operation. An additional disadvantage with speckle mode of operation is that the seeding in large scale flows or high speed flows can become exceedingly difficult and expensive as the required concentration increases. Finally, the high concentrations of tracer particles required by the Laser Speckle mode may influence or distort the flow field being studied.

4. Experimental facilities and procedures

The time-space development of the near-wake flow behind a circular cylinder impulsively accelerated to constant velocity were examined using Particle Displacement Velocimetry. The flow is created by towing the circular cylinder in the reduced scale Fluid Mechanics Research Laboratory towing tank facility. The tank is $300 \times 200 \times 600$ mm. A detailed examination showed that the motion of the towing carriage is smooth and vibration free. The towing carriage is driven by a variable D.C. motor, and the towing velocity can vary from 0 to 100 mm/sec. For the photography, a 35 mm camera (Nikon F-3) is used. To photograph the flow at regular time intervals, the photographic camera has a electric winding device. The photographic time interval available with this camera can be continuously varied up to a maximum of 6 frames per second. Two options are available to fix the camera: one by attaching it to the towing carriage, which means an observation point fixed in relation to the model, and the other by attaching it to the frame of the water tank, which means an observation point fixed in relation to the fluid. The selection of these two depends upon the flow field being photographed.

In this experiment the circular cylinder is 25.4 mm in diameter and is towed with a velocity of 22 mm/sec. The corresponding Reynolds number was 550. The fluid used in this experiment was water seeded with 4 μm metallic coated particles (TSI model 10087). For the illumination, a laser beam from a 5 Watt Argon-Ion Laser (Spectra-Physics series 2000) is steered and focused to a diameter of 3 mm using an inverse telescope lens arrangement. A cylindrical lens, with a focal length of -6.34 mm, is used to diverge the focused beam in one dimension, creating a light sheet. The laser sheet is 70 mm wide and illuminates the mid-span section of the cylinder. For the multiple exposure, the CW laser beam is modulated using a Bragg cell. In this experiment, the laser power density, I_0, of the sheet was .27 W/mm^2. In order to record the time development of the flow field, the camera was attached to the towing carriage and the frequency of which the multiple exposures were taken was set at 1.7 Hz. The aperture of the lens with a focal length of 50 mm and a spacer of 12 mm, was set at F # 5.6 and the resulting magnification factor was 0.40. For the multiple exposure, the time between exposures, T, and the exposure time, t, are chosen according to the criteria discussed in Lourenço & Krothapalli (1986), Lourenço & Whiffen (1984). The frequency of exposures was optimized to achieve the largest dynamic range, and was 30 m sec. For optimum exposure, the exposure time was 3 m sec, which corresponded roughly to (d_i/MVmax), where D is the analyzing beam diameter, V is the maximum expected velocity in the field and d_i is the particle image diameter expressed in terms of

$$d_i = (d_p^2 + d_s^2)^{\frac{1}{2}} \tag{7}$$

with d_p the particle diameter and d_s the edge spread caused by the limited response of the recording optics Adrian & Yao (1985). The exposure time and the time between exposures together with the particle image size diameter determine the technique's velocity dynamic range, defined as the largest velocity difference that can be detected in the flow field as follows Lourenço (1986).

$$(V_{max} - V_{min}) / V_{min} = [(D - 2d_i) / 2Md_i] - 1 = 6 \tag{8}$$

5. Results

In this experiment the flow was captured at several stages of its development corresponding to $t^* = 0.6, 1.2, 1.8, 2.2, 2.8, 3.2, 3.8, 4.2, 4.9, 5.2$, with $t^* = tU/D$, the non-dimensional time, where t is the time from startup, U is the free stream velocity and D is the cylinder diameter. Figure 3 a-d are typical triple exposed photographs of the flow field. As shown (Lourenço 1986), the triple exposed photograph increase the SNR and fringe visibility. The velocity data is acquired in a square mesh by digital processing of the Young's fringes, produced by point-by-point scanning of the positive contact copy of the photograph (Lourenço 1986). The scanning step size and the dimension of the analyzing beam are 0.5 mm, which corresponds to a spatial resolution of about 1.25 mm in the object plane or about 1/20 diameter of the cylinder. The fringes were processed using the methods described in the following paragraph. The resultant two-dimensional velocity fields, corresponding in figures 3a-d are shown in figures 4a-d, are a good representation of the expected flow pattern. The length of each vector is proportional to the local velocity at the point.

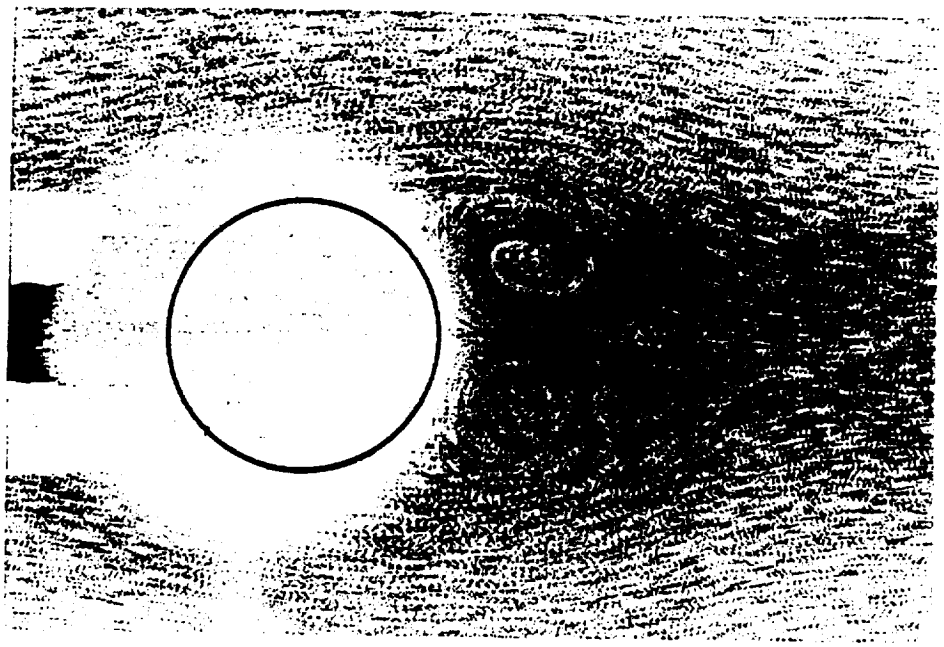

(a)

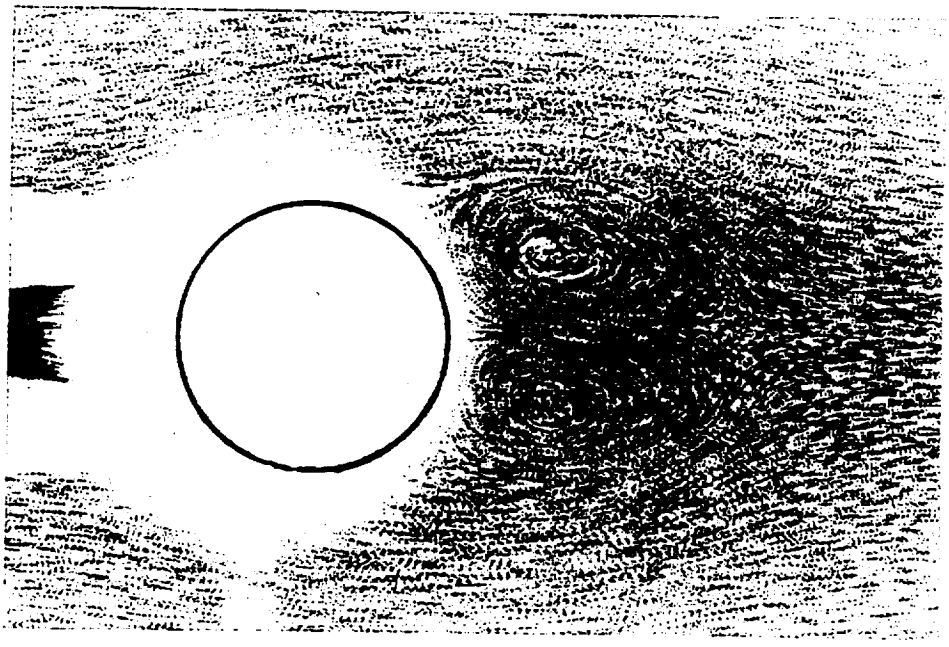

(b)

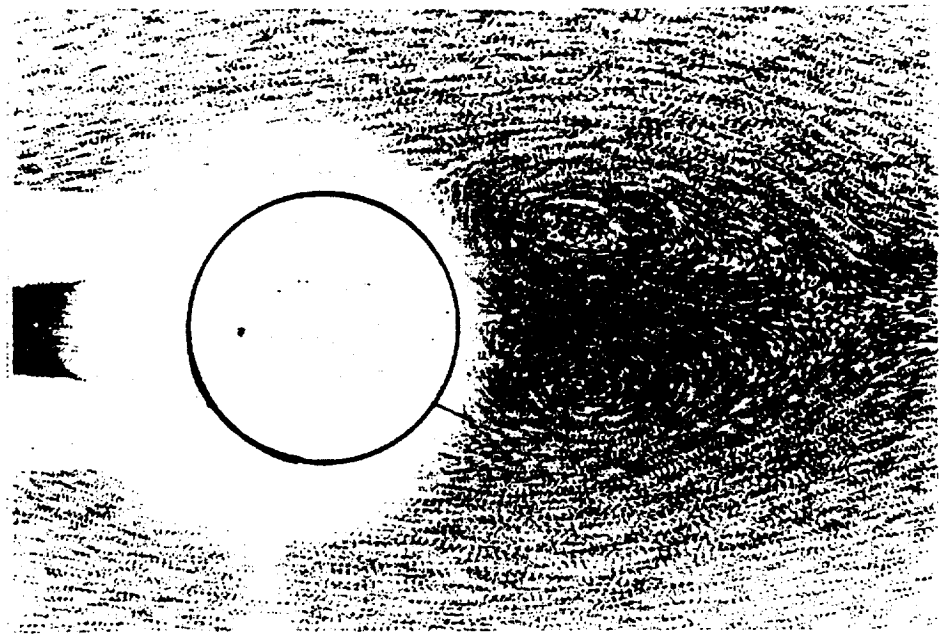

(c)

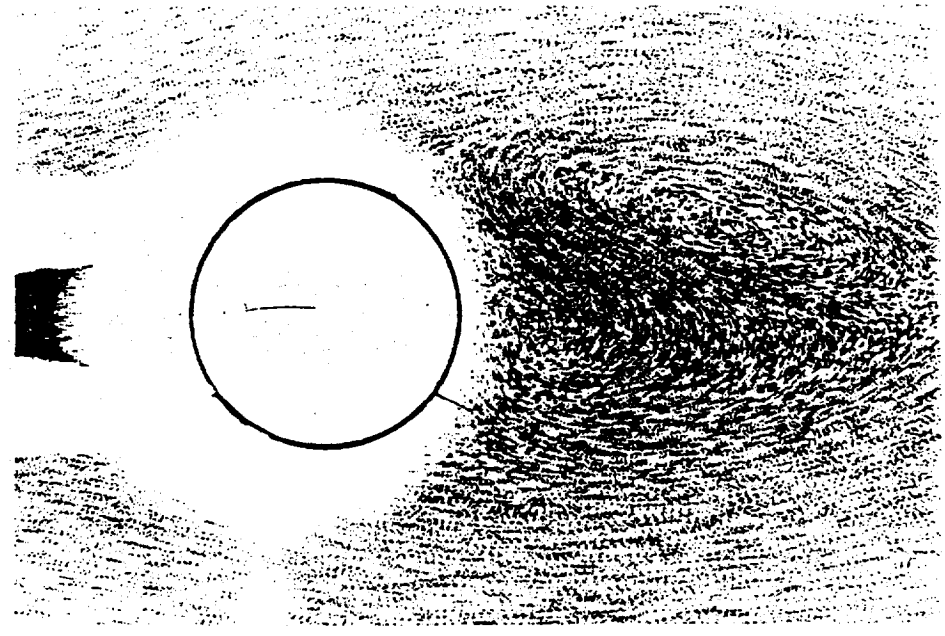

(d)

FIGURE 5. Triple exposed photographs of the wake flow field; a) $t^* = 2.2$; b) $t^* = 3.2$; c) $t^* = 4.2$; d) $t^* = 5.2$.

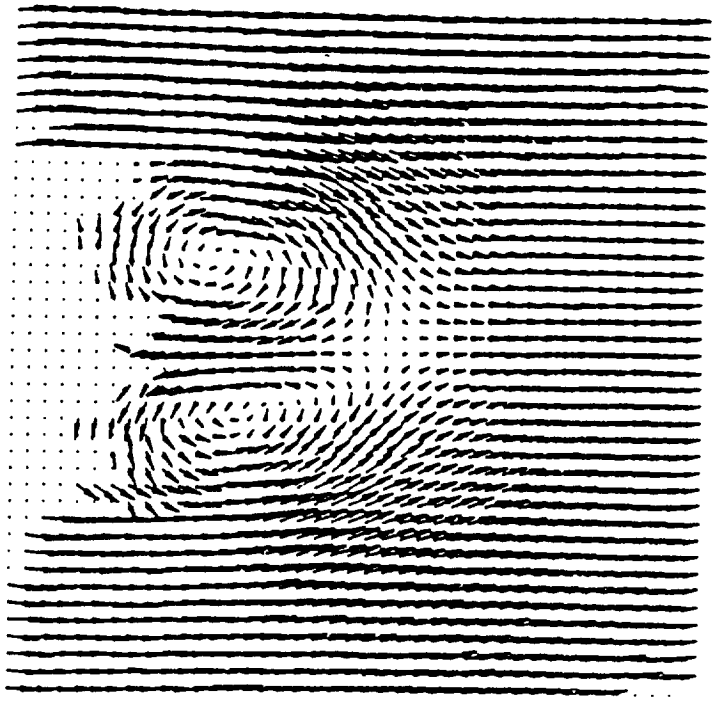

(a)

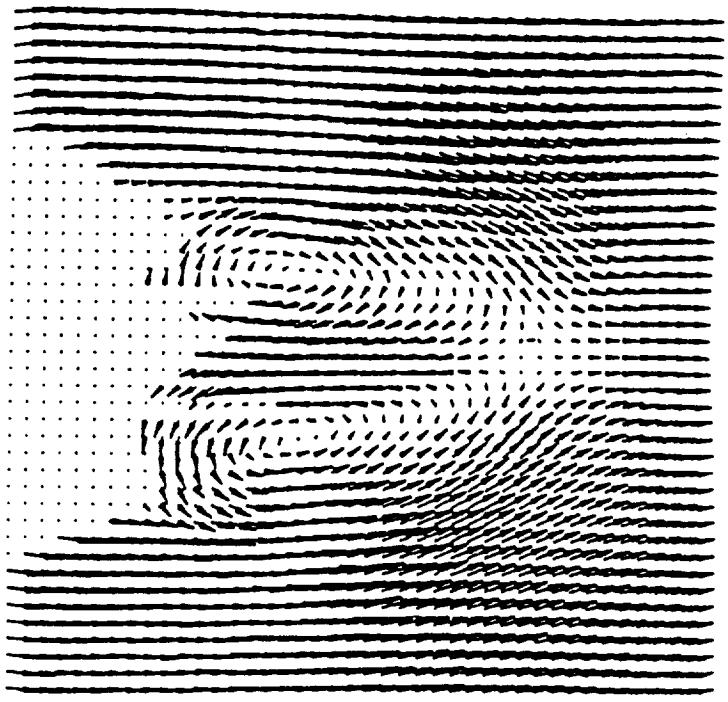

(b)

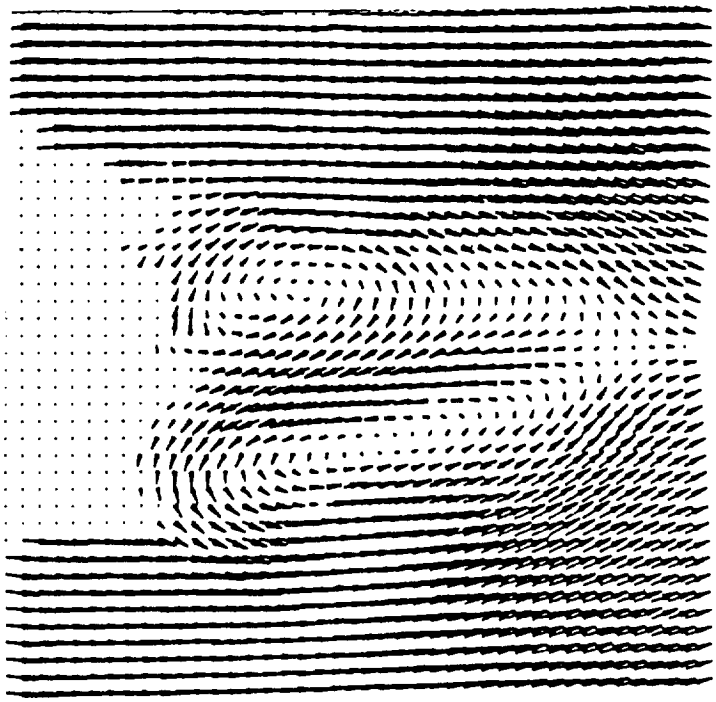

(c)

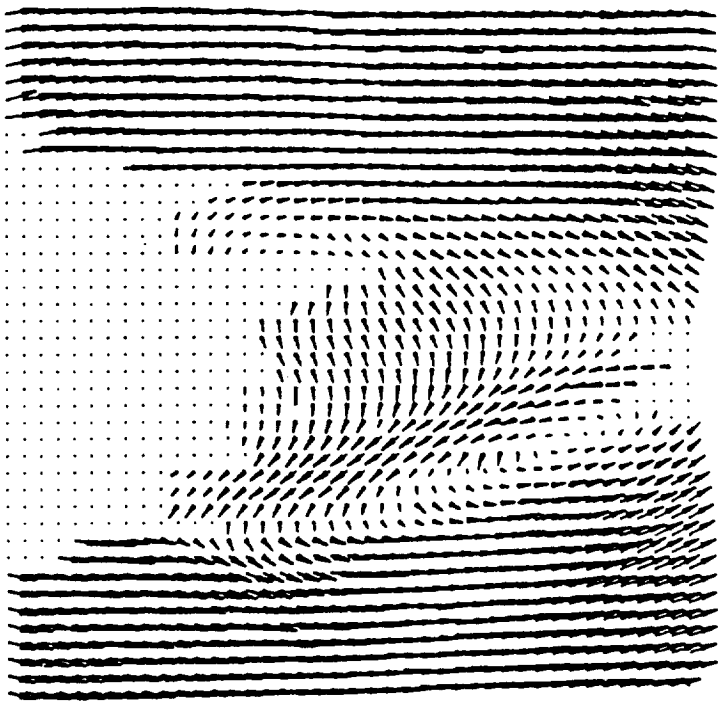

(d)

FIGURE 4. Instantaneous velocity field: a) $t^* = 2.2$; b) $t^* = 3.2$; c) $t^* = 4.2$; d) $t^* = 5.2$.

Using the velocity data, global wake characteristics such as the bubble size development versus time were determined. Figure 5 displays the development of the wake length, measured in terms of the distance between the cylinder surface and the saddle point (zero velocity) where the two counterrotating wake vortices join. These values which are plotted in terms of the non-dimensional time compare well with available experimental data by Honji & Taneda (1969) and numerical predictions by Loc (1980) and L. van Dommelen (1981). It was observed that the distance between the two twin vortices remained constant at a value of about 0.55 D throughout the experiment. This is also in good agreement with the observations reported by Honji & Taneda (1969).

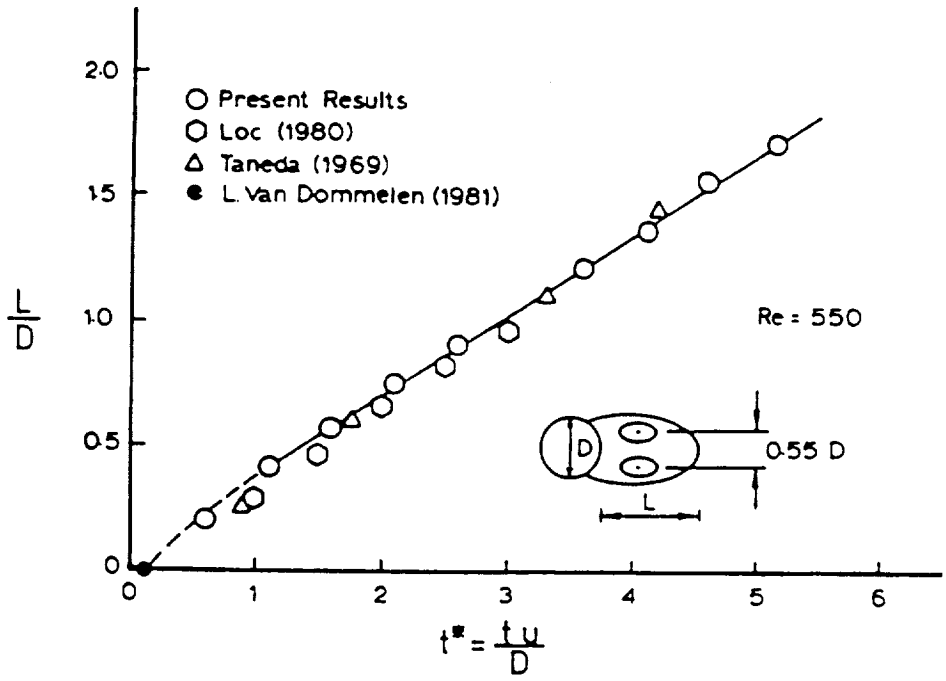

FIGURE 5. Development of the wake size with time.

Because of the high spatial resolution of these data, vorticity contours can be derived by taking spatial derivatives. Letting each grid location be labeled with indices i, j, the vorticity component at location (i, j) is

$$\Omega_{i,j} = h \left\{ \frac{V_{i+1,j} - V_{i-1,j}}{2\,\Delta x} - \frac{U_{i+1,j} - U_{j-1} - U_{i,j}}{2\,\Delta y} \right\} \qquad (9)$$

where Δx and Δy are the mesh intervals in the stream wise and cross-stream directions, respectively. Figures 6a-d show these smoothed vorticity contours, normalized with respect to the free stream velocity and cylinder diameter. Analysis of these figures together with the velocity field (figures 4a-d) reveals some interesting features.

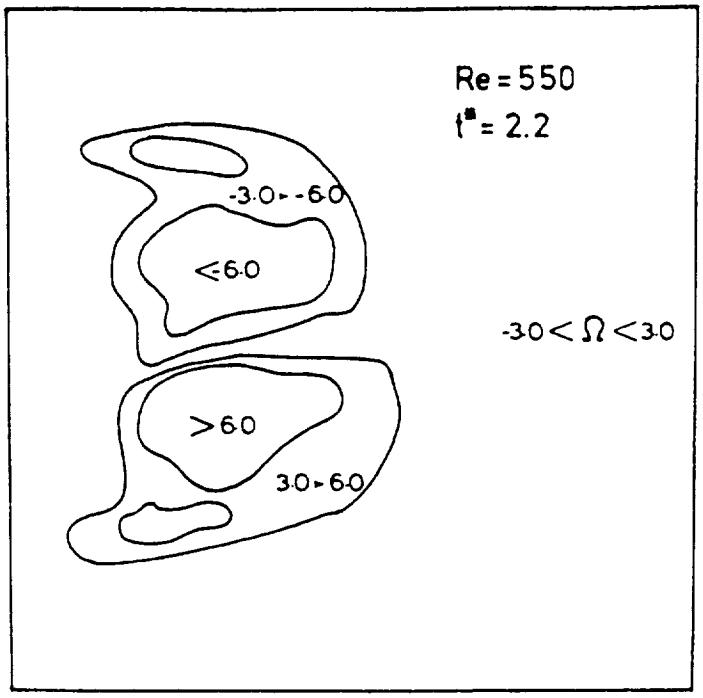
Re = 550
t* = 2.2
-3.0 ▸ -6.0
<-6.0
>6.0
3.0 ▸ 6.0
-3.0 < Ω < 3.0

(a)

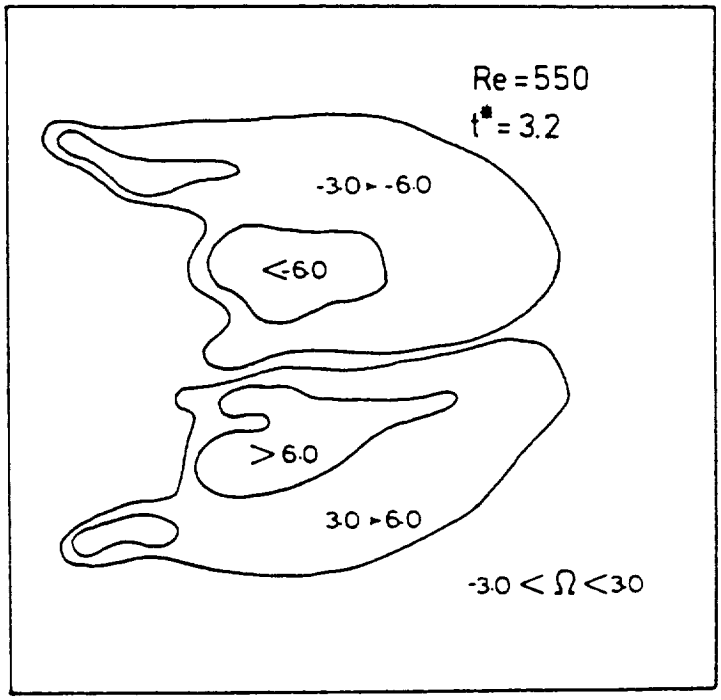
Re = 550
t* = 3.2
-3.0 ▸ -6.0
<-6.0
>6.0
3.0 ▸ 6.0
-3.0 < Ω < 3.0

(b)

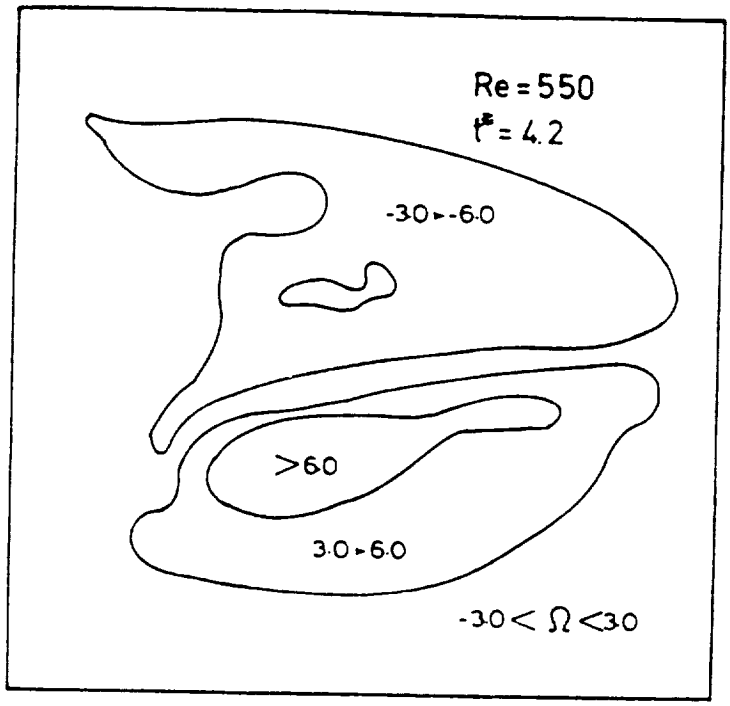

(c)

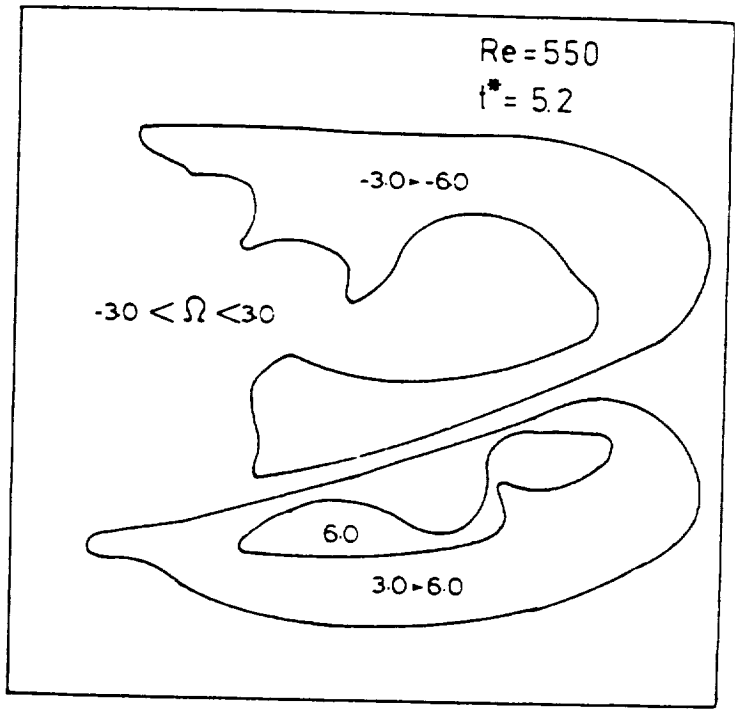

Constant vorticity contours: a) $t^* = 2.2$; b) $t^* = 3.2$; c) $t^* = 4.2$; d) $t^* = 5.2$.

Two primary regions of high vorticity form at the rear of the cylinder corresponding to the startup vortices, while two secondary high vorticity regions are observed further outward. The primary vorticity regions may possibly correspond to the «vorticity peak» reported by Bouard & Coutanceau (1980) whereas the secondary regions may be related to the breakup of the feeding sheet as suggested by the flow visualizations of Tietjens (1979). It is interesting to observe that the vorticity field displays earlier evidence of asymmetry than the streamline (velocity) picture.

6. Data processing

The fringe images were acquired and analyzed using the digital image analysis system of the Florida State University FMRL (figure 7). This system consists of the following components: a DEC LSI-11/73 host computer, Gould

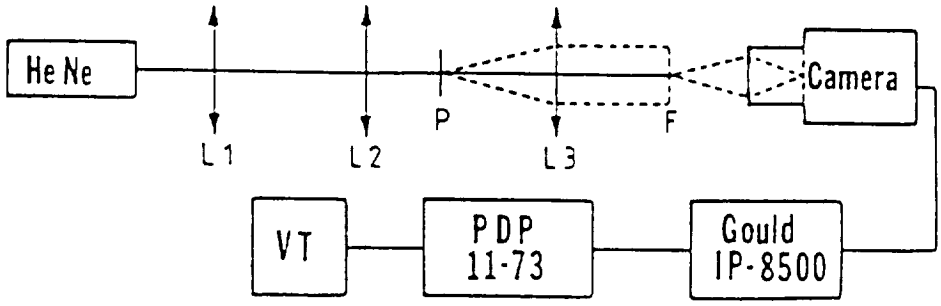

FIGURE 7. Young's fringe analysis set up.

IP-8500 Digital image processor which includes four memory tiles for storage of image data in a 512×512 formal with a resolution of 8 bit per pixel, a frame digitizer, a pipeline processor and a video output controller to convert digital to analog information for display on a color monitor. The system also includes a two-dimensional Klinger traversing mechanism with a controller for the purpose of automatically scanning the film transparencies. Two methods are available and used for fringe analysis (Lourenço & Whiffen 1984). The first one is an interactive method in the sense that it requires the assistance of an operator. The principle of the method consists of first obtaining a 1-D periodic signal from the straight fringes. This is performed by determining the fringe angle in relation to a pre-determined reference followed by an averaging of the lines of the digitized picture as follows:

$$f(m) = \sum_{n=0}^{511} I\ [m + (n-255)\tan\alpha, n] \quad 0 \leq m \leq 511 \tag{10}$$

where I(m, n) represents the digitized picture, f(m) is the resulting periodic signal and is the angle of the fringes with the n axis.

The extraction of the frequency from this signal is straightforward. The Fourier transform of f(m) displaying a peak at the frequency proportional to the velocity component parallel to the m axis. However, due to low frequency modulation of the fringes, which is a consequence of the non-uniform light intensity distribution in the diffraction halo, it is sometimes difficult to identify

this peak, especially if the fringes have low frequency. In order to remove this modulation, the fringe signal is passed through a high pass filter before processing.

The advantage of the one-dimensional averaging technique is rapidity. The computation, which includes the determination of the fringe angle by the operator and position updating of the film transparency scanning mechanism, is completed in a few seconds, typically 7-8 sec, using the PDP 11-73 computer.

The inconvenience of the one-dimensional averaging method is the need for an external adjustment of the angle of the fringes by an operator. This problem can be by passed by computing the velocity components along independent directions. Because each line of the fringe frame can be considered as a noisy periodic signal with variable phase, the automatic determination of a velocity component can be performed only by averaging over a quantity independent of the phase. The autocorrelation for each line or its Fourier transform for the power spectrum satisfies this requirement. The m velocity component can be computed from:

$$g(u) = \sum_{n=0}^{511} \left[\frac{\sum_{m} [I(m,n)I(m+u,n)]}{\sum_{m} [I(m,n)]^2} \right] \quad -511 < u < 511 \qquad (11)$$

This algorithm has been implemented using the pipeline processor of the Gould IP-8500 image processor to perform simultaneously the autocorrelation for all the lines of a frame. For an accurate estimate of the velocity magnitude and directions, four of such full image operations, yielding four autocorrelation functions, are required. From these the velocity vector is determined by selecting the values of the components which have been computed from autocorrelations having the highest SNR, and visibility. In our configuration, the determination of the velocity vector requires 4-5 seconds.

A shortcoming of the autocorrelation technique is the difficulty to measure the velocity when the fringe density is too low (less than five bright fringes, including the central one). In this case, the velocity can often be evaluated by the interactive one-dimensional averaging method. So, the two methods are complementary.

7. Overall accuracy of the technique

The overall accuracy of the technique is evaluated using the following method. A uniform flow field is created by producing a multiple exposure photograph of the still seeded water, in the water tank, with a camera moving at constant speed. For the multiple exposure photograph a number of time between exposures are used, thus resulting in photographs with particle pairs at different known distances. The range of time between exposures as well as the distance between corresponding particle images in the film plane are presented in Table 1. A large number of points (100) of these photographs (5) are analyzed using the methods described in Section 5, in order to obtain statistical information about experimental errors. These uncertainties include error introduced during the recording of the multiple exposure photograph, such as the ones introduced by distortion of the scene being recorded by the camera lens, limited film resolution, and inaccuracies due to the processing algorithms.

In the absence of a systematic bias, the standard deviation of the obtained the film transparencies using the two techniques yields the same mean value

velocity distribution is an estimate of the mean measurement error. Analysis of with a nearly equal standard deviation (Table 1). The values in Table 1 indicate that using these methods, inaccuracies of the order of 1-2 % are expected. It is believed that these inaccuracies are due to a combination of the limited resolving

TIME BETWEEN EXPOSURES (MSEC)	FRINGE FREQUENCY	RMS FRINGE FREQUENCY	MEASURED DISTANCE (uM)
22.2	33.447	0.257	194
25.0	37.045	0.208	218
28.6	42.950	0.381	249
33.3	49.037	0.710	291
40.0	60.693	1.190	350

TABLE 1

power of film using for recording (100 lines/min) and limited response of the camera lens. Another source of error which is not accounted for in this analysis is the one due in the spurious contributions on the in-plane displacement recording by the out-of-plane motions (Lourenço & Whiffen 1984, Lourenço 1986).

8. Conclusions

A technique for laser speckle velocimetry has been briefly described. Measurements of the early near-wake development behind a impulsively started circular cylinder, have been reported, which illustrated the ability of the to record, unsteady flows with accuracy.

The technique has been shown to provide both flow visualization and quantitative measurements, which include the velocity and vorticity fields.

This work is supported by NASA Ames Research Center under Grant No. NAG-2-514.

REFERENCES

ADRIAN, R. J. & YAO, C. S. 1985 Pulsed laser technique application to liquid and gaseous flows and the scattering power of seed materials. *Applied Optics*, 19, 1585-1586.

BOUARD, R. & COUTANCEAU, M. 1980 The early state of development of the wake behind an impulsively started cylinder for $40<Re<10^4$. *J. Fluid Mech.*, 101, 583-607.

COLLICOTT, S. H. & HESSELINK, L. 1985 Anamorphic optical processing of laser speckle anemometer data. *Bull. Amer. Phys. Soc.*, 30, 1728.

HONJI, H. & TANEDA, S. 1969 Unsteady flow past a circular cylinder. *J. Phy. Soc. of Japan*, 27, 1668-1677.

LOC, T. P. 1980 Numerical analysis of unsteady secondary vortices generated by an impulsively started circular cylinder. *J. Fluid Mech.*, **100**, 111-128.

LOURENÇO, L. 1986 The fundamentals and application of particle image displacement velocimetry. *Von Karman Institute Lecture Series*, Belgium.

LOURENÇO, L. & KROTHAPALLI, A. 1986 The role of photographic parameters in laser speckle or particle image displacement velocimetry. *Experiments in Fluids*, **5**, 29-32.

LOURENÇO, L. & WHIFFEN, M. C. 1984 Laser Speckle methods in fluid dynamics applications. Proc. *Int. Symp. on Appl. of Laser Anemometry to Fluid Mechanics*, Lisbon, Portugal.

MEYNART, R. 1980 Equal velocity fringes in a Rayleigh-Bernard flow by a speckle method. *Applied Optics*, **19**, 1385-1386.

SIMPKINS, P. G. & DUDDERAR, T. D. 1978 Laser Speckle methods for transient Bernard convection. *J. Fluid Mech.*, **89**, 665-671.

TIETJENS, O. 1970 *Stromungslehre*, 1st Edition, Vol. 2, Springer-Verlag, Berlin, 105-109.

VAN DOMMELEN, L. L. 1981 *Unsteady Boundary Layer Separation*. Ph. D. Thesis Cornell University.

YAO, C. S. & ADRIAN, R. J. 1984 Orthogonal compression and 1-D analysis technique for measurement of 2-D particle displacements in pulsed laser velocimetry. *Applied Optics*, **23**, 1687-1689.

APPENDIX III

Particle image displacement velocimetry measurements of a three-dimensional jet

L. Lourenco and A. Krothapalli
Department of Mechanical Engineering, Florida A&M University/Florida State University College of Engineering, P.O. Box 2175, Tallahassee, Florida 32316-2175

(Received 19 February 1988; accepted 22 April 1988)

A whole field experimental technique, commonly referred to as particle image displacement velocimetry (PIDV), is used for the measurement of the instantaneous two-dimensional velocity fields in the transition region of a three-dimensional jet issuing from a rectangular nozzle with aspect ratio 4. The experiments were performed using an air jet at a Reynolds number based on the hydraulic diameter of 3600. The rollup of the laminar shear layer into vortices and their subsequent interactions are examined.

Particle image displacement velocimetry (PIDV) is an attractive experimental technique for the nonintrusive measurement of two-dimensional velocity fields in free shear layers dominated by quasideterministic large structures. It provides an instantaneous velocity field measurement capability with good spatial resolution, from which the vorticity field can be computed accurately.

Earlier investigations[1,2] have been carried out using a technique similar to PIDV to study the mixing region of an axisymmetric jet. However, as a result of the limited dynamic range in the velocity measurements[1] or limited spatial coverage of the flow field,[2] a number of important features of the vortical structures could not be obtained. The purpose of this Letter is to establish the validity and attractiveness of the PIDV technique for accurate measurements of the instantaneous two-dimensional velocity field in a three-dimensional, time dependent, vortical, and entraining flow.

The flow field considered is a three-dimensional incompressible jet of air issuing from a rectangular nozzle of aspect ratio 4. The structure and development of such a jet is markedly different from those issuing from two-dimensional and axisymmetric nozzles.[3] One of the interesting features is the "crossover" phenomenon, which is generally characterized by the switching of the major and minor axes downstream of the nozzle exit. The physical mechanism of this phenomenon is not well understood. Recent experiments on low-aspect-ratio elliptic jets[4] suggest that an initial instability process may influence the position of the crossover point and thus the development of the jet. With this in mind, the present investigation focuses on studying the structure and growth of the mixing layer region of the jet.

A brief description of the particle image displacement velocimetry technique is given here, however, for more details see Refs. 5 and 6. The PIDV measurements of fluid flows can be described as follows: A selected cross section of the flow is illuminated by a sheet of coherent light. A pulsed laser such as a Nd:Yag laser, is normally used as the light source. The laser sheet is formed by focusing the laser beam with a spherical lens of long focal length followed by a one-dimensional expansion using a cylindrical lens. Within the illuminated sheet, the flow is made visible through small tracer particles seeded within the fluid. The illuminated particles generate resolved diffraction limited images recorded in a multiple exposure photograph. The spacing between the images of the same tracer provides a measure of the local flow velocity.

To determine this spacing, a Fourier analysis is used. A focused laser beam is used to interrogate a small area of the multiple exposure photograph transparency. The diffraction produced by coherent illumination of the multiple images in the film transparency generates Young's fringes. The fringes are oriented perpendicular to the direction of the local displacement and their spacing is inversely proportional to the magnitude of the displacement. The use of Young's fringes avoids the difficulty of locating individual image pairs in the photograph.

In this method, the sign of the velocity cannot be determined.[7] A method to resolve this ambiguity, as well as to improve the technique's capabilities to measure large velocity gradients, is incorporated in this experiment. This method,[7,2] commonly known as the "velocity bias technique," consists of recording the flow field in a moving reference frame, thus superposing a known velocity bias to the actual flow velocity. This effect may be accomplished in several ways, such as using a moving camera during the photographic recording or by optical means using scanning or ro-

tating mirrors. For the data presented here, a scanning mirror is used to displace the image during the photographic recording.

A simple low speed air supply system was used to flow air into a cylindrical settling chamber 27 cm in length and 10 cm in diameter. A honeycomb and a series of screens at the inlet of the nozzle are used to further reduce flow disturbances. The cross-section area of the contraction changes gradually from a circular cross section, 10 cm in diameter, to a rectangular nozzle. The long dimension and the short dimension of the rectangular nozzle are, respectively, 3 cm and 0.75 cm and the streamwise contours of the contraction for the two central planes are fifth-order polynomials. In order to obtain appropriate jet seeding, smoke particles in the submicron range are produced using a Rosco-type 1500 smoke generator. The smoke and ambient air are mixed in a large cylindrical settling tank (100 cm in length and 45 cm in diameter). The air–smoke mixture is then supplied to the settling chamber of the jet using a small axial fan. A second smoke generator of the same type is used to seed the outside ambient fluid surrounding the jet.

A mean velocity of 4.5 m/sec is maintained at the exit plane of the nozzle; the mean velocity profile at the exit plane is flat with a laminar boundary layer at the walls. The Reynolds numbers based on the hydraulic diameter and the small dimension of the nozzle are, respectively, 3600 and 2250.

For the illumination, a laser beam from a frequency-doubled, double-pulsed Nd:Yag laser (Spectra-Physics model DCR-11) is steered and focused to a diameter of 0.3 mm using an inverse telescope lens arrangement. A cylindrical lens with a focal length of -24.5 mm diverges the focused beam one dimensionally, creating the light sheet. The laser sheet is 45 mm wide and illuminates the central plane through the small dimension of the nozzle. A 35 mm camera (Nikon F-3) with a 150 mm macro lens loaded with 400ASA KODAK TMAX film, a film with good sensitivity at the laser light frequency, is used for the photographic recording. The lens aperture is set at $f/5.6$ and the magnification is 0.5. Two laser pulses with a duration of 10 nsec and a separation of 50 μsec are used for the double exposure recording. In this mode, the laser delivered a 15 mJ/pulse of light at the 0.532 nm wavelength. The pulse separation of 50 μsec is much smaller than any relevant time scale of the flow field, thus the double exposure photograph truly represents a flow field at a given instant of time.

The analysis of the photograph was performed by means of an integrated image analysis system based on a Gould IP-8500 digital image processor controlled by a μVAX II. The system also includes a computer controlled scanning mechanism for updating the position of the film transparency. The algorithm used to determine the velocity vector is discussed in Ref. 5, and its accuracy is estimated at 1% or better.

Typical double exposure photographs of the jet in the central plane through the small dimension of the nozzle, for two different times are shown in Fig. 1. These pictures display the flow field from the nozzle exit to a downstream location of about eight widths. The photographs were taken using the velocity shift and external seeding of the ambient medium. From these and other flow visualization pictures,

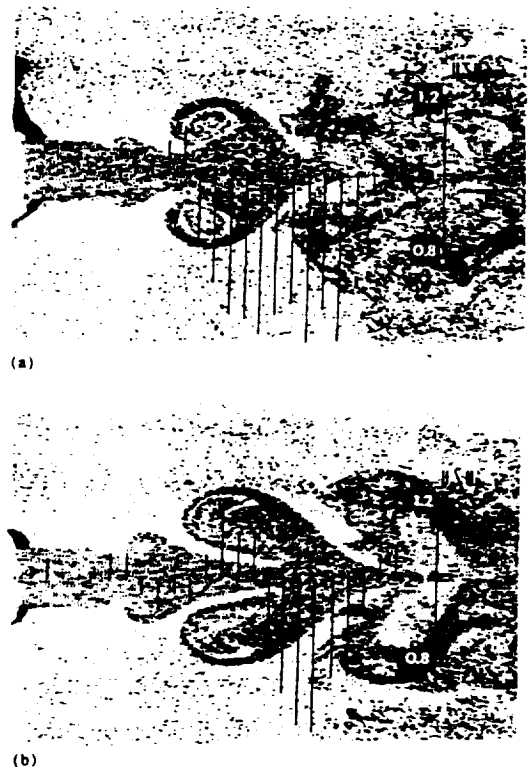

FIG. 1. Instantaneous double exposure photographs of the central plane, containing the small dimension of the jet, and superposed with the jet centerline velocity distribution.

the following observations were made. The jet consists of three regions: the region in which the initial shear layer is unstable and rolls up into discrete vortices; an interaction region in which the vortices pair with each other; and a region in which the vortices break up into random, three-dimensional motion. In spite of the relatively large aspect ratio of the nozzle exit (AR = 4), the rectangular jet organizes itself into a structure similar to that of an axisymmetric jet.[8] The pairing process is also quite similar. In this process, the trailing vortex catches up with the leading vortex, decreases in size, and passes through the leading vortex, which has slowed down and grown in size. The vortex cores rotate around each other and ultimately merge, producing a single vortex. A number of vortex pairings can occur before the vortex becomes three dimensional. The physical regions where these phenomena take place overlap and depend on the phase of the development of the jet. Strong accelerations and decelerations exhibited by the large scale vortical structures can be observed when the instantaneous axial centerline velocity distribution normalized with the jet's axial exit velocity is superimposed on the photographs (Fig. 1). The nondimensional passage frequency of the vortices before pairing is estimated to be about $St_w = 0.7$, where St_w is the Strouhal number based on the nozzle width w and the mean exit velocity U of the jet, i.e., $St_w = fw/U$. This Strouhal number is close to that of an axisymmetric jet,[9] at a comparable Reynolds number. Examination of several photograph

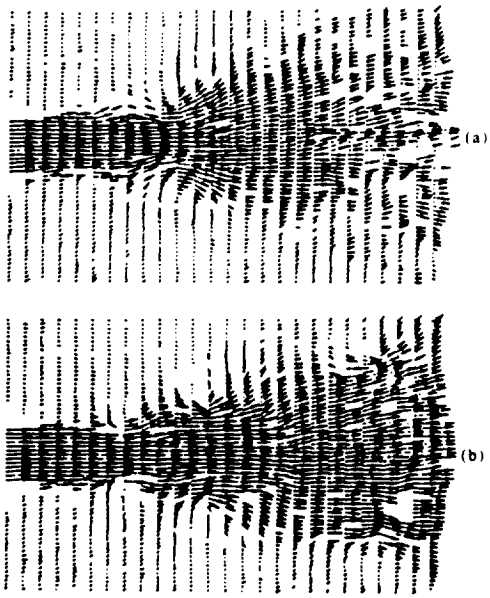

FIG. 2. Instantaneous two-dimensional velocity fields shown in the laboratory reference frame.

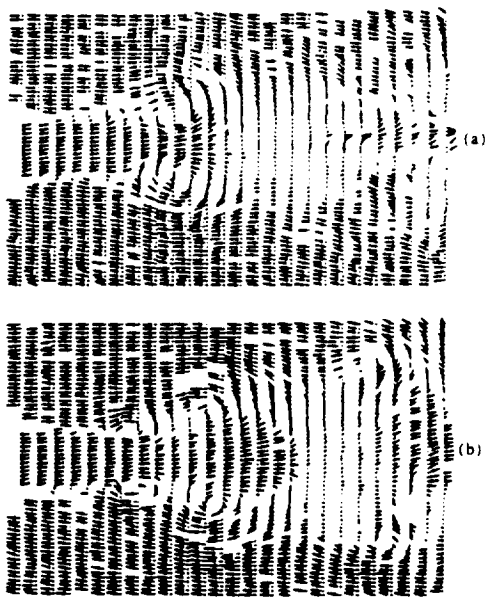

FIG. 3. Instantaneous two-dimensional velocity field shown in a reference frame moving with the convection velocity of the vortical structures.

suggests that the vortex breakdown leads to the larger spreading rate of the jet. The increased three-dimensionality enhances the mixing in the plane of the small dimension of the nozzle. No increase in mixing was observed in the central plane containing the long dimension of the nozzle.

For two typical phases in the development of the jet, shown as the double exposed photographs in Fig. 1, the instantaneous velocity fields were obtained. The results after removal of the velocity bias (i.e., in the laboratory reference frame) are shown as a series of uniformly scaled velocity vectors in Fig. 2. Because the velocity gradients are largest in the transverse direction, the velocity data were acquired using a rectangular mesh with a mesh spacing of 2 mm in the jet axial direction and 0.5 mm in the jet transverse direction. The velocity field displayed in Fig. 2, represents, with great fidelity, all the aforementioned regions of the flow field. These include the shear layers and regions with strongly three-dimensional motion. Such an accurate representation of the flow field was a consequence of our use of the velocity bias technique and the judicious management of the flow seeding procedure.

Examination of the obtained velocity fields confirms our previous analysis based on the flow visualization pictures. The jet structure can be further illuminated when the velocity field is presented in a reference frame moving with the convection velocity of the vortical structure, estimated to be 60% of the jet exit velocity (Fig. 3). In this reference frame, the large scale vortical structures, as well as the nature of the symmetric instability, are clearly observed. The instantaneous velocity profiles provide a unique means to quantify the extent of the jet unsteadiness, the existence of the coherent structures, their interactions, and subsequent generation of random three-dimensional motions.

A successful application of PIDV to study a time dependent, vortical, entraining, and three-dimensional flow field is reported. The data acquired provided quantitative and flow visualization information that revealed the nature of the instability process that occurs in the initial region of the jet. This process is consistent with previously observed features of axisymmetric jets. Furthermore, new and important quantitative information was obtained which is essential for a deeper understanding of this complex flow field.

ACKNOWLEDGMENTS

This work is supported by the Aeromechanics branch of NASA Ames Research Center under Grant No. NAG 2-314. The grant monitor is Dr. C. A. Smith, whose cooperation and understanding is much appreciated.

[1]R. Meynart, Phys. Fluids 26, 2074 (1983).
[2]C. C. Landreth, R. J. Adrian, and C. S. Yao, Exp. Fluids 6, 119 (1988).
[3]A. Krothapalli, D. Baganoff, and K. Karamcheti, J. Fluid Mech. 107, 201 (1981).
[4]C. M. Ho and E. Gutmark, J. Fluid Mech. 179, 383 (1987).
[5]L. M. Lourenco and A. Krothapalli, Exp. Fluids 5, 29 (1987).
[6]L. M. Lourenco and A. Krothapalli, *Laser Anemometry in Fluid Mechanics-III* (Ladon-Institute Superior Technico, Lisbon, Portugal, 1988), p. 161.
[7]L. M. Lourenco, A. Krothapalli, J. M. Buchlin, and M. L. Riethmuller, in *Aerodynamic and Related Hydrodynamic Studies Using Water Facilities*, AGARD CP-413 (NATO, Brussels, 1986), paper 23.
[8]E. E. Bouchard, Ph.D. dissertation, Stanford University, 1982.
[9]H. A. Becker and T. A. Massaro, J. Fluid Mech. 31, 435 (1968).

APPENDIX IV

Vortex Interactions in the Transition Region of a Rectangular Jet

A. Krothapalli, L. Lourenco, and C. Shih

Department of Mechanical Engineering
Florida A&M University and Florida State University
Tallahassee, FL 32316-2175, U.S.A

Paper presented at IUTAM Symposium on Separated Flows and Jets, Novosobirsk, USSR, July 1990.

Abstract

This paper describes an experimental investigation of the large scale vortical structures in the transition region of a rectangular jet of aspect ratio 4 at a Reynolds number, based on the equivalent diameter, of 4500. The instantaneous two dimensional flow for the first 4 equivalent diameters in the jet was measured using the Particle Image Displacement Velocimetry technique. This technique provides an instantaneous velocity field measurement capability with good spatial resolution, from which the vorticity field can be computed accurately. The kinematics of the vortex interaction process are described in terms of the formation and evolution of coherent-vorticity distributions. An important observation is that the interaction process of cylindrical vortices is not unique and consists of several different events. The paper describes two of such processes which are typical of rectangular jets.

1. Introduction

Since the clear and vivid experiments of Brown[1], the presence of large scale vortical structures in the transition region of jets have been recognized to play a significant role in the downstream development of a jet. There have been several review articles describing the nature of these structures and their relevance to the overall understanding of the turbulence, and the most recent and comprehensive of these is given by Hussain[2]. Because of their simple geometry, most previous investigators have focused their attention in understanding the transition region of either an axisymmetric jet (eg. Becker and Massaro[3]) or a two-dimensional jet (eg. Rockwell and Niccolls[4]) . More recently, Ho and Gutmark[5] and Hussain and Husain[6] have studied jets exiting from low aspect ratio elliptic nozzles. These studies provided better understanding of the nature of the mixing processes that takes place in an elliptic jet. The role of large vortical structures on the deformation (cross-over phenomenon) of a rectangular jet was convinsingly pointed out by Abramovitch[7]. In the present investigation, we attempted to study the transition region of a rectangular jet with a relatively new experimental technique commonly known as Particle Image Displacement Velocimetry (PIDV). This technique will provide the instantaneous velocity field in a selected plane of the flow field with sufficient accuracy to obtain the vorticity field. The transition region of a jet is best characterized by the study of the instantaneous flow, with the hope that a more detailed knowledge may lead to some ability to control its characteristics.

In the past, many researchers have attempted to identify, by flow visualization and conditionally sampled statistical measurements, typical kinematic features of the instantaneous flow. Such an approach, although will yield useful information in flows which are typically two dimensional and have a dominant frequency at which many of the significant events take place, may prove to be difficult to implement in three dimensional jets. Here, with the use of the PIDV technique, the study of the vortex dynamics, especially in the region where large scale structures are present, is made much simpler with the measurement of instantaneous vorticity. A brief description of the technique is given below, but for more details reference may be made to a recent review article by Lourenco et.al[8] .

The PIDV technique can be described as follows: A selected cross section of the flow is illuminated by a sheet of coherent light. A pulsed laser, such as a Nd:Yag laser, is normally used as the light source. The laser sheet is formed by focusing the laser beam with a spherical lens of long focal length followed by a one-dimensional expansion using a cylindrical lens. Within the illuminated sheet, the flow is made visible through small tracer particles seeded in the fluid. The illuminated particles generate resolved diffraction limited images which are recorded in a multiple exposure photograph. The spacing between the images of the same tracer provides a measure of the local fluid velocity. To determine this spacing, a Fourier analysis is used. A focused laser beam is used to interrogate a small area of the multiple exposure photograph transparency. The diffraction produced by coherent illumination of the multiple images in the film transparency generates Young's fringes. The fringes are oriented perpendicular to the direction of the local displacement and their spacing is inversely proportional to the magnitude of the displacment. In this method, the sign of the velocity can not be determined. A method to resolve this ambiguity, as well as to improve the dynamic range for the velocity measurement, is incorporated in this experiment. The method consists of recording the flow field in a moving reference frame, thus superposing a known velocity bias to the actual flow velocity. This is accomplished by optical means using a scanning mirror.

2. Apparatus and Instrumentation

A simple low speed air supply system was used to flow air into a settling chamber 25 cm in length and 7.5 cm in diameter. A honeycomb and a series of screens at the inlet of the settling chamber were used to reduce the flow distrubances. The cross-section area of the nozzle contraction changes gradually from a circular cross section, 7.5 cm in diameter, to a rectangular nozzle. The long (L) and short (W) dimensions of the rectangular nozzle are 3cm and 0.75 cm respectively and the streamwise contours of the contraction are fifth-order polynomials. The contoured nozzle has a contraction ratio of 19.6:1 over a length of $1.6D_i$, where D_i is the inlet diameter. In order to obtain appropriate jet seeding, smoke particles in the sub-micron range are produced using a Rosco-type 1500 smoke generator. The smoke and ambient air are mixed in a large cylindrical settling tank (100 cm in length and 45 cm in diameter). The air-smoke mixture is then supplied to the settling chamber of the jet using small axial fan. A second smoke generator of the same type is used to seed the outside ambient fluid surrounding the jet. To minimize ambient distrubances the whole apparatus is placed in a rectangular room ($183cm \times 183cm \times 100cm$) made of transparent walls.

For the illumination, a laser beam from a frequency-doubled, double-pulsed Nd:Yag laser (Spectra-Physics model DCR-11) is steered and focused to a diameter of 0.3 mm using an inverse telescope lens arrangement. A cylindrical lens with a focal length of -24.5 mm diverges the focused beam one dimensionally, creating the light sheet. The laser sheet is 4.5 cm wide and illuminates the central plane through the small dimension of the nozzle. Two laser pulses with a duration of 10 nsec and a separation of $50\mu sec$ are used for the double exposure recording. The pulse separation of $50\mu sec$ is much smaller than any relevant time scale of the flow field, thus the double exposure photograph truly represents a flow field at a given instant of time. The photographs were taken at random and some times on different days.

The analysis of the photographs was performed by means of an integrated image analysis system based on Gould IP-8500 digital image processor controlled by a $\mu VAXII$. The system also includes a computer controlled scanning mechanism for updating the position of the film transparency. The algorithm used to determine the velocity vector is discussed in Ref. 8, and its accuracy is estimated at 1% or better. The velocity vectors were obtained in a cartesian grid (60 × 80). Using a central finite difference scheme, the instantaneous vorticity was obtained with an estimated accracy of about 5%.

In addition to the use of PIDV technique, a laser sheet flow visualization study was conducted. A thin laser sheet was used to illuminate a plane of interest within the flow field. The image was captured by a video camera at 30Hz frame rate. Three different planes are selected for this study: the two central planes along the major and minor axes, and a plane along the diagonal of the nozzle exit (i.e 45° to the major and minor axes.

Initial Conditions:

The nozzle employed in the present investigation is designed to produce a top-hat mean velocity profile with laminar boundary layers at the nozzle exit wall. A mean centerline velocity of 4.5 m/sec is maintained at the exit plane of the nozzle. The centerline turbulence intensity is about 3%. The laminar boundary layer profile at the nozzle exit, as measured by a single normal hot-wire, is of Blasius type. The average momentum thickness along the long and short dimensions of the nozzle are about 0.08 mm and 0.09 mm respectively. The Reynolds number based on the small dimension of the nozzle exit, and the exit mean velocity is 2250. On the basis of arguments put forth by Abramovitch[7], a proper length length scale to be used in defining the Reynolds number for a rectangular jet is the equivalent diameter taken as $D_e = 2\sqrt{ab} = 2W$, where a and b are semi- major and smi-minor axes respectively. The corresponding Reynold number ($Re = \frac{U_e D_e}{\nu}$) for the present experiment will be 4500. The use of such a length scale to characterize a jet is also supported by the experimental data of Hussain and Husain[6] for elliptic jets.

3. Results and Discussion

Typical double exposure photographs of the jet in the central plane through the small dimension of the nozzle, for two different times, are shown in figure 1. The pictures display the flow field from the nozzle exit to a downstream location of 8 widths. From a number (about 100) of similar photographs and flow visualization pictures the

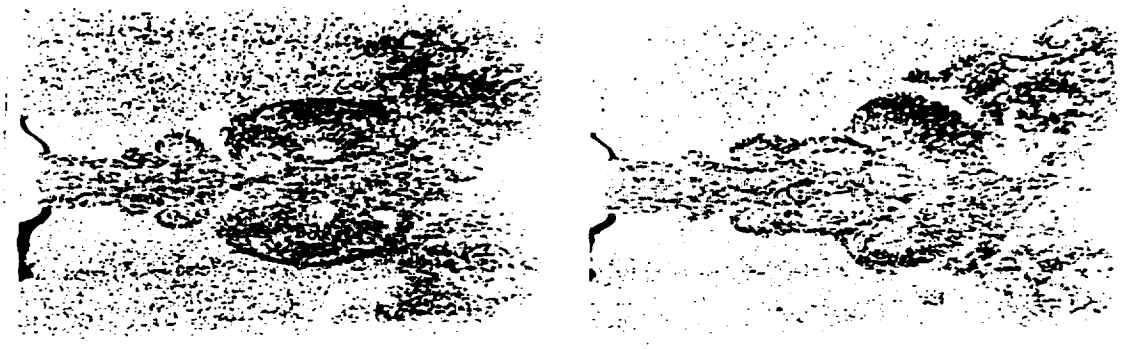

Figure 1. Instantaneous double exposure photographs of the central plane containing the small dimension of the nozzle.

near field ($X/W \leq 20$; where X is the coordinate along the centerline of the jet with its origin located at the nozzle exit) of the jet can be characterized by three distinct regions. The first region in which the initial shear layer is unstable and rolls up into discrete vortices; an interaction region in which two or more vorticies interact with each other; and a region in which vortices break up into three dimensional motion. From flow visualization pictures, a cylindrical vortex rolled up as a rectangle is observed at 1.4 widths downstream of the nozzle exit. Further downstream the individual vortices interact with each other; consequently, the jet spreads very rapidly in the minor axis plane. Such interactions take place in the region $2.0 \leq X/W \leq 6.0$. For $X/W > 6$ the large vortical structures become highly three dimensional.

The passage frequency of the vortices at a given location can be obtained by studying the frequency spectra of the hot-wire signal at that location. With this in mind, frequency spectrum was obtained for various positions in the shear layers surrounding the jet column for $0.5 \leq X/W \leq 6.0$. Figure 2 shows a selected sample of these taken in central planes of major and minor axes. The ordinate is the amplitude plotted with an arbitrary linear scale. The spectrum at the nozzle exit (X/W =0.5) shows a distinct peak at 120Hz. This peak frequency has the same value around the circumference of the jet. The Strouhal number based on the intial momentum thichkness is 0.0213 in the minor axis plane, and 0.024 in the major axis plane. At X/W = 1.0, in addition to the peak at 120Hz, several other prominent peaks are observed at 148, 176, 210, 246, and 282Hz. These peaks are the same in the two central planes. Based on this and flow visualization observations, it is suggested that a single cylindrical vortex is shed in an instant. Further downstream (i.e $X/W \geq 4$) a single prominant broad band peak is observed at 72Hz in the central XY plane. This frequency represents the so called the "preferred mode" in jets. The corresponding Strouhal number based on the equivalent diameter ($St = \frac{fD_e}{U_e}$) is 0.24. It is generally observed that the preferred Strouhal number is approximately proportional to the Strouhal number of the shear layer mode[9] (i.e the vortex passage frequency at the end of the potential core (X/W =4) is simply a fraction of the shear layer mode frequency). However, in the present study such a relationship is not observed. It may be suggested that the regular sequence of amalgamations of vorticies (i.e pairing process) observed in axisymmetric and plane jets does not take

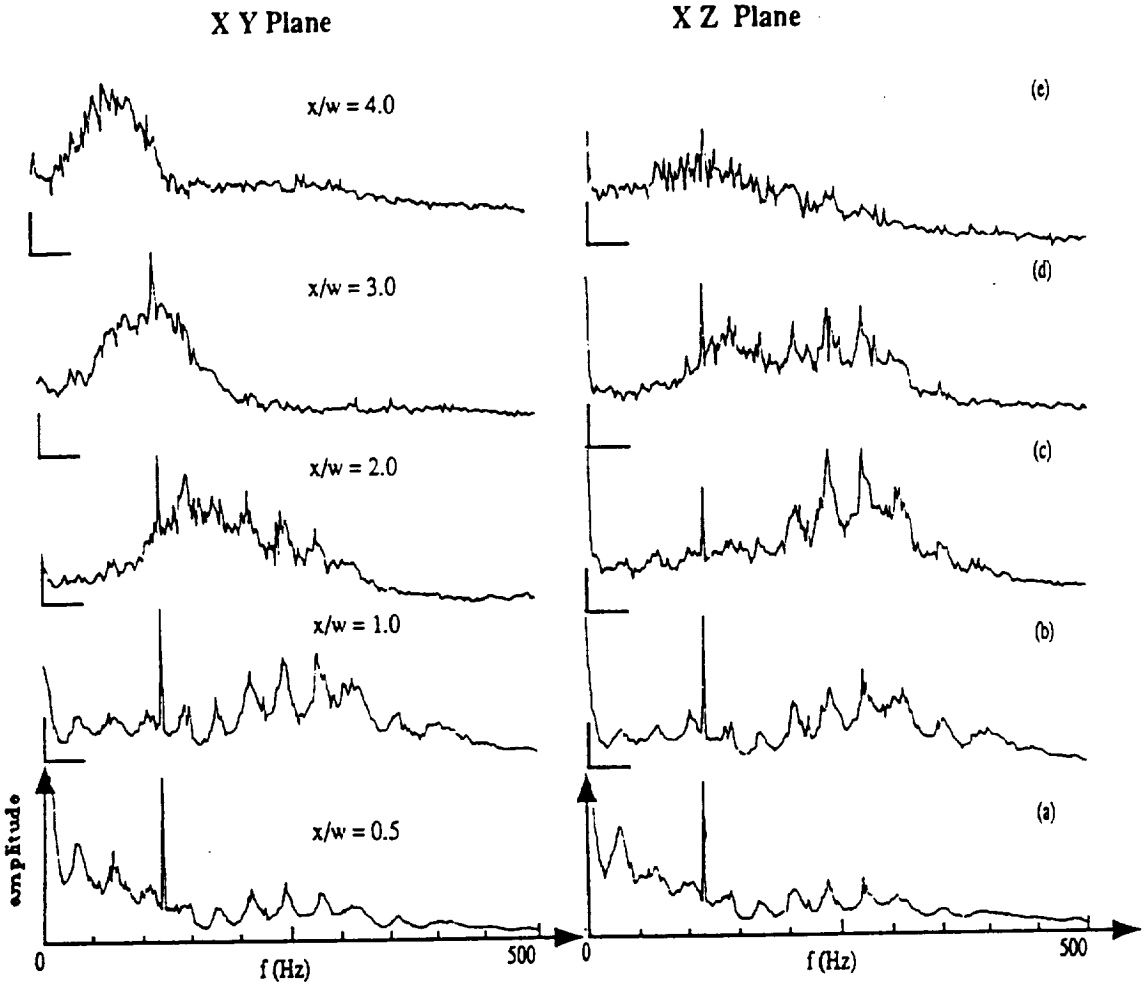

Figure 2. Evolution of frequency spectra in the shear layers of the minor axis (XY) and major axis (XZ) planes.

place. Further confirmation of this can be found later in the paper. The prominant peaks observed at higher frequencies (>120Hz) are believed to represent the effect of the corner "streamwise vorticies" that are generated due to uneven boundary layer structure at the nozzle exit. This aspect is presently being investigated.

Figure 3a shows a typical instantaneous velocity field corresponding to the double exposed photograph in figure 1a. The results after removal of velocity bias are shown as a series of uniformly scaled velocity vectors. Because of the velocity gradients are largest in the transverse direction, the velocity data were acquired using a rectangular mesh (60 × 80) with a mesh spacing of 1 mm in the axial direction and 0.5 mm in the transverse direction. Using a central finite difference scheme the instantaneous vorticity and strain rates are calculated, and shown in figure 3. Also included in the figure are the instantaneous Reynolds stresses corresponding to a typical phase shown in figure 1a. These results represent, with great fidelity, the aforementioned regions of the flow field. Superposition of the three Reynolds stresses on the vorticity plot shows that the

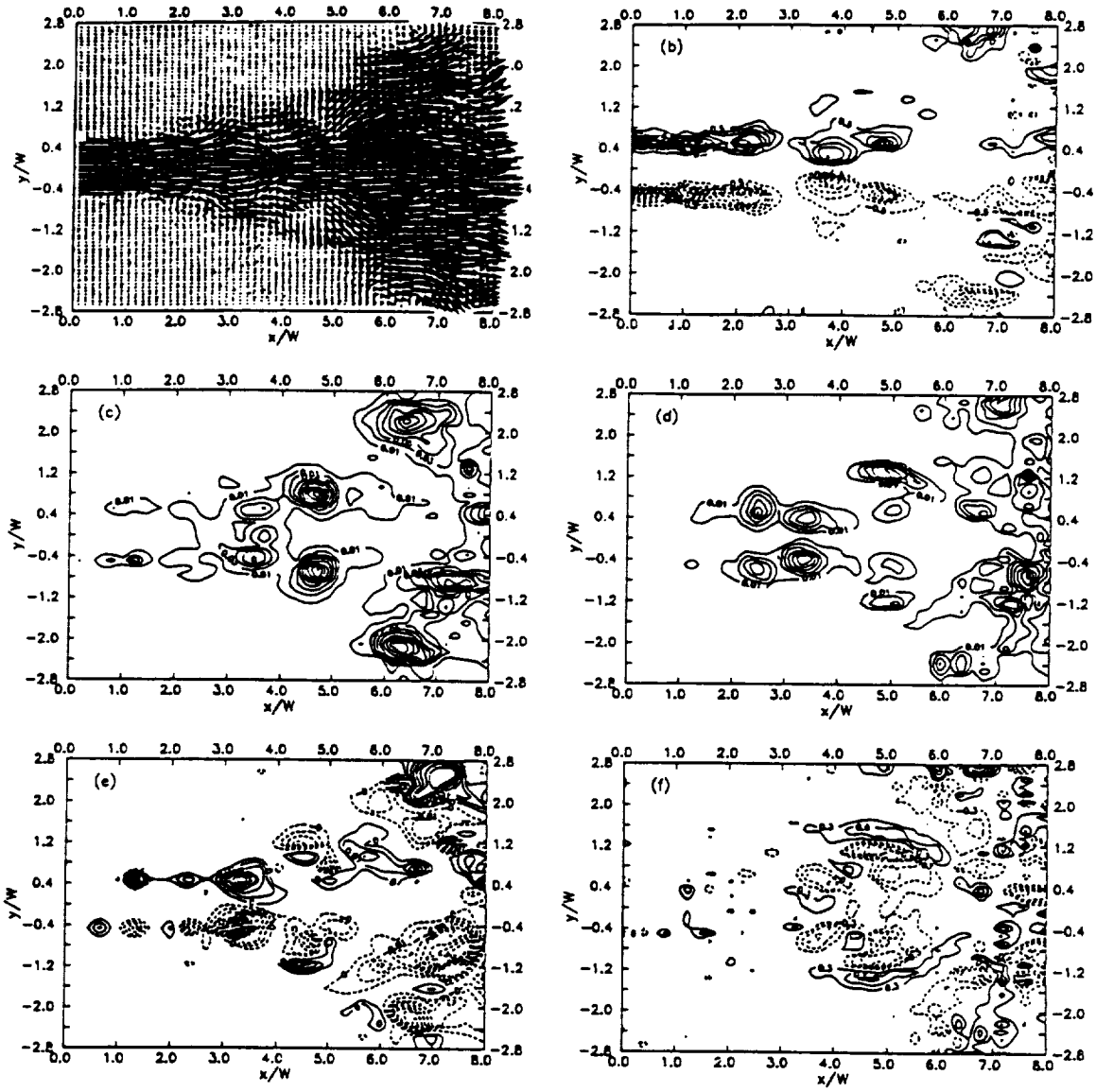

Figure 3. Instantaneous quantities corresponding to the photograph in figure 1a. a) Two-dimensional velocity field, b) Normalized vorticity field, c) $\frac{u'^2}{U_e^2}$, d) $\frac{v'^2}{U_e^2}$, e) $\frac{u'v'}{U_e^2}$, f) $\frac{\partial w'}{\partial z}$.

peaks for these quantities lie away from the vorticity peaks associated with the large vortical structures. The Reynolds stress and vorticity patterns show a strong symmetry with respect to the jet centerline. The nature of three dimensionality generated can be observed in a plot of the instantaneous strain rate (figure 3f). Similar results are obtained for a number (47) of photographs representing individual events that take place in the transition region of the jet. After careful examination of the instantaneous double exposed photographs, and the flow visualization pictures, it is suggested that there are more than one type of multiple vortex interactions occur in the transition region of the jet.

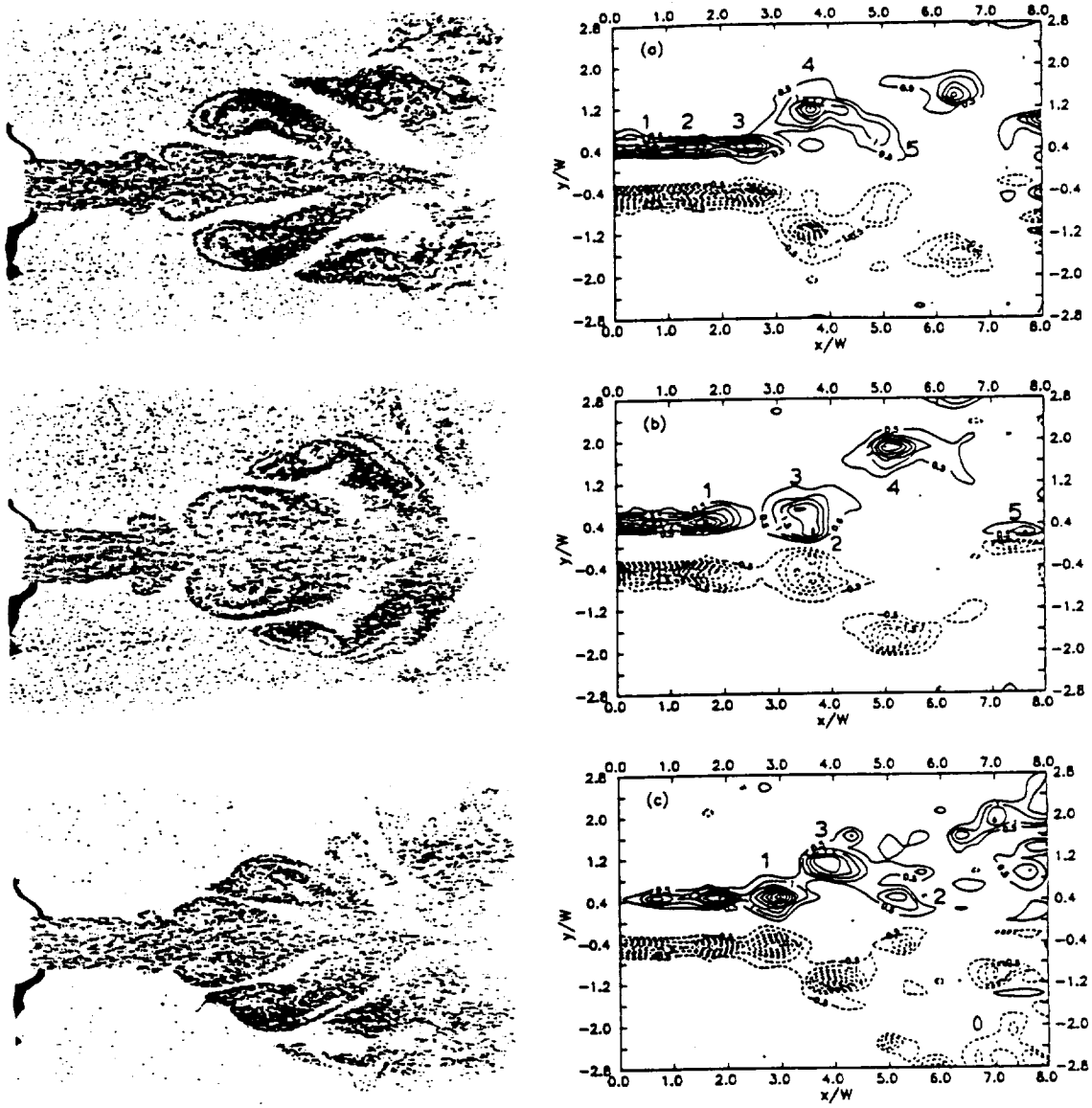

Figure 4. A sequence of a vortex interaction process; Left: double exposure photographs; Right: corresponding vorticity maps.

With the use of two dimensional spatial cross-correlations between a selected set of instantaneous velocity fields, two typical sequences of vortex interactions are selected and presented in figures 4 and 5. Included in these figures are the double exposure photographs and and their corresponding vorticity distributions. In each figure, the first photograph (a) represents the beginning of a sequence, and the following two pictures (b) and (c) depict the progressive development of a vortex interaction process. In this study, the flow organizes itself symmetrically with respect to the jet centerline. To guide the following discussion, individual vorticies in the figures are numbered as shown. The initial shear layer emanating from the nozzle lip roll up into a succession of cylindrical vorticies. Three such vorticies are identified in figure 4a. Two successive vorticies 2 and

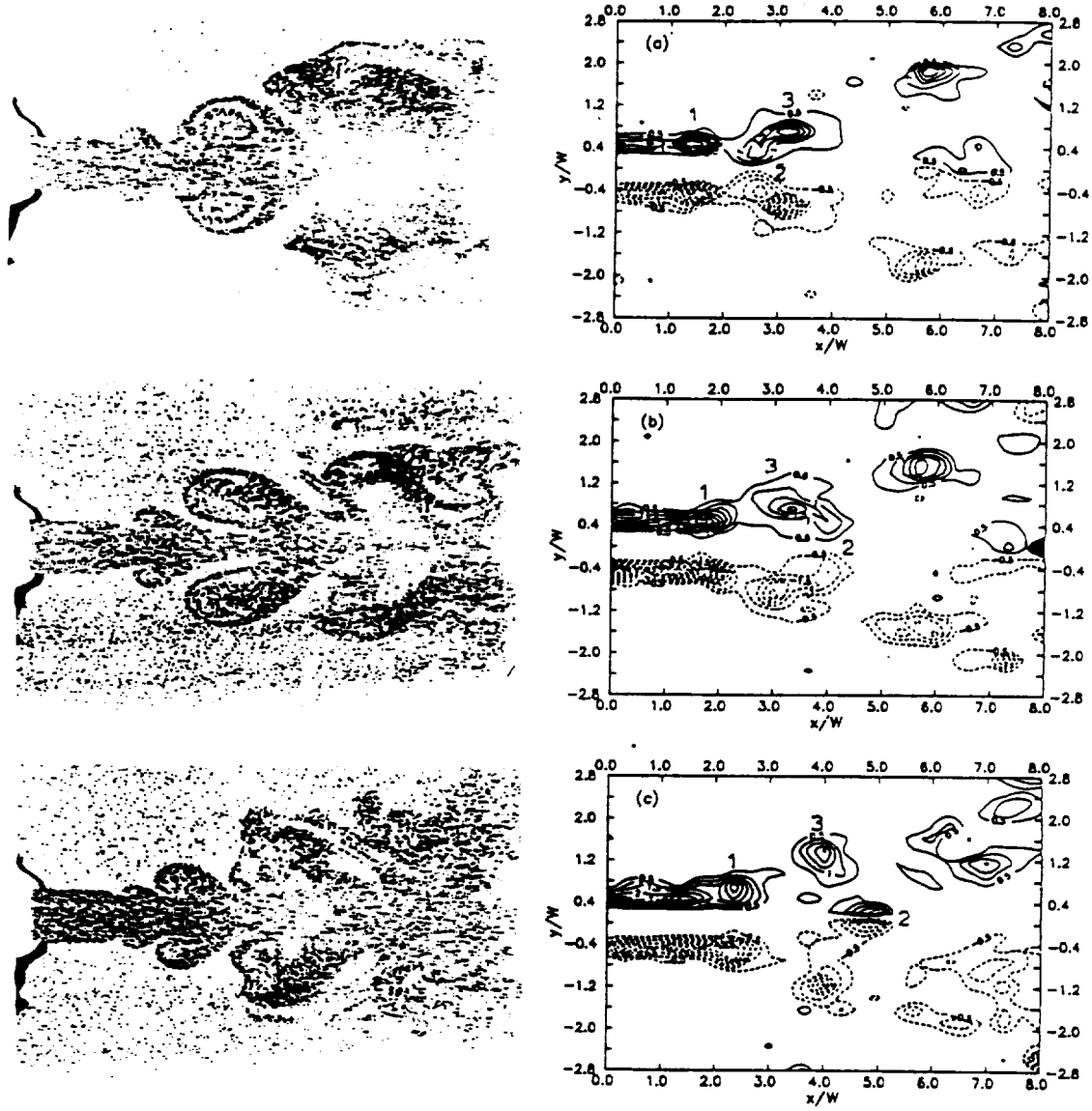

Figure 5. A sequence of a vortex interaction process; Left: double exposure photographs; Right: corresponding vorticity maps.

3 interact with one another in such a way that the trailing vortex 2 catches up with vortex 3 (figure 4b), proceeds to and moves at a high speed through the leading vortex (figure 4c). During this process, the leading vortex 3 moves away from the jet centerline resulting in enhanced spreading of the jet in the minor axis plane. In the mojor axis plane, like in the case of an elliptic jet[5,6] , the cylindrical vortices are bent and distorted in the lateral direction. A different type of vortex interaction process is shown in figure 5. As before, two successive vorticies 2 and 3 begin to interact with each other in figure 5a, and at later times produce patterns different from those observed in the previous sequence. Yet a third type of vortex arrangement can be seen in figure 1, where two successive vorticies appear to move together without significant interaction between

them. In the present experiment, we have observed more than three different types of vortex interactions. Careful examination of the pictures from the video tape suggest that the different interactions noted above occur repeatedly. Based on the limited amount of data, it may be argued that the different types of interactions observed here are a conesquence of the presence of "stream-wise corner vortices" and their interactions with cyclindrical vorticies surrounding the jet. Further investigations are clearly needed to unravel the different facets of the vortex interactions observed here.

4. Concluding Remarks

This exploratory experiment, for the first time provided information regarding the vortex formation and their subsequent interactions in the transition region of a rectangular jet. This description of the interactions between the cylindrical vorticies is greatly aided by the instantaneous velocity field measurements and their corresponding vorticity fields.

Our data suggest that there are more than one type of vortex interaction processes occur in the transition region before the jet becomes highly three dimensional. Two such processes are described in this paper. Present results indicate that the "stream-wise vortices" generated at the corners of the nozzle exit, due to uneven boundary layer structure, may have significant influence on the development of the transition region of a rectangular jet.

The cylindrical vorticies once formed and shed; generate energetic level coherent vorticity and turbulence production in between the vortical structures. To properly characterize the jet structure in the initial region, our experiment indicates that the detailed description of the instantaneous flow of the individual events may be necessary for better understanding of the physics of transition in three dimensional jets.

Acknowledgments

The support of NASA Ames Research center for the development of the PIDV technique is appreciated. Mr. Todd Lasalle and Ms Melissa Styer have been very helpful in reducing the data to a presentable form.

5. References

1. Brown, G. B., " On Vortex Motion in Gaseous Jets and Origin of Their Sensitivity to Sound", Proceedings of the Physical Society of London, 47, 1935, pp 703 - 731.
2. Hussain, A. K. M. F., " Coherent Structures and Turbulence", Journal of Fluid Mechnics, 173, 1987, pp 303 - 356.
3. Becker, H. A., and Massaro, T. A., " Vortex Evolution in a Round Jet", Journal of Fluid Mechnics, 31, 1968, pp 435 - 448.
4. Rockwell, D. O., and Niccolls, W. O., " Natural Breakdown of Planar Jets", Transactions of ASME: Journal of Basic Engineering, 94, 1972, pp 720 - 730.
5. Ho, C. M., and Gutmark, E., "Vortex Induction and Mass Entrainment in a Small Aspect Ratio Elliptic Jet", Journal of Fluid Mechnics, 179, 1987, pp 383 - 405.
6. Hussain, F., and Husain, H., "Elliptic Jets. Part 1: Characterstics of unexcited and excited jets", Journal of Fluid Mechnics, 208, 1989, pp 257 - 320.
7. Abramovich, G, N., " On the Deformation of the Rectangular Turbulent Jet Cross-Section", Int. Journal of Heat and Mass Transfer, 25, 1982, pp 1885 - 1894.

them. In the present experiment, we have observed more than three different types of vortex interactions. Careful examination of the pictures from the video tape suggest that the different interactions noted above occur repeatedly. Based on the limited amount of data, it may be argued that the different types of interactions observed here are a conesquence of the presence of "stream-wise corner vortices" and their interactions with cyclindrical vorticies surrounding the jet. Further investigations are clearly needed to unravel the different facets of the vortex interactions observed here.

4. Concluding Remarks

This exploratory experiment, for the first time provided information regarding the vortex formation and their subsequent interactions in the transition region of a rectangular jet. This description of the interactions between the cylindrical vorticies is greatly aided by the instantaneous velocity field measurements and their corresponding vorticity fields.

Our data suggest that there are more than one type of vortex interaction processes occur in the transition region before the jet becomes highly three dimensional. Two such processes are described in this paper. Present results indicate that the "stream-wise vortices" generated at the corners of the nozzle exit, due to uneven boundary layer structure, may have significant influence on the development of the transition region of a rectangular jet.

The cylindrical vorticies once formed and shed; generate energetic level coherent vorticity and turbulence production in between the vortical structures. To properly characterize the jet structure in the initial region, our experiment indicates that the detailed description of the instantaneous flow of the individual events may be necessary.

Acknowledgments

The support of NASA Ames Research center for the development of the PIDV technique is appreciated. Mr. Todd Lasalle and Ms Melissa Styer have been very helpful in reducing the data to a presentable form.

5. References

1. Brown, G. B., " On Vortex Motion in Gaseous Jets and Origin of Their Sensitivity to Sound", Proceedings of the Physical Society of London, 47, 1935, pp 703 - 731.
2. Hussain, A. K. M. F., " Coherent Structures and Turbulence", Journal of Fluid Mechnics, 173, 1987, pp 303 - 356.
3. Becker, H. A., and Massaro, T. A., " Vortex Evolution in a Round Jet", Journal of Fluid Mechnics, 31, 1968, pp 435 - 448.
4. Rockwell, D. O., and Niccolls, W. O., " Natural Breakdown of Planar Jets", Transactions of ASME: Journal of Basic Engineering, 94, 1972, pp 720 - 730.
5. Ho, C. M., and Gutmark, E., "Vortex Induction and Mass Entrainment in a Small Aspect Ratio Elliptic Jet", Journal of Fluid Mechnics, 179, 1987, pp 383 - 405.
6. Hussain, F., and Husain, H., "Elliptic Jets. Part 1: Characterstics of unexcited and excited jets", Journal of Fluid Mechnics, 208, 1989, pp 257 - 320.
7. Abramovich, G, N., " On the Deformation of the Rectangular Turbulent Jet Cross-Section", Int. Journal of Heat and Mass Transfer, 25, 1982, pp 1885 - 1894.

8. Lourenco, L., Krothapalli, A., and Smith, C. A., " Particle Image Velocimetry" Advances in Fluid Mechanics Measurements, Ed: M. Gad-El-Hak, Springer-Verlog, 1989, pp 128 - 199.
9. Ho, C. M., and Huerre, P., " Perturbed Free Shear Layers", Annual Review of Fluid Mechanics, 16, 1984, pp 365 - 424.

REPORT DOCUMENTATION PAGE

Form Approved
OMB No. 0704-0188

1. AGENCY USE ONLY *(Leave blank)*	2. REPORT DATE	3. REPORT TYPE AND DATES COVERED
	July 1991	Contractor Report

4. TITLE AND SUBTITLE

The Development of Laser Speckle Velocimetry for the Study of Vortical Flows

5. FUNDING NUMBERS

NAG2-314

6. AUTHOR(S)

A. Krothapalli

7. PERFORMING ORGANIZATION NAME(S) AND ADDRESS(ES)

Fluid Mechanics Research Laboratory
Department of Mechanical Engineering
FAMU/FSU College of Engineering
Tallahasseee, Florida 32306

8. PERFORMING ORGANIZATION REPORT NUMBER

A-91187

9. SPONSORING/MONITORING AGENCY NAME(S) AND ADDRESS(ES)

Ames Research Center
Moffett Field, CA 94035-1000

10. SPONSORING/MONITORING AGENCY REPORT NUMBER

NASA CR-177589

11. SUPPLEMENTARY NOTES

Point of Contact: Steve Dunagan, Ames Research Center, MS T-042, Moffett Field, CA 94035-1000
(415) 604-4562 or FTS 464-4562

12a. DISTRIBUTION/AVAILABILITY STATEMENT

Unclassified — Unlimited
Subject Category 35

12b. DISTRIBUTION CODE

13. ABSTRACT *(Maximum 200 words)*

A research program was undertaken to develop a new experimental technique commonly known as "particle image displacement velocimetry" to measure an instantaneous two dimensional velocity field in a selected plane of the flow field. This technique was successfully developed and applied to the study of several aerodynamic problems. This report presents a detailed description of the technique and a broad review of all the research activity carried out in this field. A list of technical publications is also provided.

The application of PIDV to unsteady flows with large scale vortical structures is demonstrated in a study of the temporal evolution of the flow past an impulsively started circular cylinder.

The instantaneous two dimensional flow in the transition region of a rectangular air jet was measured using PIDV and the details are presented. This experiment clearly demonstrates PIDV's capability in the measurement of turbulent flows.

Preliminary experiments were also conducted to measure the instantaneous flow over a circular bump in a transonic flow. Several other experiments now routinely use PIDV as a non-intrusive measurement technique to obtain instantaneous two dimensional velocity fields.

14. SUBJECT TERMS

Laser speckle velocimetry, Particle image displacement velocimetry, Vortical flows, Non-invasive measurements

15. NUMBER OF PAGES

118

16. PRICE CODE

A06

17. SECURITY CLASSIFICATION OF REPORT	18. SECURITY CLASSIFICATION OF THIS PAGE	19. SECURITY CLASSIFICATION OF ABSTRACT	20. LIMITATION OF ABSTRACT
Unclassified	Unclassified		